Eimeria bovis-mediated modulation of the host cell cholesterol metabolism

Penny Humaidah Hamid

INAUGURAL-DISSERTATION zur Erlangung des Grades eines **Dr. med. vet.**
beim Fachbereich Veterinärmedizin der Justus-Liebig-Universität Gießen

édition scientifique
VVB LAUFERSWEILER VERLAG

1. Auflage 2014

1st Edition 2014

Printed in Germany

édition scientifique
VVB LAUFERSWEILER VERLAG

STAUFENBERGRING 15, D-35396 GIESSEN
Tel: 0641-5599888 Fax: 0641-5599890
email: redaktion@doktorverlag.de

www.doktorverlag.de

Aus dem Institut für Parasitologie
der Justus-Liebig-Universität Gießen

Betreuerin: Prof. Dr. med. vet. habil. Anja Taubert DVM, DipEVPC

Eimeria bovis-mediated modulation of the host cell cholesterol metabolism

INAUGURAL-DISSERTATION
zur Erlangung des Grades eines
Dr. med. vet.
beim Fachbereichs Veterinärmedizin
der Justus-Liebig-Universität Gießen

eingereicht von

Penny Humaidah Hamid

Tierärztin aus Trenggalek, Indonesien

Gießen 2014

Mit Genehmigung des Fachbereichs Veterinärmedizin

der Justus-Liebig-Universität Gießen

Dekan	:	Prof. Dr. Dr. h.c. Martin Kramer
Gutachterin	:	
		Prof. Dr. Anja Taubert
		Prof. Dr. Sybille Mazurek
Prüfer	:	Prof. Dr. Joachim Geyer
Tag der Disputation	:	16.10.2014

PUBLICATIONS FROM THIS WORK

Original papers

1. **Hamid P.**, Hermosilla C., Kleinertz S., Hirzmann J., Taubert A. (2013). Erfolgreiche Replikation: *Eimeria bovis* moduliert den wirtszelleigenen Cholesterolhaushalt. *KompaktVet* 5: 4
2. Hamid, P.H., Hirzmann, J., Hermosilla, C., Taubert, A., 2014. Differential inhibition of host cell cholesterol de novo biosynthesis and processing abrogates Eimeria bovis intracellular development. Parasitology research 113, 4165-4176.
3. **Hamid P.**, Hirzmann J., Kerner K., Gimpl G., Lochnit G., Hermosilla C., Taubert A. (2014). *Eimeria bovis* infection modulates endothelial host cells cholesterol metabolism for successful replication (manuscript in preparation)

Presentations at conferences

1. **Hamid P.**, Hermosilla C., Kleinertz S., Hirzmann J., Lochnit G., Taubert A. *Eimeria bovis* modulates endothelial host cell cholesterol metabolism for successful replication. Jahrestagung der Deutschen Veterinärmedizinischen Gesellschaft, Fachgruppe Parasitologie und parasitäre Krankheiten: 8.-10.7.2013, Gießen
2. **Hamid P.**, Kleinertz S., Hermosilla C., Hirzmann J., Lochnit G., Taubert A. *Eimeria bovis* modulates endothelial host cell cholesterol metabolism for successful replication. 24th International Conference of the World Association for the Advancement of Veterinary Parasitology (WAAVP), 25.-29.8.2013, Perth, Australien
3. **Hamid P.**, Kleinertz S., Hermosilla C., Hirzmann J., Lochnit G., Taubert A. *Eimeria bovis* modulates endothelial host cell cholesterol metabolism for successful replication. "ApiCowplexa": Apicomplexa in farm animals, 31.10.13-02.11.13, Kusadasi, Türkei
4. **Hamid P.**, Kleinertz S., Hermosilla C., Hirzmann J., Taubert A. Host cell cholesterol esterification blockage inhibits *Eimeria bovis* development *in vitro*. "ApiCowplexa": Apicomplexa in farm animals, 31.10.13-02.11.13, Kusadasi, Türkei
5. **Hamid P.**, Hermosilla C., Kleinertz S., Hirzmann J., Lochnit G., Taubert A. *Eimeria bovis* modulates endothelial host cell cholesterol metabolism for successful replication. International Coccidiosis Conference, 26.-30.09.14, Dresden
6. **Hamid P.**, Hermosilla C., Hirzmann J., Taubert A. Differential inhibition of cholesterol synthesis and processing abrogates *Eimeria bovis* intracellular development. International Coccidiosis Conference, 26.-30.09.14, Dresden
7. **Hamid P.**, Hirzmann J., Kerner K., Lütjohann D., Hermosilla C., Taubert A. *Eimeria bovis* modulates endothelial host cell cholesterol metabolism for successful replication. Jahrestagung der Deutschen Veterinärmedizinischen Gesellschaft, Fachgruppe Parasitologie und parasitäre Krankheiten: 30.6.-2.7.14, Leipzig
8. **Hamid P.**, Hirzmann J., Hermosilla C., Taubert A. Differential inhibition of host cell cholesterol *de novo* biosynthesis and processing abrogates *Eimeria bovis* intracellular development. Jahrestagung der Deutschen Veterinärmedizinischen Gesellschaft, Fachgruppe Parasitologie und parasitäre Krankheiten: 30.6.-2.7.14, Leipzig
9. **Hamid P.,** Hermosilla C., Hirzmann J., Taubert A. Differential inhibition of host cell cholesterol *de novo* biosynthesis and processing abrogates *Eimeria bovis* intracellular development. PARATROP 2014 – Joint meeting of Parasitology and Tropical Medicine, 16.-19.7.2014, Zürich, Switzerland
10. **Hamid P.**, Hermosilla C., Hirzmann J., Kerner K., Lütjohann D., Taubert A. *Eimeria bovis* modulates endothelial host cell cholesterol metabolism for successful replication. PARATROP 2014 – Joint meeting of Parasitology and Tropical Medicine, 16.-19.7.2014, Zürich, Switzerland

ABBREVIATIONS

25-OHC	25-hydroxycholesterol
ACAT	acetyl-CoA acetyltransferase
acLDL	acetylated LDL
ADHP	10-acetyl-3,7-dihydroxyphenoxazine
BHQ	black hole quencher
BLAST	basic local alignment search tool
BSA	bovine serum albumin
BUVEC	bovine umbilical vein endothelial cell
$CaCl_2$	calcium chloride
cDNA	complementary DNA
CE	cholesterol ester
CH25H	cholesterol 25-hydroxylase
CHO	chinese hamster ovary
Ct	cycle threshold
CTCF	corrected total cell fluorescence
DAPI	4',6-diamidino-2-phenylindole
DMSO	dimethylsulfoxide
DNA	deoxyribonucleic acid
dNTP	deoxynucleotidetriphosphate
DTT	dithiothreitol
Ebmic4	*Eimeria bovis* microneme protein
ECGM	endothelial cell growth medium
EDTA	ethylenediaminetetraacetic acid
ER	reticulum endoplasmic
FACS	fluorescence activated cell sorting
FAM	6-carboxy-fluorescein
FCS	fetal calf serum
FITC	fluorescein isothiocyanate
GAPDH	glyceraldehyde-3-phosphate
HBSS	hank's balanced salt solution
HCl	hydrogen chloride
HDL	high density lipoprotein
HEX	hexachloro-6-carboxy-fluorescein
HMGCR	3-hydroxy-3-methylglutaryl-CoA reductase
HMGCS	3-hydroxy-3-methylglutaryl-CoA synthase
HRP	horseradish peroxidase
IC_{50}	inhibitory concentration 50
IMC	inner membrane complex
KCl	potassium chloride
kDa	kiloDalton
KH_2PO_4	potassium dihydrogen phosphate
LB	luria bertani
LD	lipid droplet

LDL	low density lipoprotein
LDLR	low density lipoprotein receptor
LE	late endosome
MBCD	methyl-β-cyclodextrin
MECGM	modified endothelial cell growth medium
MFI	mean fluorescence intensity
$MgCl_2$	magnesium chloride
$MgSO_4$	magnesium sulfate
mRNA	messenger ribonucleic acid
MTT	3-(4,5-dimethylthiazol-2-yl)-2,5 diphenyl tetrazolium bromide
Na_2HPO_4	disodium phosphate
NaCl	sodium chloride
NaN_3	sodium azide
NL	neutral lipids
NTC	non template control
OD	optical density
OLR	oxidized low density lipoprotein/ (lectin-like) receptor
OPG	oocysts per gram
ORP	OSBP related protein
OSBP	oxysterol binding protein
p.i	post infection
PBS	phosphate buffered saline
PCR	polymerase chain reaction
PE	phycoerythrin
PMN	polymorphonuclear
PV	parasitophorous vacuole
PVM	parasitophorous vacuole membrane
qPCR	quantitative real-time polymerase chain reaction
RE	recycling endosome
RIN	RNA integrity number
RNA	ribonucleic acid
RT	reverse transcriptase
SD	standard deviation
SDS	sodium dodecyl sulfate
SOAT	sterol-O-acyltransferase
SQLE	squalene epoxidase
SREBP	sterol regulatory element binding protein
TAE	tris acetate EDTA
TBS	tris-buffered saline
TBST	tris-buffered saline + tween
TET	tetrachloro-6-carboxy-fluorescein
TGN	trans-Golgi network
tRNA	transfer RNA
VLDL	very low density lipoprotein

TABLE OF CONTENTS

TABLE OF FIGURES AND TABLES

Figures

Tables

1 INTRODUCTION

Eimeria bovis represents one of the most pathogenic *Eimeria* species causing cattle coccidiosis (Daugschies and Najdrowski, 2005). During its longlasting intracellular first merogony (14-18 days of duration) *E. bovis* forms large macromeronts of > 400 µm size containing > 120,000 merozoites in host endothelial cells (Hammond, 1946). Given that the invading sporozoite stage alone cannot provide all components necessary for this nutrient and energy demanding process, the parasite needs to scavenge molecules from the host cell. Especially for the offspring's membrane production, large amounts of cholesterol are indispensable for a successful replication process.

Overall, cholesterol is needed for several reasons during macromeront formation: *i*) for the enormous enlargement of the host cell plasma membrane, *ii*) for the formation of the parasitophorous vacuole and *iii*) for the formation of a multitude of merozoites I. Interestingly, cholesterol auxotrophy has been reported for some closely related apicomplexan parasites, such as *Toxoplasma gondii*, *Cryptosporidium parvum* and *Plasmodium yoelii* (Coppens et al., 2000, Labaied et al, 2011, Ehrenmann et al., 2013). However, cholesterol is an irreplaceable component of cellular membrane biogenesis in the eukaryotic system exhibiting several pivotal physiological functions (Ohvo-Rekila et al., 2002) and its metabolism is tightly regulated in the mammalian system (Brown and Goldstein, 1986, Goldstein and Brown, 1990, Chang et al., 2006). To meet their cholesterol requirements for optimal parasite proliferation, *T. gondii, P. yoelii* and *C. parvum* scavenge cholesterol from their host cell by exploiting different pathways of cholesterol acquisition in a parasite-specific manner (Coppens et al., 2000; Labaied et al., 2011, Ehrenmann et al., 2013).

So far, little data are available on *E. bovis*-triggered modulation of the host cell cholesterol metabolism. Transcriptomic and proteomic analyses of *E. bovis*-

infected host cells indicate a parasite-induced alteration of cholesterol acquisition pathways in general (Taubert et al., 2010, Lutz et al., 2011), but do not deliver detailed data. Therefore, the current work intends to analyze the interference of *E. bovis* with its endothelial host cell on the level of low density lipoprotein-mediated cholesterol up-take and cellular cholesterol *de novo* synthesis via the mevalonate biosynthesis pathway. In addition, cholesterol processing in the host cell and parasite-mediated lipid droplet formation is analyzed in more detail and, overall, parasite-specific actions are highlightened.

2 LITERATURE REVIEW

2.1 Eimeria bovis

2.1.1 General introduction

Eimeria bovis belongs to the class Coccidia within the phylum Apicomplexa (Levine, 1980, Adl et al., 2005). Apicomplexan parasites are characterized by their unique apical complex (**Fig. 2.1.)**. The main components of the apical complex are: polar-ring complex, subpellicular microtubules, micronemes, rhoptries and dense granules (Chobotar and Scholtyseck, 1982). The polar-ring complex is localized at the very anterior part of apicomplexan invasive stages and consists of a ring of microtubules. The hollow-shaped conoid is located in the middle of the apical complex. Additionally, subpellicular microtubules are arising and anchored to this apical polar ring. These longitudinal subpellicular microtubules are associated with the inner membrane complex (IMC) which are important for the apicomplexan shape and physical stability (Morrissette and Sibley, 2002, de Souza and Attias, 2010).

The rhoptries, micronemes and dense granules are well known as highly specialized apicomplexan secretory organelles being indispensable for parasite gliding motiliy as well as for host cell invasion activity. Thus, their secreted products are required for three essential apicomplexan parasite actions: *i*) gliding motility, *ii*) host cell invasion and *iii*) early intracellular life establishment by parasitophorous vacuole (PV) formation (Dubremetz et al., 1998, Morrissette and Sibley, 2002, Souza, 2006, Ravindran and Boothroyd, 2008, Blackman and Bannister, 2001). The rhoptries are tear drop-shaped organelles which are connected by a thin duct to the apical part of the parasite. The rhoptry numbers can vary from two to more than six depending on the apicomplexan genus, species and stage [e. g. sporozoites, merozoites, bradyzoites, tachyzoites, metrozoites, (Blackman and Bannister, 2001)]. Rhoptry content secretion occurs shortly after parasite adhesion to the host cell membrane and rhoptric molecules have been

described to participate in the parasite-cell membrane tight junction formation during the active host cell invasion process (Dubremetz et al., 1998, Sibley, 2010). Furthermore, different rhoptry proteins have been described to be present either in the pheripheral or in the transmembrane part of intracellularly formed PVs (Sam-Yellowe, 1996). In this context, a merozoite-specific 22-kDa rhoptry protein of *E. nieschulzi* has been reported to be present in the PV membrane shortly after host cell invasion (Rick et al., 1998). In contrast to rhoptries, the micronemes are small elliptic-shaped organelles dispersed within the apical third of the parasite (**Fig. 2.1.**). These organelles are also relevant for host cell recognition, binding and gliding motility (Dubremetz et al., 1998). The dense granules are cytoplasmic, spherical-shaped organelles. Their contents are ultramicroscopically dense owing to their high protein concentration. The secretion of these proteins occurs after parasite internalization. Proteins of dense granule origin are components of the PV membrane and of the intravacuolar membranous network (Mercier et al., 2005).

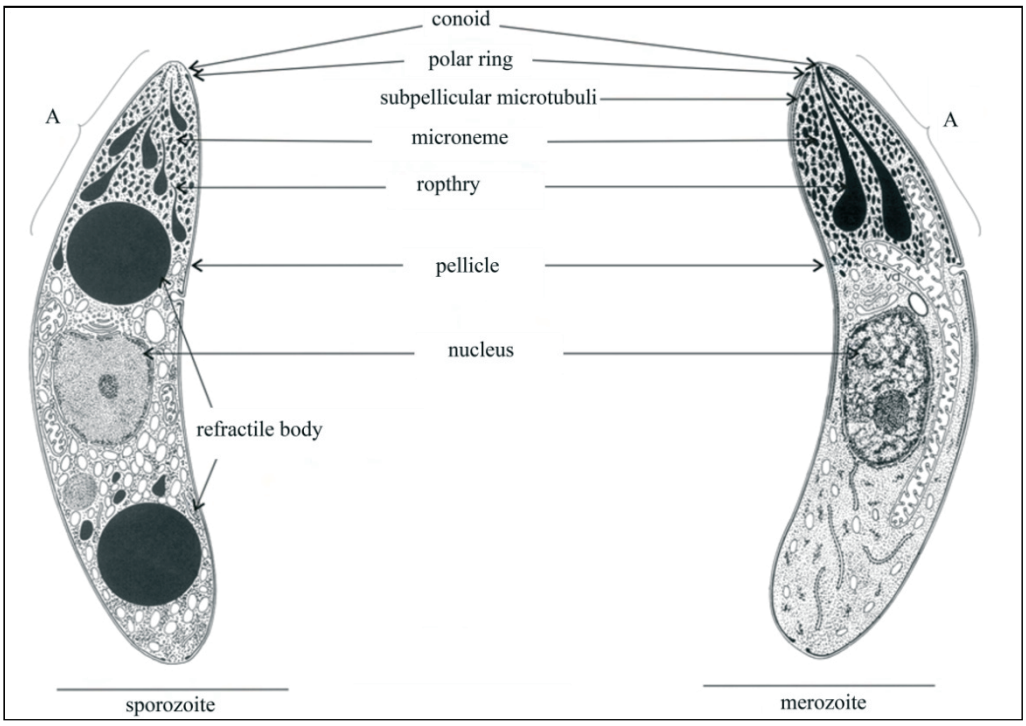

Fig. 2.1. Morphology of coccidian invasive stages (sporozoites and merozoites).
A: Apical complex. The image was adapted from Scholtyseck, 1979.

Endogenous invasive stages of *E. bovis* are the sporozoites, merozoites, macro- and microgametocytes. The invasive sporozoite stage of *E. bovis* is 15.6 µm long with 3.3 anterior and 3.7 µm wide. *E. bovis* sporozoites are characterized by one large refractile body at the posterior part of the body and one or two smaller refractile bodies situated proximal of the parasites nucleus (Hammond et al, 1968). In total, the sporozoite stage possesses 24 subpellicular microtubules (Robberts and Hammond, 1970) and several amylopectin granules which are located in between the nucleus and the posterior refractile body (Speer, 1988).

Merozoites I stage are approximately 13.5 µm long and 1.4 µm wide. As invasive stage it shows active flexing and gliding motility movements. *E. bovis* merozoites I possess 22 subpellicular microtubules being elongated from the anterior polar-ring. Furthermore, merozoites I have two club-shaped rhopthries in the apical complex. In contrast to sporozoite micronemes, the merozoite I micronemes are rather tortuous and often with unclear borders. The nucleus is located in the posterior third of the body (Sheffield and Hammond, 1966) and is surrounded by amylopectin granules (Speer, 1988). Other organelles, such as the endoplasmatic reticulum, are adjacent to nucleus with its rough cisternae in the anterior and posterior region. The Golgi complex is situated close to the anterior part of nucleus (Sheffield and Hammond, 1966). Merozoites II are shorter than first generation merozoites with 6-7 µm of length (Hammond et al., 1963).

2.1.2 Bovine coccidiosis and E. bovis life cycle

The prevalence of bovine coccidiosis is generally high and can reach up to 100% in young animals (Fox, 1985, Cornelissen et al., 1995, Faber et al., 2002). The tenacious sporulated *Eimeria*-oocysts are found ubiquitously in the environment resulting in infections of calves and young cattle, the most susceptible age group. Calves at an age of 3 weeks to 6 months are in particular susceptible to clinical bovine coccidiosis, which rather reflects lack of immunity than age resistance (Gräfner and Graubmann, 1979). Nonetheless, high prevalences have also been reported to occur in yearlings (Cornelissen et al., 1995, Faber et al., 2002). Thus,

it is most probable that all animals kept under conventional farming conditions unavoidably are exposed to *Eimeria* spp. infections worldwide (Bürger et al., 1983, Faber et al., 2002, Daugschies and Najdrowski, 2005). Infected animals may suffer from severe diarrhoea with sometimes even lethal outcome. However, given that the infection pressure is rather low, the animals were not infected by the most pathogenic *Eimeria* spp. or that the animals have previously been exposed and developed protective immunity against homologue *Eimeria* species (Hermosilla et al., 1999, 2012, Taubert et al., 2008, Suhwold et al., 2010), coccidial infections are not necessarily associated with clinical disease.

Infection-induced, impaired performance, mortality and anticoccidial treatment costs frequently result in considerable economic losses (Fitzgerald et al., 1980; Fox, 1985, Daugschies and Najdrowski, 2005, Hermosilla et al., 2006). Presumably, the economic losses due to subclinical disease even exceed those resulting from clinical coccidiosis (Fitzgerald, 1980, Bürger et al., 1983, Faber et al., 2002) as the former occurs much more frequently and may though impair intestinal physiology, feed conversion and animal growth (Fox, 1985, Gräfner et al., 1985, Cornelissen et al., 1995). According to Fitzgerald (1980), the worldwide annual costs due to bovine coccidiosis in cattle approximate 731 million US $. Matjila and Penzhorn (2002) estimated that the loss in profit within cattle industry reaches up to US $400 million/year since animals having survived severe clinical coccidiosis always show retarded growth and most probably will never become profitable again (Fox, 1985, Daugschies and Najdrowski, 2005).

Apicomplexan cattle *Eimeria* spp. all share a similar monoxenous life cycle, with an endogenous (parasitic) and an exogenous (environment) phase of life. They are all strictly host specific (monoxenous) enteropathogens which develop within specific host cells at specific sites of the intestinal mucosa. Most detailed studies on the biology of bovine coccidiosis have been carried out so far with *E. bovis*. Until now, thirteen different cattle *Eimeria* species (i. e. *E. alabamensis*, *E. aubernensis*, *E. bovis*, *E. brasiliensis*, *E. bukidnonensis*, *E. canadensis*, *E.*

cylindrical, *E. ellipsoidalis*, *E. illinoisensis*, *E. pellita*, *E. subspherica*, *E. wyomingensis*, *E. zuernii*) have been reported to occur worldwide. The most pathogenic species in cattle coccidiosis are *E. bovis* and *E. zuernii*, causing the classical 'stable coccidiosis' and *E. alabamensis* as the ethiological agent of 'pasture coccidiosis'. Extremely high doses of oocysts (10^8) are necessary to experimentally induce clinical 'pasture coccidiosis' with *E. alabamensis* (Hooshmand-Rad et al., 1994), whilst much lower doses of oocysts (10^4) of *E. bovis* and (10^5) of *E. zuernii* result in clinically apparent 'stable coccidiosis'. *E. bovis/E. zuernii*-infected animals frequently show a severe haemorrhagic typhlocolitis (Daugschies et al., 1986, Hermosilla et al., 1999) with weight losses, dehaydration and even sudden death. In contrast, *E. alabamensis*-coccidiosis is rather characterized by profuse catharralic enteritis (Hooshmand-Rad et al., 1994).

Under *in vitro* conditions, free-released sporozoites from oocysts might invade various cell types of different hosts. However, further development has been exclusively reported to occur within host cells of bovine origin and few gamonts and oocysts were only obtained in fetal gastrointestinal cells *in vitro* (Hermosilla et al., 2002). In the natural host, after the oral uptake of sporulated oocysts, free-released sporozoites of *E. bovis* must traverse the intestinal mucosa epithelium without considerable alterations (Behrendt et al., 2004), in order to infect host endothelial cells of the central lymph capillaries of the ileal villi (Hermosilla et al., 2006, 2012, Taubert et al., 2006a, 2010). Host cell invasion is accompanied by the release of parasitic antigens from diverse organelles located in the anterior part of the sporozoites (e. g. micronemes, rhoptries, dense granules) which play a significant role in host cell recognition, penetration through the host cell plasma membrane and the formation of the PV membrane (Heise et al., 1999a, b). Within the PV, sporozoites of *E. bovis* transform into trophozoites and then into first generation of meronts. One of the peculiarities of *E. bovis* is that intracellular sporozoites develop into huge macromeronts reaching sizes of up to 207-435 µm *in vivo* (Hammond et al, 1946) being accompanied by efficient modulation of infected host cells. Thus, cytoskeletal changes (Hermosilla et al., 2008), apoptosis

inhibition (Lang et al., 2009) and modulation of the host cell metabolism (Taubert et al., 2010, Lutz et al., 2011, Hermosilla et al., 2012) were reported. During macromeront formation, the lobes of spheroidal blastophores are subdivided from the meront cytoplasm. The anterior part of the offspring (merozoites I) is formed earlier than the posterior part. There is a thick inner membrane underneath to form the plasma membrane with the conoid opening in the offspring. This membrane is elongated forming a bud of early merozoites I stages containing cellular compartments, i. e. rhoptries, nucleus and Golgi apparatus. This membrane complex grows further forming the posterior body of the merozoites I. The individualized merozoites I are completely formed but still attached by their posterior part to the blastophore. When the merozoites I are released *in vivo,* this connection is solved (Hammond et al, 1946, Morrissette and Sibley, 2002). The free-released merozoites I then migrate to the caecum and colon in order to infect epithelial host cells where they undergo the second merogony resulting in 30-36 merozoites II (Hammond et al, 1963). Free-released merozoites II then start sexual reproduction, the gamogony, and form intracellular macro- and microgamonts in caecum/colon epithelial host cells. After syngamy (fertilization of a female macrogamont by a male motile microgamete) the zygote is formed which further develops into the oocyst stage. After the rupture of infected epithelial host cell, un-sporulated oocysts are shed via the faeces into the environment and the exogenous phase of the life cycle begins. Within this phase, oocysts undergo sporogony (asexual replication) resulting in infectious sporulated oocyts containing four sporocysts with two sporozoites each. The speed of successful sporogony strongly depends on adequate environmental conditions, such as optimal humidity, oxygen and temperature ranges.

2.1.3 Modulation of the host cell by E. bovis infections

During first merogony, *E. bovis* intracellular development leads to a massive alteration of its host cell and the endothelial host cell has to tolerate a ~10-fold enlargement and the formation of >120,000 merozoites within its cytoplasm. Given that endothelial cells are are highly immunoreactive cells being able to

produce a broad range of adhesion molecules, cytokines and proinflammatory chemokines upon activation thereby initiating leukocyte trafficking e. g. by recruiting polymorphonuclear neutrophils (PMN), NK cells, T lymphocytes and monocytes to the site of infection (for reviews see Tedder et al., 1995, Ebnet and Vestweber, 1999, Wagner and Roth, 2000) it appears likely that this cell type will actively defend intracellular parasitism.

In order to study both, parasite-triggered mechanisms allowing for successful replication and host cell derived defense actions, Hermosilla et al. (2002) established suitable *in vitro* cultures allowing for the entire merogony I, i. e., the development from the moment of host cell invasion to merozoite I production. An exemplary culture is depicted in **Fig. 2.2**.

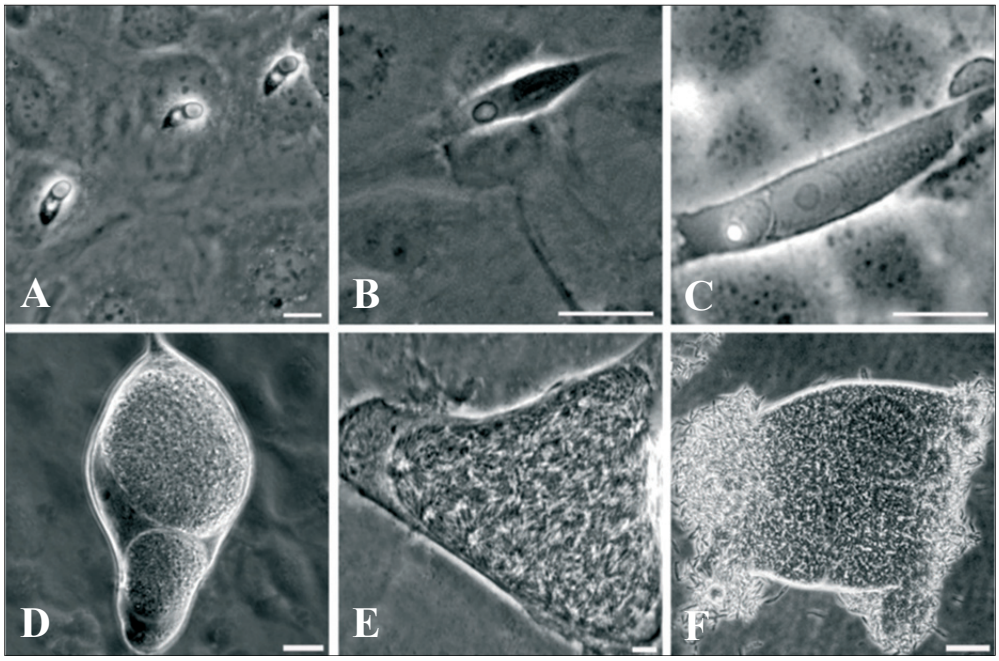

Fig. 2.2. *E. bovis* merogony I in bovine endothelial cells.
A: 1-5 days p.i.; B: 5-8 days p.i.; C: 8-12 days p.i.; D: 12-18 days p.i.; E: 18-23 days p.i.; F: 23 days p.i. onwards. Scale bars: 10 µm.

General profiling analyses heading for an overview of *E. bovis*-triggered host cell modulation throughout merogony I on both, the transcript and protein level revealed a multitude of functional categories to be altered in infected cells (Taubert et al., 2010, Lutz et al., 2011, Hermosilla et al., 2012) that may support

the parasites needs during intracellular development. However, host cell immune reactions were equally induced as molecules related to carbohydrate and lipid host metabolism as well as cellular transport and energy production (Taubert et al., 2010, Lutz et al., 2011, Hermosilla et al., 2012).

Targeted analyses on host cell defense mechanisms showed that endothelial host cells indeed react upon *E. bovis* invasion and intracellular development. Thus, several immunoregulatory molecules, such as adhesion molecules and chemokines were up-regulated in host cells (Hermosilla et al., 2006, Taubert et al., 2006a) and leukocyte adhesion to *E. bovis*-infected monolayers was enhanced relative to non-infected controls (Hermosilla et al., 2006; Taubert et al., 2007). Interestingly, comparative analyses revealed these reactions as considerably lower in *E. bovis*-infected host cells when compared to those induced by other coccidian parasites (Taubert et al., 2006b) indicating active counter-regulation by *E. bovis*. In agreement, *E. bovis* infections actively downregulated TNFα-stimulated PMN adhesion to infected host cells (Hermosilla et al., 2006).

Massive host cell enlargement needs to be supported by structural elements, such as the cytoskeleton. *E. bovis* infections caused a significant accumulation and re-organization of several cytoskeletal elements (Hermosilla et al., 2008). As such, actin, α-tubulin, acetylated tubulin and spectrin molecules were found altered in *E. bovis*-infected host cells forming compact structures adjacent to the macromeront (Hermosilla et al., 2008). Given that cytoskeletal elements do not only influence cell shape and mechanical properties but are also considerably involved in cellular transport (Ross et al., 2008, Balint et al., 2013), these modifications of the host cell cytoskeleton may be of outstanding importance for parasite proliferation.

Parasite invasion and the final enlargement of the host cell far beyond the physiological size causes considerable stress to the host cell (Frias et al., 2007, Fisch et al., 2007) and cell stress, in turn, is well known to trigger apoptosis

(Green and Reed, 1998, Green, 2000). The parasite, however, depends on a live host cell to complete its development. In consequence and in agreement to other related parasites, such as *E. necatrix, E. tenella* (del Cacho et al., 2004), *Cryptosporidium parvum* (Chen et al., 1999, 2001), *Theileria parva* (Heussler et al., 1999, 2001, Kuenzi et al., 2003), *Toxoplasma gondii* (Goebel et al., 1998, 1999, Caamano et al., 2000, Luder and Gross, 2005, Carmen et al., 2006, Keller et al., 2006) and *Plasmodium* spp. (Doolan and Hoffman, 2000, van de Sand, 2005), *E. bovis* was demonstrated to actively block host cell apoptosis by the up-regulation of anti-apoptotic molecules thereby preventing early host cell death and guaranteeing its prolonged intracellular survival (Lang et al., 2009).

2.2 Cholesterol

Cholesterol is an essential constituent of plasma membranes of most eukaryotic cells, where it is distributed non-randomly in structural and kinetic pools (Schroeder et al., 1991, Liscum & Underwood, 1995). In contrast, prokaryotic cell structures are devoid of cholesterol (Alberts, et al., 2008). The highest abundance of cholesterol is found in the plasma membranes although being present in differing proportions depending on the cell type (Lange, 1991, Ohvo-Rekila et al., 2002). Thus, in the liver cell plasma membrane cholesterol contents account for 17 % of total lipids, for 23 % in the red blood cell plasma membrane and for 22 % in myelin, whilst membranes of mitochondria and endoplasmic reticulum contain only 3 and 6 % of total lipids, respectively (Alberts, et al., 2008).

Cholesterol is an important regulator of physicochemical membrane properties by altering the fluidity and permeability of membanes (reviewed by Ohvo-Rekila et al., 2002, Ikonen, 2008). Cholesterol also modulates the functions of membrane proteins and participates in several membrane trafficking and transmembrane signalling processes (Simons and Toomre, 2000, Parton and del Pozo, 2013). Moreover, cholesterol metabolites function as signal transducers and solubilizers of other lipids (for review see Ikonen, 2008).

2.2.1 ***Cellular cholesterol sources***

Cellular cholesterol is either *de novo* synthesized by the mevalonate biosynthesis pathway or internalized from extracellular sources via lipoprotein up-take. Comparing these pathways quantitatively, a 70: 30 contribution of *de novo* synthesis vs. dietary intake was proposed (Grundy, 1983).

Cholesterol is synthesized in the endoplasmic reticulum *de novo* via the multistep enzymatic mevalonate biosynthesis pathway using acetyl-CoA as substrate (Liscum, 2004; for an overview on enzymatic steps see **Fig. 2.3.**). Within this pathway, the rate-limiting step is the conversion of HMG-CoA to mevalonate by HMG-CoA reductase activity. Given that mevalonate is also utilized for the synthesis of non-sterol isoprenoids, the squalene synthase (+ downstream acting molecules) may be considered as the first enzyme that determines the switch topwards sterol biosynthesis (Bergstrom et al., 1995).

Excess free cholesterol is toxic for cells and, in consequence, it is either effluxed from the cell or detoxified via biochemical cholesterol modification. The endoplasmic reticulum harbours enzymes for key cholesterol processing steps. Thus, cholesterol hydroxylation to generate oxysterols takes place in the ER rendering cholesterol to more hydrophilic. In general, oxysterols, such as 24-, 25- or 27-hydroxycholesterol, are present in cells only in minor amounts (approximately 1:1000 compared to cholesterol). In addition, cholesterol is modified via esterification leading to cholesteryl ester formation. Correspondingly, excess cellular free cholesterol activates acyl-coenzyme A: sterol acyltransferase (SOAT) (syn. acyl-coenzyme A: cholesterol acyltransferase, ACAT) enzymatic activity promoting cholesteryl ester formation. SOAT1 and SOAT2 are mainly located in the endoplasmic reticulum as integral membrane proteins. Whilst SOAT1 mRNA is ubiquitously expressed in mammalian tissues, SOAT2 is mainly active in the liver and small intestine (Chang et al., 2009). SOATs mediate the covalent binding of cholesterol and long-chain fatty acyl-CoA to form cholesteryl esters. In almost all cell types cholesteryl esters are present at

low levels in cytosolic organelles, the lipid droplets (LDs). Cholesteryl esters may accumulate in cells and are generally stored in cytosolic LDs (see **2.2.2**) which can rapidly release free cholesterol upon demand by cholesteryl ester hydrolase activities (Buhman et al., 2000, Chang et al., 2006).

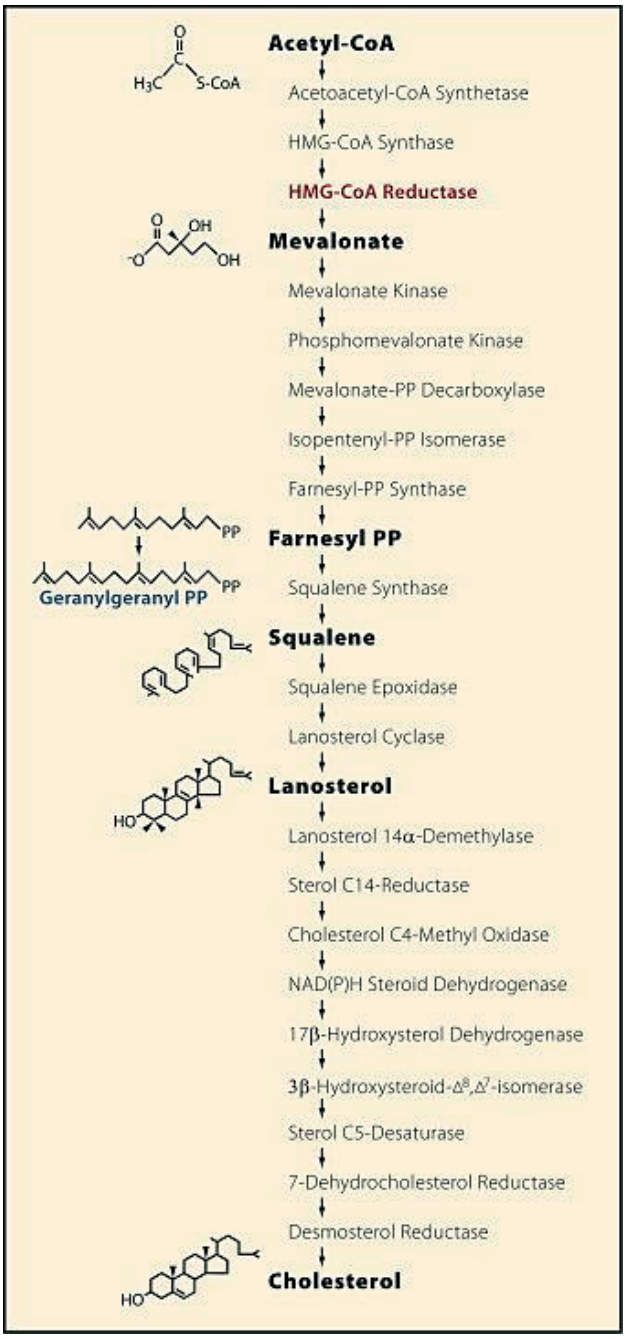

Fig. 2.3. Cholesterol synthesis via the mevalonate pathway in mammalian cells.
Acetyl-CoA is converted to cholesterol by at least 20 enzymes. Four key intermediates (mevalonate, farnesyl pyrophosphate squalene, lanosterol) are highlighted in black. Geranylgeranyl pyrophosphate, is a nonsterol isoprenoid derived from farnesyl pyrophosphate. Other nonsterol isoprenoids derived from farnesyl pyrophosphate (dolichol, heme A, ubiquinone) and from isopentyl pyrophosphate (isopentyl group of tRNAs) are not shown. (The figure and the legend are taken from Goldstein et al., 2006)

Exogenous acquisition of cholesterol is mediated via lipoprotein internalization. The general structure of lipoproteins is depicted in **Fig. 2.4**. The most important cholesterin-transporting molecule in the blood is the low density lipoprotein (LDL) particle. The LDL molecule contains 47-51 % of cholesteryl esters and 10-12 % of non-esterified cholesterol rendering LDL particles as the richest cholesterol carrier molecule amongst other lipoprotein subclasses, such as chylomicrons, VLDL and HDL (Jonas, 2004). LDL particles have a mass of approximately 3,000 kDa and measure ~22 nm in diameter (Brown and Goldstein, 1986). Cholesterol molecules are located in the hydrophobic core of LDL with polar OH-group esterified to long-chain fatty acid. The core contains around 1,500 cholesterol molecules and is surrounded by a monolayer of lipoprotein membrane which is composed of ~800 phospholipid and 500 unesterified cholesterol molecules. LDL particles furthermore contain one apoprotein B-100 molecule in the outer sheet which mediates specific binding to the LDL receptor (LDLR) on cell surfaces (Albert et al, 2008).

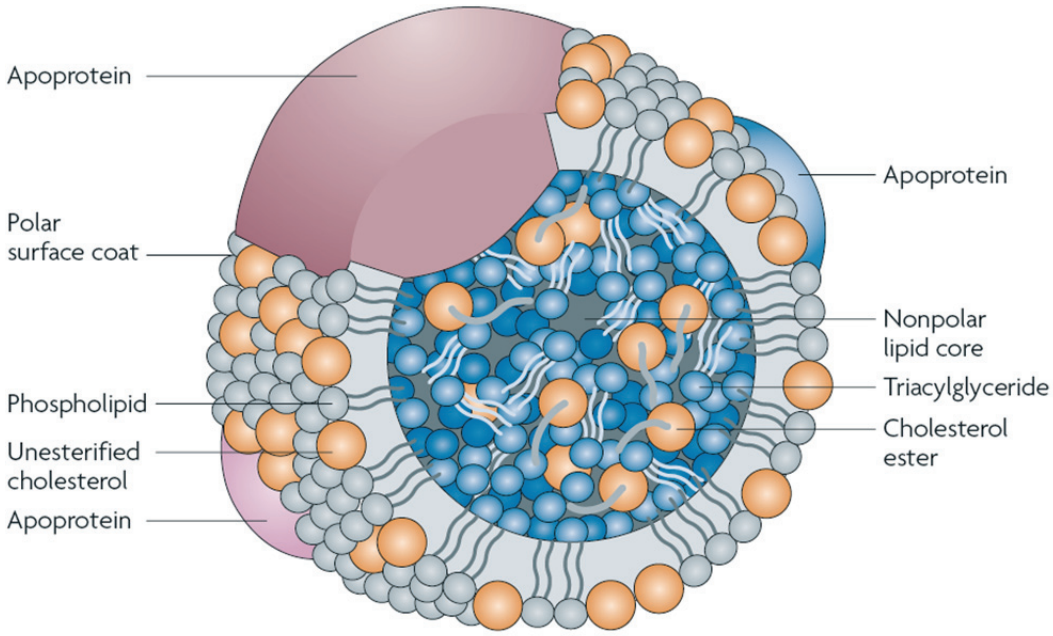

Fig. 2.4. General structure of a lipoprotein. The core is primarily composed of triacylglycerides and cholesterol esters. They are encased by a phospholipid monolayer. Apolipoproteins embedded in the phospholipid layer confer structural and functional properties to the molecule. (Figure and figure legend are taken from Wasan et al., 2008)

Cellular LDL-uptake is performed by LDL receptor (LDLR)-mediated endocytosis (Brown and Goldstein, 1975a, b; Brown et al., 1975) involving clathrin coated pits of the cell membrane. An overview of the LDLR-mediated endocytosis procedure is given in **Fig. 2.5**. The LDLR is concentrated in certain regions of the plasma membrane being specialized for receptor-mediated endocytosis. These regions form pits, i. e. plasma membrane invaginations, which are lined with clathrin molecules. The invagination rapidly occurs when LDL binds to LDLRs and the molecules are endocytosed. The clathrin molecules are recycled from endocytosed vesicle by ATPase heat shock cognate 70 (HSC70) and auxilin activities resulting in uncoated vesicles which are transported intracellularly (McMahon and Boucrot, 2011). The LDL/LDLR complex fuse with early sorting-endosomes. The LDL molecules then dissociate from LDLR due to acidic pH conditions in the endosome and are hydrolized to cholesterol and protein molecules. The LDLR molecules are recycled to the plasma membrane through endocytic recycling compartments. Early-endosome contents are processed to late endosome via vesicular transport and or endosome transformation.

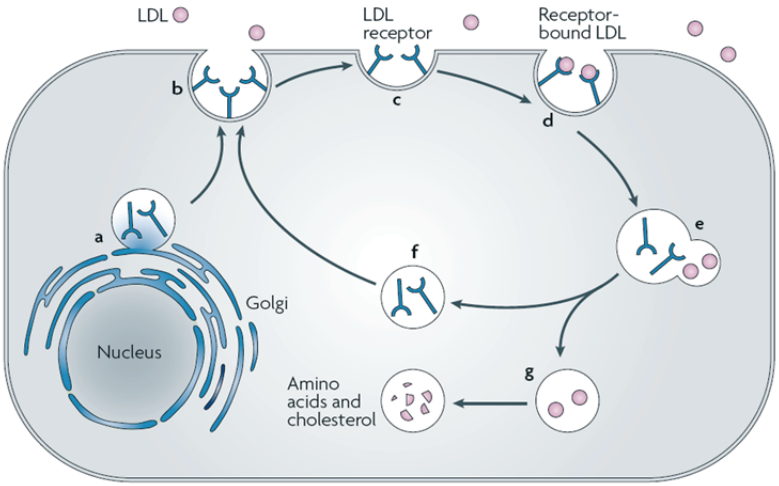

Fig. 2.5. LDL receptor-mediated endocytosis pathway. The entire cycle lasts approximately ten minutes. **a** | Nascent LDLrs are synthesized and packaged into vesicles in the Golgi complex. **b** | The vesicles are transported to and fuse with the plasma membrane. **c** | Functional LDLrs on the plasma membrane are clustered within clathrin-coated pits. **d** | LDL particles associate with LDLrs through interactions of the ligand-binding domain and ApoB100. **e** | Endocytosis of the coated pit internalizes the LDLr complex. Fusion with lysosomes decreases the pH of the vesicle causing the dissociation of LDL from the receptor. **f** | Intact receptors are transported back to the plasma membrane for re-use. **g** | The LDL particles are degraded into cholesterol and amino-acid components. (Figure and figure legend are taken from Wasan et al., 2008)

2.2.2 *Cytosolic lipid droplets (LDs)*

LDs (syn. lipid bodies) represent spherical, lipid-rich organelles that are found in the cytoplasm of most eukaryotic cells. Besides their function as lipid storage organelles, they are also reported as dynamic and multifunctionally active organelles being involved in several aspects of lipid metabolism, membrane trafficking, cell signaling and in inflammation (for reviews see Bozza et al., 2007, Farese and Walter, 2009, Beller et al., 2010, Melo et al., 2011). LDs are composed of a neutral lipid core (containing mainly triacylglycerol, cholesteryl esters and diacylglycerol) being surrounded by a single phospholipid monolayer equipped with associated proteins that mediate protein-protein interactions (Bozza et al., 2007, Melo et al., 2011). Cytosolic LDs are actively formed and increasing numbers are induced upon adequate stimuli. Furthermore, the volume/size of LDs can be enhanced either by augmentation of local lipid synthesis (Kuerschner et al., 2008) or by LD fusion (Olofsson et al., 2009).

LD formation is a multienzymatic and complex process involving fatty acid activation, synthesis of neutral lipids, remodeling and synthesis of phospholipids and integration of accessory proteins in LDs monolayered membrane (Pol et al., 2014). LDs appear to be produced in the endoplasmic reticulum, and their outer monolayer is proposed to originate from one of the endoplasmic reticulum bilayered membranes (Fujimoto et al., 2008). LDs are well-known for their capacity to store lipids for both purposes, as metabolic energy carriers and as membrane percursor molecules. LDs are mobilized upon demand for energy by the activity of specific lipases or other metabolic enzymes. LDs are sites of key enzymes of cholesterol metabolism and fatty acid synthesis indicating that both anabolic and catabolic steps of lipid metabolism occur in LDs (Brasaemle et al, 2004; Fujimoto et al, 2004). LDs also involved in cellular lipid and protein trafficking by direct contact of LD with other cellular membranes facilitating lipid transfer (Murphy et al., 2009). The actual composition of lipids and LD-associated proteins varies between different cell types and physiological states (Bickel et al., 2009).

Besides acting as feeder organelle and host-derived nutrient supplier, LDs also play a role in inflammatory responses since they are described as sites of storage and synthesis of cytokines, chemokines and growth factors especially in immune cells (Bozza et al., 2007). Furthermore, they were reported to be elicited in response to inflammatory stimuli (for review, see Melo et al., 2011). Whithin inflammatory cells, LDs contain arachidonyl lipids for eucosanoid synthesis and relevant enzymes, such as cyclooxygenase, prostaglandin E2 synthase, lyoxygenases and leukotriene C4 synthase (reviewed by Bozza et al., 2007 and Melo et al., 2011). Pathogen-induced LD formation was reported for bacterial, viral, fungal and parasitic infection suggesting a role of LDs in intracellular survival and pathogen replication (d'Avila et al., 2008, van der Meer-Janssen et al., 2010).

2.2.3 *Intracellular cholesterol transport and regulation of homeostasis*

Cellular cholesterol transport is a highly complex multistep process. Cholesterol distribution within the cell, its processing and trafficking is summarized and described in **Fig. 2.6.**, according to Simons and Ikonen (2000).

Overall, cholesterol is permanently transported within the cell, either by vesicular, membrane-associated mechanisms or by non-vesicular routes. Non-vesicular transporting either uses direct membrane contacts or cytosolic lipid transfer proteins involving several organelle-specific molecules (reviewed in Ikonen, 2008). However, so far, only some molecules being involved in cholesterol transporting are known, such as the Nieman Pick C (NPC1 and NPC2) molecules.
Given that excess cellular cholesterol contens are toxic for the cell, cholesterol may either be biochemically modified and stored, i. e. in LDs (see **2.2.2**), or it is effluxed. In the latter case it may be taken up by HDL particles, acting as major cholesterol acceptors and key molecules in the reverse cholesterol transport to liver cells (Tall, 1998, Ohashi et al., 2005, Yokoyama, 2005).

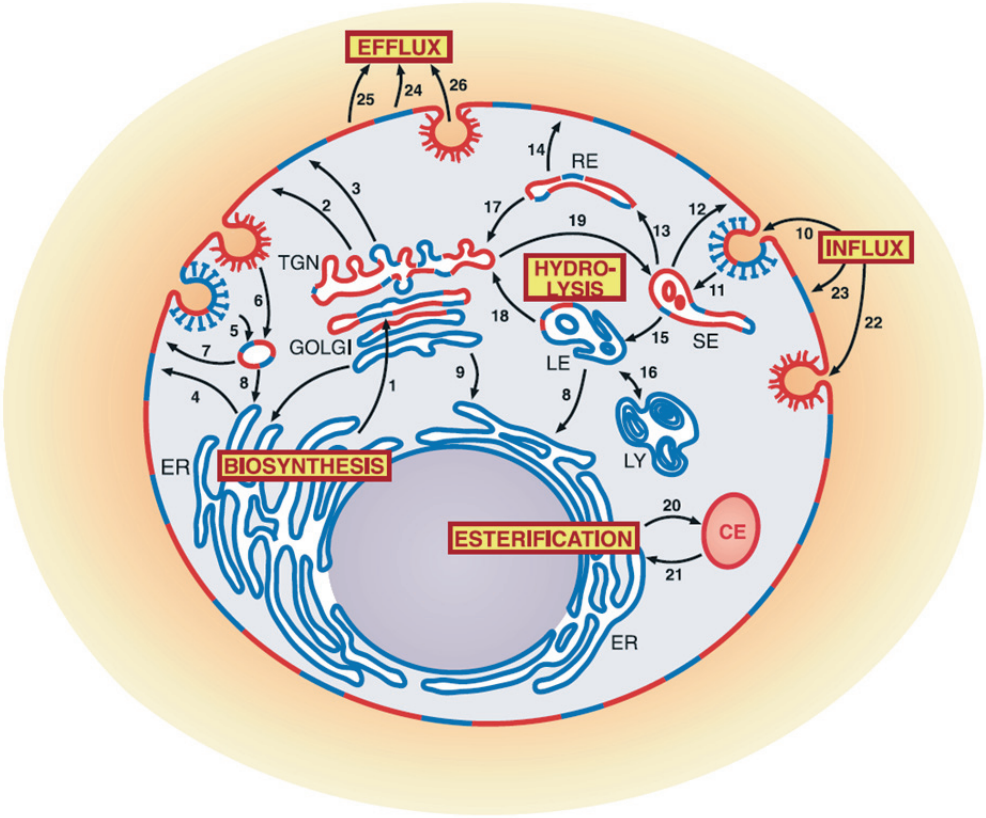

Fig. 2.6. Schematic presentation of cellular cholesterol distribution, processing, and trafficking circuits. Cholesterol is synthesized in the endoplasmic reticulum (ER). Part of it is transported via the Golgi complex (**1**) and the trans-Golgi network (TGN) to the plasma membrane, where it is distributed either to raft (**2**, red) or nonraft (**3**, blue) microdomains. The majority of cholesterol, however, takes a Golgi-bypass route (**4**) to the cell surface. Cholesterol can be internalized from the plasma membrane by endocytosis via clathrin-coated vesicles (**5**) or other pathways, including caveolae (**6**). Endocytosed rafts are found in sorting and recycling endosomes. From the endocytic circuits, cholesterol may be recycled to the surface (**7**) or transported back to the ER (**8**). Also, retrograde routes from the Golgi complex (**9**) recycle cholesterol to the ER. There may also be a route involving transport via caveolae to the ER. Cholesterol is endocytosed in LDL via clathrin-coated pits (**10**) and transported to sorting endosomes (SE; **11**). From there, it can be recycled to the surface either via a rapid route (12) or through slower circuits involving recycling endosomes (RE; **13**, **14**). Cholesterol is also transported to late endocytic structures [**15**, late endosomes (LE) and lysosomes (LY)] that can fuse with each other (**16**). Sorting, recycling, and late endosomes communicate with the exocytic pathway at the level of the TGN (**17** through **19**), thus exchanging cholesterol between the endocytic and exocytic routes. Cholesterol esters in LDL are hydrolyzed prior to release from the endocytic organelles, but cholesterol returning to the ER may become re-esterified. Cholesterol esters (CE) are deposited in cytosolic lipid droplets (**20**) from where cholesterol can be mobilized upon ester hydrolysis (**21**). Cholesterol and cholesterol esters can also be exchanged directly between circulating lipoproteins and the plasma membrane. Caveolae have been implicated in the uptake of cholesterol esters from HDL (**22**), and free cholesterol can be taken up from LDL (**23**).Cholesterol can be released from cells, both from nonraft (**24**) and raft domains (**25**), the latter potentially involving caveolae (**26**). In some cases, this may involve endocytic uptake and resecretion of lipoproteins. (Figure and figure legend are taken from Simons and Ikonen, 2000)

Cholesterol homeostasis is tightly regulated to prevent toxic effects but to meet the needs of cellular cholesterol delivery (Brown and Goldstein, 1986, Goldstein and Brown, 1990). The cellular cholesterol concentration itself plays a pivotal role in cholesterol homeostasis. Whilst too high cholesterol concentrations block the mevalonate biosynthesis pathway and LDLR expression and enhance cholesterol esterification and storage (Goldstein and Brown, 1990, Brown and Goldstein, 1986, Brown et al., 1975b, **Fig. 2.7.**), low cholesterol levels induce the gene transcription of HMGCR and other relevant molecules via a highly complex activation process of special transcription factors, the so-called Sterol Regulatory Element Binding Proteins, SREBPs (Edwards et al., 2000, Shimano, 2001, Horton et al., 2002, Eberle et al., 2004). Besides being regulated via cholesterol levels, cholesterol homeostasis is also controlled by 25-hydroxycholesterol (25-OHC). Oxysterols, such as 24-, 25- and 27-OHC are produced in low concentrations in various tissues (Russell, 2000). In general, oxysterols are synthesized when cholesterol levels are high. High 25-OHC levels lead to the blockage of SREBPs thereby lowering cholesterol *de novo* synthesis (Radhakrishnan et al., 2007).

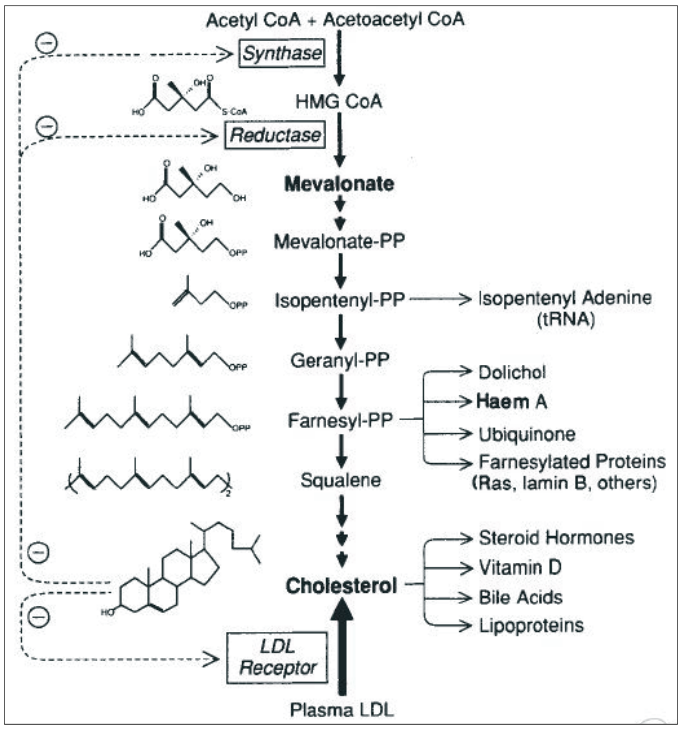

Fig. 2.7. Regulation of cholesterol homeostasis [according to Brown and Goldstein (1990)].

2.3 Modulation of host cell cholesterol metabolism by protozoan parasites

Coccidian parasites in general and some apicomplexan parasites in particular have been described as auxotrophic in their capability to synthesize cholesterol by themselves (Furlong, 1989, Coppens et al., 2000, Bano et al., 2007, Labaied et al., 2011, Ehrenman et al., 2013, Bansal et al., 2005, Coppens, 2013). Thus, cholesterol auxothrophy was reported for the coccidian parasites *T. gondii* and *C. parvum* (Coppens et al., 2000, Ehrenman et al., 2013); furthermore apicomplexan *Plasmodium* subspecies are considered as defective in cholesterol synthesis (Labaied et al., 2011). Given that the developing parasite stages of these obligate intracellular replicating protozoans indeed do contain cholesterol, they must scavenge this molecule from their host cell by exploiting different cellular pathways. Interestingly, different cholesterol synthesis-deficient parasites appear to follow different strategies of cholesterol scavenging characterizing the modulation of host cell cholesterol metabolism as a parasite-specific process.

Most data on the presence of cholesterol in coccidian stages or on coccidia-triggered host cell cholesterol exploitation concern *T. gondii* infections. In *T. gondii* tachyzoite stages, cholesterol was reported to be concentrated in the rhoptries and pellicules (Foussard et al., 1991a, b). Furthermore, free cholesterol was detected in the apical complex, the wide posterior-end of rhoptry membranes, inner membrane complex, the apicoplast and in the remaining mother-cell residue of the nascent tachyzoites (Coppens et al., 2000, Coppens and Joiner, 2003). Overall, lipid profiling experiments revealed cholesterol as the most abundant molecule in isolated rhoptries when compared to other lipid classes. Apart from the free form, cholesterol was also present in the esterified form in *T. gondii* (Besteiro et al., 2008, Charron and Sibley, 2002). It is worth noting that *T. gondii* itself has the capacity to express enzymes promoting cholesterol esterification (Nishikawa et al., 2005, Lige et al., 2013).

Coppens et al. (2000) experimentally proved *T. gondii* as auxothrophic for cholesterol synthesis since tachyzoites revealed unable to convert radioactive

substrates of the mevalonate biosynthesis pathway to form cholesterol. They additionally showed that parasite growth is enhanced by addition of free or LDL-incorporated cholesterol to the cell culture medium. However, the mode of cholesterol acquisition by *T. gondii* appears to be host cell-dependent, since different strategies were described in different host cell types. Thus, in CHO cells *T. gondii* exclusively utilized cholesterol derived from internalized LDL particles and did not profit from *de novo* synthesized cholesterol (Coppens et al., 2000). In contrast, transcriptomic data on *T. gondii*-infected fibroblasts indicated an up-regulation of molecules involved in the mevalonate biosynthesis pathway (Blader et al., 2001). In addition, cellular *de novo* synthesis but not LDL-mediated up-take proved essential for parasite growth in macrophages as indicated by statin treatments and the use of LDLR knock-out cells (Nishikawa et al., 2011). However, up to date, all *T. gondii*-related reports indicate that only one alternative pathway is exploited by the parasite at a time.

Overall, host cell cholesterol plays a crucial role already very early in *T. gondii* infection, i. e., when the parasite initially invades the host cell. Thus, host cholesterol governs parasite entry by modulating secretory-organelles discharge. Furthermore, it influences parasite internalization and contributes to the formation of the PV membrane (Coppens and Joiner, 2003, Cruz et al., 2013).

In *T. gondii*-infected host cells, exogenously supplied cholesterol is inserted in the parasite plasma membrane and cholesterol-rich organelles and is furthermore esterified for LD deposition (Coppens et al., 2000, Charron and Sibley, 2002, Sehgal et al., 2005, Nishikawa et al., 2005). Accordingly, host and parasite esterification activity was shown to be essential for parasite intracellular growth (Sonda et al., 2001). Correspondingly, *T. gondii* infection leads to enhanced cytoplasmic LD formation in skeletal muscle cell cultures indicating these organelles as a source of lipids for parasite survival (Gomes et al., 2014).

Host cellular LDL acquisition involves the LDL receptor (LDLR)-based endocytic pathway in *T. gondii*-infected host cells (Coppens et al., 2000). So far, the transport of LDL-derived cholesterol to the intracellular parasite residing within its PV is not fully understood. It is evidenced that compounds interfering with endolysosomal function disrupt cholesterol delivery towards the parasite (Coppens et al., 2000). Thus, the parasite appears to use a vesicle-based transport of host endolysosomal organelles being supported by transporter-like proteins present in the PV and parasite plasma membrane (Sehgal et al., 2005). Furthermore, *T. gondii* reorganizes the microtubule system around the PV and uses this system to sequester lysosomes from the host cell to the PV space (Coppens et al., 2006). Interestingly, microtubules form deep invatinations of the PV membrane leading to double membrane structures, termed "Host Organelle Sequestring Tubulo Structures", which are thought to be involved in endosome-mediated cholesterol delivery to the parasite (Laliberte and Carruthers, 2008). Electron microscopic analyses evidenced that gold-labelled LDL is indeed transported through these microtubule protrusions and found inside the PV as intact vesicular entities (Coppens et al., 2006).

The delivery of LDL-derived cholesterol in addition requires host-P-glycoprotein-based pumps, since delivery of cholesterol towards PV is inhibited in respective knock-out fibroblasts (Bottova et al., 2009). In *T. gondii*-infected skeletal muscle cells, increased numbers of LD are formed and recruited to the PV. Since direct contacts of LDs with the PV and parasite membrane were observed, the authors hypothesize a discharge of their contents as lipid delivery sytem (Gomes et al., 2014). However, given that LD enhancement was not observed in fibroblasts, which were also present in skeletal muscle cell cultures, these features appear to be cell type-specific.

The apicomplexan parasites *Plasmodium yoelii* and *P. berghei* also contain host cell-delivered cholesterol in the PV of their intrahepatic stages (Bano et al., 2007, Labaied et al., 2011). Furthermore, *Plasmodium* merozoites were shown to

integrate lipids derived from the erythrocyte membrane into the nascent PV (Ward et al., 1993). *Plasmodium* blood stages, which are residing within erythrocytes, mainly acquire cholesterol from circulating HDL particles and deliver cholesterol via a tubulovesicular network (Grellier et al., 1990). In hepatic stages, *Plasmodium* spp. appear to salvage cholesterol from both host cellular pathways, i. e. LDL-mediated up-take and *de novo* synthesis (Grellier et al., 1994, Labaied et al., 2011). However, host cellular cholesterol acquisition does not appear to be essential for optimal parasite proliferation since neither the reduced expression of LDLR nor the blockage of the mevalonate biosynthesis pathway interfered significantly with parasite development (Labaied et al., 2011). The authors interpret these results by a moderate parasite need of sterols and by an adaptive reaction to cholesterol-restricted conditions in terms of alternative source utilization. Although abundant LD formation was also reported for *P. berghei*- or *P. falciparum*-infected host cells (Rodriguez-Acosta et al., 1998, Vielemeyer et al., 2004), no cholesteryl ester formation was detected in *Plasmodium*-infected cells implying a certain lack of lipid storage activity (Nawabi et al., 2003, Palacpac et al., 2004, Vielemeyer et al., 2004, Coppens and Vielemeyer, 2005) which may argue for a continuous cholesterol acquisition from the host cell as hypothesized by Coppens (2013).

By far less data are available on other apicomplexan parasites. *C. parvum* mainly acquires cholesterol from LDL particles and from micellar lipoproteins being internalized by enterocytes (Ehrenman, 2013). To a minor degree, *C. parvum* also scavenges *de novo*-synthesized cholesterol since treatments of parasite cultures with lovastatin or zaragozic acid had moderate effects on parasite proliferation (Ehrenmann et al., 2013). Furthermore, the NPC1L-mediated vesicular transport appeared to play a pivotal role for cholesterol acquisition within infected enterocytes (Ehrenmann et al., 2013). The involvement of membrane cholesterol in parasite entry and internalization was described for several other protozoa, such as *Babesia bovis* (Okubo et al., 2007), *Trypanosoma cruzi* (Fernandes et al., 2007) or *Leishmania* spp. (Pucadyil et al., 2004, Tewary et al., 2006). Furthermore, the

modulation of host cell gene transcripts being associated with cholesterol metabolism were also shown for *L. amazonensis* (Lecoeur et al., 2013) and *T. cruzi* (Nagajyothi et al., 2011, Chiribao et al., 2014). In the latter case, enhanced LD formation was observed *in vitro* in infected macrophages suggesting infection-induced lipid storage activities (Melo et al., 2003, 2006). Furthermore, accumulation of cholesterol and LDL was measured in *in vitro* cultures and in tissues of *T. cruzi*-infected mice (Johndrow et al., 2014) confirming an important role of lipids in this parasite infection.

To date, data on cholesterol and its delivery in *Eimeria*-infected host cells are almost absent. The only report is given by Taubert et al. (2010) indicating that the gene transcription of several molecules being involved in the *de novo* mevalonate biosynthesis pathway and in the LDL-promoted cholesterol cellular up-take are up-regulated in *E. bovis*-infected endothelial host cells in times of macromeront formation.

3 MATERIALS AND METHODS

3.1 Cell culture

3.1.1 *Primary endothelial cell isolation and cultivation*

Materials

1. Puck's buffer: 8 g/l NaCl, 0.4 g/l KCl, 0.012 g/l $CaCl_2$, 0.154 g/l $MgSO_47H_2O$, 0.39 g/l NaH_2PO_4, 0.15 g/l KH_2PO_4, 1.1 g/l glucose (all Roth, Karlsruhe)
2. Collagenase solution: 0.025 g collagenase type II (Worthington Biochemical Corp., NJ, USA, LS004174) in 100 ml Puck's buffer, sterile filtered using a 0.2 µm syringe filter (Millipore)
3. Endothelial Cell Growth Medium (ECGM) containing supplement (complete ECGM, PromoCell, Heidelberg, C-22010)
4. Fetal Calf Serum [(FCS), Biochrom, Berlin, S 0415)]
5. Hank´s Balanced Salt Solution (HBSS): 1X HBSS (Gibco, 24020-117) with 6 g HEPES/l, 1 % penicillin-streptomycin (Pen-Strep, PAA Laboratories, Coelbe), pH 7.4 ± 0.3
6. Medium 199 (Sigma-Aldrich, Steinheim, M0393)
7. Modified ECGM: 150 ml complete ECGM supplemented with 350 ml medium 199 containing 1 % Pen-Strep and 2 % FCS
8. RPMI 1640 medium (Sigma-Aldrich, R0883)

Method

Endothelial cells originated from bovine umbilical cords from calves born by *sectio caesarea* were supplied by the Clinic of Large and Small Animals, Justus Liebig University Giessen, and the Clinic for Cattle, University of Veterinary Medicine Hannover, Germany. Umbilical cords were kept and transported in HBSS buffer at 4ºC temperature and isolated according to Jaffe et al. (1973). Briefly, one side of the umbilical cord vein was closed with an artery clamp. Then, collagenase solution was infused into the vein lumen, the vein was closed and incubated at 37ºC in 5 % CO_2 atmosphere for 20 min. Thereafter, the

umbilical vein was gently massaged, unclamped and RPMI 1640 medium was infused to wash the endothelial cells into a 50-ml plastic tube. Collagenase was inactivated by the addition of 1 ml FCS per 25 ml solution. The solution was centrifuged (600x*g*, 10 min), and the pellet was resuspended in complete ECGM. The cells were seeded in 75 cm^2 cell culture flasks and fed every 2-3 days until confluency. BUVEC were cultivated using modified ECGM after the first passage. First to fifth BUVEC passages were used for *E. bovis* infection experiments *in vitro*.

3.1.2 *Endothelial cell subcultivation and cryopreservation*

Materials

1. Trypsin buffer: 137 mM NaCl, 5 mM KCl, 7 mM $Na_2HPO_42H_2O$, 5.5 mM Glucose, 0.8 mM Tris-Base (all Roth), 2.5 g trypsin (Serva, Duisburg, 37294.02)
2. Versen buffer: 137 mM NaCl, 2 mM KCl, 8.1 mM $Na_2HPO_42H_2O$, 1.4 mM KH_2PO_4, 5.3 mM EDTA (all Roth), sterile filtered (0.2 µm syringe filter)
3. Trypsin-Versen buffer: 1 part trypsin buffer + 4 parts versen buffer

Method

10 ml Trypsin-Versen buffer were added to each 75 cm^2 tissue culture flask containing confluent BUVEC layers and incubated for 10 min at 37ºC. Flasks were shaken to facilitate cell detachment. Then 10 ml modified ECGM were added and the solution was collected in a 50 ml tube and centrifuged (600x*g*, 10 min). The pellet was resuspended in ECGM medium and splitted into three new flasks. For cryopreservation, the pellet was resuspended in medium containing 10 % DMSO. Cells were then incubated for 30 min at 4ºC, and stored at -80ºC. For longer storage, cells were transferred to liquid nitrogen (-196ºC). Thawing of BUVEC was performed by transferring the frozen cells directly into a 37ºC-waterbath. After defrosting, modified ECGM was added immediately and the samples were washed (600x*g*, 10 min) to remove DMSO. The pelleted cells were

resuspended in modified ECGM and cultivated in three flasks for further cultivation.

3.2 Parasite preparations

3.2.1 *Experimental animals*

Male Holstein Frisian calves were purchased from a local farmer at the age of 2 weeks, treated with Baycox® (Bayer) and Halocur® (Intervet) in the second week after birth, assessed for parasitic infections and when deemed parasite free, maintained under parasite-free conditions in autoclaved stainless stell cages (Woetho) until experimental *E. bovis* infection. They were controlled for parasitic infections coprologically every 3 days. They were fed with milk substitute (Hemo Mischfutterwerke) and commercial concentrates (Raiffeisen). Drinking water and sterilized hay were given *ad libitum*.

3.2.2 *Animal infections with E. bovis*

At an age of 8-10 weeks calves were infected orally with sporulated *E. bovis* oocysts. Therefore, sporulated oocysts were washed three times with distilled water and centrifuged (400x*g*,10 min). The supernatant was discarded and pelleted oocysts were resuspended in sterile distilled water. Calves were infected orally with 5 x 10^4 oocysts and monitored during infection. The faeces were analyzed coproscopically for oocysts applying MacMaster technique three times a week. Briefly, 4 g faeces were mixed with sugar solution (specific density 1.27). The solution was then mixed thoroughly and filtered. Then, both sides of a McMaster counting chamber were filled and allowed to stand for 5 min. The samples were analysed microscopically applying a 10 x 10 magnification. The number of oocysts per gram faeces (OPG) was calculated by summing-up the oocyst counts of the two chambers and multiplying the total with the factor 50. The faeces were collected for oocyst isolation when OPG values exceed >1000.

3.2.3 *Oocyst isolation from the faeces*

Materials

1. Sugar solution prepared at the spesific density of 1.3
2. 4 % (w/v) potassium dichromate (Roth) solution

Method

Faeces were meshed, mixed in tap water and filtered gradually using 300, 150 and 80 µm pore-sized filters. Filtered faeces were sedimented in tap water for 2 h. The supernatants were discarded and the pellets were mixed with sugar solution (1.3 specific density). Oocysts/sugar-solutions were adjusted to 1.15 final specific density, placed in plastic backets and covered with glass plates. Surfaces should be covered without any bubbles such that floting oocysts could directly attach to the glass. The glass plate was washed with tap water every two hours and respective suspensions were controlled microscopically for oocyst numbers. Solutions containing less than 5 oocysts per vision field were discarded. The oocysts were centrifuged (400x*g*, 10 min) and mixed 1:1 with 4 % (w/v) potassium dichromate. Solutions were stirred daily to infuse air and to improve the sporulation process. The oocysts were monitored microscopically for sporulation for up to 3 weeks. After sporulation, the oocysts were centrifuged (400x*g*, 10 min), resuspended and kept in potassium dichromate (2 % final concentration) at 4ºC until further use.

3.2.4 *Oocyst excystation*

Materials

1. Excystation medium: 0.4 % (w/v) trypsin (Serva), 8 % bovine bile obtained from the local slaughter house (Giessen, Germany) in HBSS medium (Gibco), sterile filtered using a 0.2 µm syringe filter (Milipore).
2. Incubation medium: 2 mM L-cystein (Serva, 17880.01), 20 mM natrium hydrogencarbonat (Roth).
3. Percoll gradient:

Percoll stock solution: 9 parts Percoll (GE Healthcare, UK, 17-0891-01) and 1 part 1.5 M NaCl.

a. 50 % Percoll solution: 5 parts Percoll stock solution and 5 parts 0.15 M NaCl. The gradient was prepared by centrifugation (15,000 rpm, 20 min).
b. 60 % Percoll solution: 6 parts Percoll stock solution and 4 parts 0.15 M NaCl. The gradient was prepared by centrifugation (15,000 rpm, 20 min).

Method

The oocysts were pelleted (400x*g*, 10 min), mixed with 4 % natrium hypochlorite solution and stirred on ice for 20 min followed by centrifugation (200x*g*, 5 min). The supernatants were collected and diluted 1:1 in distilled water. The suspension was centrifuged (400x*g*, 10 min) and pelleted oocysts were resuspended in a small amount of distilled water. This oocyst suspension was carefully layered on a 60 % percoll gradient followed by centrifugation (400x*g*, 20 min). Oocysts in specific layers of the resulting gradient were carefully aspirated, microscopically checked and layered onto a 50 % percoll gradient followed by centrifugation (400x*g*, 20 min). The oocysts present in the gradient layer were collected and resuspended in a 75 cm^2 flask containing 50 ml excystation medium. Then, CO_2 was infused into the solution for 20 s and the flasks were incubated overnight at 37ºC in 100% CO_2 atmosphere. Then the oocysts were sedimented (400x*g*, 10 min), incubated in sterile excystation medium for 2-3 h and controlled microscopically for sporozoite release. When ≥ 90 % of the sporozoites were excysted, the specimens were washed thrice in sterile PBS (400x*g*, 15 min) and once in modified ECGM. Finally, the sporozoites were counted a Neubauer chamber.

3.2.5 ***E. bovis in vitro infection***

Infection experiments were performed by utilizing at least three different BUVEC isolates to account for biological variation between individuals. As primary cells exhibit a limited life span, BUVEC passaged less than 10 times were used in all experiments. Infections were performed by adding freshly excysted sporozoites to 80-90 % confluent BUVEC monolayers. The infected cells were kept overnight at

37ºC, 5 % CO_2. Extracellular sporozoites were removed 24 h p. i. by medium change. Initial infection rates were calculated by microscopic counting. Therefore, photos were taken randomly at 10 power vision fileds of the infected cell layer using a phase contrast microscope (IX81, Olympus). Infection rates waere calculated by the following formula:

$$\text{Infection rate} = \frac{\text{number of infected cells}}{\text{total number of cells}} \text{ X } 100\ (\%)$$

For cholesterol staining and pulse-labelling BUVEC were grown on coverslips placed in 12-well cell culture plates and infected with $2x10^4$ *E. bovis* sporozoites. For cholesterol quantification, BUVEC in 25 cm^2 flasks were infected with 5 x 10^5 sporozoites. For medium enrichment and inhibition assays, BUVEC grown in 24-well plates were infected with 2 x 10^4 sporozoites. For cholesterol depletion, BUVEC grown in 6-well plates were infected with 10^4 sporozoites. For qPCR analysis, BUVEC cultivated in 25 cm^2 flasks were infected with 5 x 10^5-10^6 sporozoites. For immunoblotting, BUVEC in 175 cm^2 flasks were infected with 6 x 10^6 sporozoites.

3.3 Cholesterol-related assays

3.3.1 Cholesterol staining

Materials

1. Filipin (Sigma-Aldrich, F9765), working solution 0.05 mg/ml in PBS containing 10 % FCS
2. 2 % paraformaldehyde (Sigma-Aldrich, P6148)
3. 1 % glycine (Roth) in 1X PBS
4. Prolong antifading mounting medium without DAPI (Life Technologies, P7481)
5. 1X PBS containing 10 % FCS
6. PBS: 171 mM NaCl, 3.4 mM KCl, 10 mM Na_2HPO_4, 1.9 mM KH2PO4 (all Roth), pH 7.4

Method

In order to visualize free cholesterol in infected host cells and in parasite invasive stages, polyene antibiotic filipin staining was performed (Coppens et al., 2000, Gimpl and Gehrig-Burger, 2007). Therefore, infected BUVEC (1, 8, 14 and 17 days p. i.) grown in coverslips were washed with PBS and invasive stages (sporozoites and merozoites I) were dropped onto poly-$_L$-lysine coated coverslips. Specimens were fixed in 4 % paraformaldehyde (10 min), and washed three times in PBS and were incubated in 1 % glycine PBS (10 min) to quench non-specific signals followed by three washing in PBS. The samples were stained by filipin (2 h, in the dark, at RT) and washed in PBS. Coverslips were then mounted in antifading mounting medium and analyzed using a fluorescence microscope (DMI 4000B, Leica, Heidelberg, Germany) applying the UV filter set (340-380 nm excitation, 430 nm pass filter).

3.3.2 Cholesterol quantification

Materials

1. Amplex-red® cholesterol assay kit (Life Technologies, A12216)
2. Catalase (Sigma-Aldrich, C1345)
3. Cholesterol standard (Sigma-Aldrich, C8667)
4. Hexane isopropanol (3:2, v:v, all Roth)
5. Isopropanol Nonidet P-40 [(NP40), 9:1, v:v, all Roth]

3.3.2.1 Total lipid extraction

Lipid extraction from *E. bo*vis-infected (4, 8 and 17 days p. i) and control BUVEC were performed by extraction in hexane:isopropanol according to Hara and Radin (1978). The cells were washed twice in ice-cold PBS to remove any traces of medium. Then, the cells were trypsinized and total cell numbers were counted using a Neubauer chamber. Afterwards, cell suspensions were washed in PBS and centrifuged (400x*g*, 10 min). The supernatant was discarded and hexane:isopropanol (3:2, v:v) was added to the cells. Homogenization of the cells was performed by utilizing stainless steel beads (Sigma-Aldrich) for 10 min in a

homogenizer. After homogenization, the solution was centrifuged (8,000x*g*, 1 min) and the supernatant was collected. The extraction was repeated once for each sample. The supernatants were then combined and dried manually under gentle liquid nitrogen stream.

3.3.2.2 Total cholesterol quantification

Total lipid extracts were reconstituted in 500 µl solvent isopropanol: NP40 (9:1) (Robinet et al., 2010) followed by sonication in a waterbath (RT, 30 min). Using 96-well black clear-bottom plates (Greiner Bio-One), 5 µl of each sample were treated with catalase [(5 µl of 0.5 mg/ml) in 40 µl of 1x reaction buffer (37ºC, 15 min)] before the enzyme cocktail of the Amplex-red® kit was added. Cholesterol standard (applying a titration of 10, 5, 2.5, 1.25, 0.625, 0.325 and 0 µM) and blanks (solvent only) were included in every experiment. Fifty microliters of enzyme mixture (0.1 M potassium phosphate buffer, pH 7.4; 0.25 M NaCl, 5 mM cholic acid, 0.1 % Triton X-100, 0.3 U/ml cholesterol oxidase, cholesterol esterase, 1.3 U/ml HRP, and 0.4 mM ADHP) were added and incubated (37ºC, 15 min). Resorufin formation was measured by fluorescence intensities (excitation wavelength of 530 nm, emission wavelength of 580 nm) in the Varioskan™ Flash Multimode Reader (Thermo scientific). Total cholesterol of the samples was extrapolated to the values of the cholesterol standard. The total cholesterol content of each sample was normalized to its total cell number counts.

3.3.3 Sterols enrichment

Materials

1. Cholesterol (Sigma-Aldrich, C8667)
2. Desmosterol (Sigma-Aldrich, D6513)
3. Ethanol (Roth)

Method

To estimate effects of sterol enrichment on *E. bovis* first meront development, cholesterol and desmosterol, a cholesterol intermediate precursor, were supplemented in excess to infected BUVEC. Both sterols were solubilized in

ethanol (Xu et al., 2005) and supplied for 30 days of culture. Therefore, infected monolayers were washed. Cholesterol and desmosterol were added in MECGM at 5 µM final concentration. All experiments were performed using 5 different BUVEC isolates. BUVEC supernatants were collected at 20, 23, 26 and 29 days p. i. At the end of the culture period (30 days) merozoites I were collected together with the trypsinized cells. Cell supernatants were centrifuged (400x*g*, 15 min) and pelleted merozoites I were processed for *E. bovis* microneme protein 4 (Ebmic4)-specific qPCR (see **3.7.2**) for quantification. In addition, macromeront growth in treated and non-treated infected BUVEC were also monitored. The size of meronts was estimated microscopically using an inverted IX81 microscope (Olympus) equipped with a software for size measurements (cellSens 1.7, Olympus).

3.3.4 Cholesterol pulse-labelling

Materials

1. Endothelial cell basal medium without supplement (Promocell, C-22110)
2. Fluorescent cholesterols: dansyl and rhodamine cholesterol/cholestanol (kindly supplied by Prof. Dr. Gerald Gimpl, University of Mainz, Germany)
3. Medium 199
4. Methyl-β-cyclodextrin (MBCD, Sigma-Aldrich, C4555)
5. Prolong antifading mounting medium without DAPI (Life Technologies, P7481)

Method

To visualize sterol incorporation into *E. bovis* macromeronts, dansyl cholesterol (Wiegand et al., 2003), was delivered to the cell culture via MBCD complexes, consisting of mixture of cholesterol and MBCD molar ratio 1:10 (Christian et al., 1997). At 17 days p. i, dansyl cholesterol (3.8 µM final concentration) was added to the culture (1 h, 37ºC, 5 % CO_2) and washed-off twice with PBS. Coverslips were mounted in antifading mounting medium and the samples were analyzed applying a DAPI filter setting in a fluorescence microscope (Olympus IX81). To

analyze the ability *E. bovis* sporozoites ability to incorporate cholesterol, sporozoites were pulse-labelled with dansyl cholesterol. The method was adapted from *T. gondii* tachyzoite pulse-labelling described by Sehgal et al. (2005). Briefly, freshly excysted sporozoites were incubated in the basal medium containing dansyl cholesterol-MBCD-complexes as described above (1 h, 37ºC, 5 % CO_2), washed twice with PBS and pelleted by centrifugation (600x*g*, 15 min) to remove free dansyl-cholesterol-complexes. The sporozoites were resuspended in PBS and dropped onto poly-$_L$-lysin coated glass coverslips. The samples were mounted in antifading mounting medium and analyzed applying a DAPI filter setting in a fluorescence microscope. Additionally, endothelial cells were pulse-labelled with rhodamine cholesterol-MBCD complexes (1:10, 1 h, 37ºC), washed with basal medium and infected with sporozoites. Infected BUVEC were incubated (1 h, 37ºC, 5 % CO_2) and analyzed applying a TRITC setting filter in a fluorescence microscope (Olympus IX81).

3.3.5 Cholesterol depletion prior to infection

Materials

1. Methyl-β-cyclodextrin (MBCD)
2. Modified endothelial cell growth medium (PromoCell C22010 and Sigma-Aldrich M0393)

Method

To assess the role of cholesterol in the early phase of *E. bovis* infection, BUVEC and sporozoites both were depleted of cholesterol according to Christian et al., (1997). Infection with non-depleted sporozoites and BUVEC infection therewith served as negative controls. For host cell depletion, BUVEC were incubated in 10 mM MBCD (30 min), infected with 10^5 freshly excysted sporozoites and washed in plain MECGM. For sporozoites depletion sporozoites were incubated with 10 mM MBCD (30 min), washed in plain MECGM and used for infection. All treatments were performed in 6-well plates by using 5 different BUVEC isolates in 2 independent experiments. The medium was removed from treated BUVEC

layers 24 h after treatments to remove any remaining free sporozoites. The infection rates (see **3.2.5**) were estimated in 10 randomly chosen power vision fields.

3.4 Lipid droplet-related assays

3.4.1 Lipid droplet staining

3.4.1.1 Nile red staining

Materials

1. 4 % paraformaldehyde
2. Nile red in DMSO (Cayman Chemical, USA, CAYM600055), working solution diluted 1:1000 according to manufacturer's intructions

Method

Nile red is a LD- and neutral lipid-specific dye (Brown et al., 1988, Greenspan et al., 1985). Free parasite stages and infected/non-infected BUVEC were washed in PBS and fixed in 4 % paraformaldehyde (RT, 10 min). Thereafter, cells were washed twice in PBS and stained in Nile Red (15 min, RT, in the dark). After staining, samples were washed thrice in PBS and mounted in PBS prior to fluorescence microscopy (FITC filter, Olympus IX81). Images were processed using the cellSens 1.7.

3.4.1.2 Bodipy 493/503 staining

Materials

1. 4 % paraformaldehyde
2. Bodipy 493/503 (Life Technologies, D3922), working solution 1 µg/ml
3. Prolong antifading mounting medium supplemented with DAPI (Life Technologies, P36941

Method

Bodipy 493/503 is a sensitive LD-specific dye (Gocze and Freeman, 1994). After fixation in 4 % paraformaldehyde, the cells were stained with bodipy 493/503 (10

min, RT, in the dark), washed three times in PBS and mounted in PBS prior to microscopy by applying FITC filter. Images were processed using the cellSens 1.7 software. For confocal microscopic analyses, the cells were processed as follows: After bodipy 493/503 staining, samples were washed thrice in PBS and mounted in antifading medium supplemented with DAPI prior to microscopy. Images were acquired using a Leica confocal microscope (TCS SP2, Heidelberg, Germany) equipped with a krypton/argon laser. Images were processed with Adobe Photoshop CS3 (Adobe). Bodipy 493/503 staining signals were acquisited at excitation/emmission of 500/510 nm. UV light was applied for DAPI staining.

3.4.1.3 Osmium tetroxide staining

Materials

1. Fixative: 2 % paraformaldehyde containing 0.1 % glutaraldehyde (EM grade Sigma-Aldrich, G7526)
4. Osmium tetroxide (Sigma-Aldrich, 201030), working solution: 0.1 %

Method

For an alternative LD staining, osmium tetroxide was used according to Melo et al. (2011). Therefore, cells were washed four times in PBS, fixed with fixative (RT, 30 min) and osmium tetroxide-stained (RT, 30 min). The samples were washed thrice in PBS, mounted in PBS and analyzed in brightfield conditions (Olympus IX81).

3.4.2 Lipid droplet quantification

3.4.2.1 Flow cytometry analysis

Materials

1. Bodipy 493/503, working solution: 1 µg/ml
2. Paraformaldehyde 4 %
3. Trypsin buffer (for preparation see **3.1.2**)

Method

To measure the relative abundance of lipid droplets in control and *E. bovis*-infected endothelial cells, relative fluorescence intensities induced by bodipy 493/503 staining were determined by fluorescence activated cell sorting (FACS). This method was described elsewhere in a different system (Gimm et al., 2010) and adapted to endothelial cells. BUVEC were trypsinized at days 8, 17 and 21 p. i. and pelleted in PBS (400x*g*, 3 min, 4ºC). The resuspended cells were stained with bodipy 493/503 (10 min, on ice) and washed twice in 1 ml PBS followed by centrifugation (400x*g*, 3 min, 4ºC). The cells were resuspended in 100 µl PBS and transferred to 5-ml FACS tubes containing 200 µl of PBS. The cells were processed in a FACSCalibur™ flow cytometer (Becton-Dickinson [BD], Heidelberg, Germany) by laser excitation at 488 nm (FL2-H channel). Fluorescence intensities were acquired by the Cell Quest Pro software (BD).

3.4.2.2 Semiquantitative assay of lipid accumulation

Intracellular lipid droplet increment in single cells was reportedly quantified by automatic image analysis (McDonough et al., 2009). This method was modified in this experiment by utilizing the software ImageJ (NIH, USA, http://imagej.nih.gov/ij/download.html) with quantification procedures being adapted from different systems (Burgess et al., 2010; Gavet and Pines, 2010) to compare the relative fluorescence intensity signals obtained from *E. bovis*-infected cells with those of non-infected ones. The terms of area (in pixel), integrated intensity and mean fluorescence values were obtained from the "set measurements" mode of the "analyze menu" in the software. The total fluorescence intensity of the cells was normalized to background intensities and termed as corrected total cell fluorescence (CTCF) intensity. The CTCF intensity was calculated by following formula:

CTCF = integrated intensity – (area of selected cell x mean fluorescence of background readings).

Infected BUVEC from inhibitor treated and non-treated groups (see **3.6.2**) were grown on coverslips. The samples were stained with bodipy 493/503 (see **3.4.1.2**) at 2, 6, 10, 14 and 18 days p. i. Cells were analyzed via fluorescence microscopy applying FITC settings. Lipid droplets were identified as bright green dots. Images were acquired by cellSens 1.7 software in TIFF format followed by ImageJ processing. The cell fluorescence intensities were estimated from different single cells (n=10) of each experimental condition.

3.4.2.3 Oleic acid enrichment

Materials

1. Bovine serum albumin (BSA) fraction V (Roth, 8076.1)
2. Modified endothelial cells growth medium
3. Oleic acid (Sigma-Aldrich, O1008)

Method

To enhance lipid droplet generation in host cells, oleic acid was supplemented in BSA formulation complexes (Martin and Parton, 2011). Direct conjugation was performed by mixing oleic acid-free BSA with oleic acid at the molar ratio of 6:1 (oleic acid: BSA). To control for oleic acid cytotoxicity for BUVEC, MTT assays (see **3.6.1**) were performed in preliminary experiments. Therefore, oleic acid was applied at different concentrations covering 200 µM to 2.5 µM. According to these preliminary assays, the following experimental conditions were chosen: BUVEC were treated with 5 µM oleic acid/BSA complexes for an induction period 1 h, then the concentration was lowered to 2.5 µM to prevent lipotoxicity. These treatments were repeated every two days from 8 days p. i onwards. The experiments were performed in 12-well plates using 3 different BUVEC isolates. The effects of oleic acid enrichment on merozoite I production were assessed by Ebmic4-specific qPCR (see **3.7.2**).

3.5 Low density lipoprotein-related assays

3.5.1 Quantification of surface LDL receptor expression

Materials

1. Accutase (Sigma-Aldrich, A6964)
2. Mouse anti-human LDLR primary antibody (Antibody online, USA, ABIN235770). This antibody coss-reacts with the bovine receptor.
3. Goat anti-mouse IgG2b isotype-phycoerythrin (PE) secondary antibody (Southern Biotech, USA, 1090-09)
4. Washing solution: PBS containing 0.01 % NaN_3 (Sigma-Aldrich, S8032)
5. Lipoprotein-deficient serum (Sigma-Aldrich, S5394)
6. Endothelial cell basal medium

Method

The surface expression of the LDL-receptor (LDLR) was estimated in infected and non-infected BUVEC applying a flow cytometry technique. BUVEC grown in 25 cm^2 flasks were infected using 7.5 x 10^5 sporozoites per flask. The cells were cultured in lipoprotein-deficient serum (36-48 h, 37ºC, 5 % CO_2). Prior to LDLR measurements the medium was removed and cells were detached using accutase treatment (37ºC, 5 min). The cells were centrifuged (400x*g*, 5 min, 4ºC) and the supernatants were discarded. The samples were resuspended in washing solution transferred to V-shaped 96-microtiter plates (Greiner Bio-One) and pelleted (400x*g*, 5 min, 4ºC). The supernatants were discarded and the cells were reacted with monoclonal antibodies against LDLR (1:25, 50 µl/well, RT, 1 h). After centrifugation (400x*g*, 5 min, 4ºC), pelleted cells were washed (400x*g*, 5 min, 4ºC) and incubated in 50 µl of secondary antibodies (diluted 1:50, 5 µg/ml, 30 min, in the dark). Secondary antibody controls were included for each experiment for signal normalization. After incubation, cells were washed (400x*g*, 5 min, 4ºC), resuspended in 100 µl PBS, transferred to 5 ml-FACS tubes (Greiner Bio-One) containing 200 µl of 1x PBS and processed by FACSCalibur™ flow cytometer (Becton-Dickinson, Heidelberg, Germany) in the FL1-H channel (red) using the software Cell Quest Pro (Becton-Dickinson).

3.5.2 Low density lipoprotein (LDL) binding assay

Materials

1. 3 % NaN_3
2. 4 % paraformaldehyde
3. Bodipy-labeled LDL (Life Technologies, L-3483)
4. Bodipy-labeled acetylated LDL (Life Technologies, L-3485)
5. Endothelial cells basal medium
6. Lipoprotein-deficient serum (Sigma-Aldrich, S5394)
7. Prolong antifading mounting medium without DAPI

Method

The binding of non-modified LDL and acetylated-LDL to receptors on the surface of infected cells and non-infected controls was estimated qualitatively using bodipy-labelled molecules. Therefore, BUVEC were grown on coverslips and infected with 2 x 10^4 *E. bovis* sporozoites. At 17 days p. i., cell layers were incubated in endothelial cell basal medium devoid of FCS and supplemented with 10 % lipoprotein deficient-serum for 36-48 h before being further processed. Then bodipy-labelled LDLs (both 10 µg/ml) were added to the medium and cells were incubated at 4ºC for 1 h followed by 4 h of incubation at 37ºC. Then, the cells were washed in PBS to remove unbound labelled LDLs. Samples were fixed in 4 % paraformaldehyde (10 min) and washed with PBS. Coverslips were mounted in antifading medium prior to fluorescence microscopy. To compare the relative binding and uptake activities between control and infected cell populations, BUVEC were treated with 3 % NaN_3 (5 min, RT) to inhibit receptor recycling and washed with ice-cold PBS. Monolayers were detached by accutase treatment (5 min, 37ºC), washed in PBS (400x*g*, 5 min) and kept on ice. Cells were then processed via flow cytometry (see **3.4.2.1**).

3.5.3 Low density lipoprotein (LDL) enrichment

LDL was supplemented (10 mg/ml final concentration) to BUVEC (n=5) cultures. This method was adapted from Coppens et al. (2000). Therefore, infected BUVEC (see **3.2.5**) were washed with MECGM to remove free sporozoites. LDL was

supplemented from 10 days p. i. onwards. Cell supernatants containing released merozoites I were collected at 20, 23, 26 and 29 days p. i. At the end of culture period (30 days p. i.) merozoites I were collected together with trypsinized cells. BUVEC supernatants were centrifuged (400x*g*, 15 min) and merozoites I were processed for Ebmic4 qPCR (see **3.7.2**). Besides merozoite I production, macromeront growth was also monitored from 10 days p. i. onwards (see **3.6.2**).

3.6 Inhibition assays

Materials

1. Inhibitors:
   a. C75 (C5490, Sigma-Aldrich) was dissolved in DMSO (Sigma-Aldrich, D8418) as stock solution and titrated 1: 2 covering 200 µM to 6.25 µM concentrations
   b. CI976 (C3743, Sigma-Aldrich) was dissolved in DMSO as stock solution and titrated 1: 2 covering 200 µM to 6.25 µM concentrations
   c. Lovastatin (L0790000, Sigma-Aldrich) was dissolved in aceton (Roth) as stock solution and titrated 1: 2 covering 200 µM to 1.58 µM concentrations
   d. Zaragozic acid (Z2626, Sigma-Aldrich) was dissolved in ethanol (Roth) as stock solution and titrated 1: 2 covering 200 µM to 6.25 µM concentrations
2. Isopropanol containing 0.04 N HCl (all Roth)
3. 3-(4,5-dimethylthiazol-2-yl)-2,5-diphenyltetrazolium bromide [(MTT), Sigma-Aldrich, M2128]

3.6.1 Toxicity assay

For toxicity assays, BUVEC were trypsinized, counted and 5 x 10^3-10^4 cells were seeded in each well of a 96-well plate. Cells were cultured in 200 µl MECGM to confluency. The inhibitors (C75, CI976, lovastatin, zaragozic acid) were substituted at indicated concentrations. Cytotoxic effects of the compounds on endothelial cell were measured by three parameters: active metabolism, alteration of the cell morphology and cell numbers. Cell metabolism was analyzed by MTT assays which estimates mitochondrial activities (van Meerloo et al., 2011,

Sylvester, 2011). MTT assays were performed 24 and 96 hours post inhibitors application. Therefore, 20 µl of 5 mg/ml MTT working solution were added to medium in each well. Plates were incubated (4 h, 37ºC, 5 % CO_2), the supernatants were removed, and 150 µl acidic isopropanol were added. After incubation (30 min, 37ºC, 5 % CO_2), formazan production was analyzed at 590 nm using a Varioskan™ Flash Multimode fluorometer. Each sample was processed as 5-fold preparation. The percentage of viable cells was calculated relative to control cells using the following formula:

$$\frac{\text{(test sample absorbance-background absorbance)}}{\text{(control absorbance-background absorbance)}} \text{ x 100 \%}$$

The alteration of the cell morphology was assessed microscopically considering intracellular vacuolization and cell death. Cell proliferation at 7, 10, 13, 16 and 19 days post inhibitor application was measured by direct counting of trypsinized cells in a neubauer chamber. The concentration of each compound that did not affect cell proliferation for more than 5 days was chosen for inhibition assay.

3.6.2 Inhibition of E. bovis proliferation in vitro

Infected BUVEC monolayers (see **3.2.5**) were washed to remove free sporozoites. Compounds were added at the following doses: lovastatin: 1, 0.5, 0.1, 0.05, 0.01 and 0.005 µM; zaragozic acid, CI976 and C75: 5, 2.5, 0.5, 0.25, 0.05 and 0.025 µM. Each dose was tested in 5 BUVEC isolates. BUVEC treatments were performed up to 30 days p. i. Initial infection rates of treated and non-treated cells were estimated microscopically in 10 randomly chosen areas at 2, 6, 10, 14, 18, 22, 26 and 30 days p. i. To estimate the numbers of merozoites I being produced in treated and non-treated BUVEC cultures, supernatants were collected at 20, 23, 26, 29 days p. i. and at the end of culture period (30 days p. i.), merozoites I were collected together with trypsinized cells. Cell culture supernatants were pelleted (400x*g*, 15 min) and processed for Ebmic4 qPCR (see **3.7.2**). To determine the median inhibition effects of the compounds, a non-linear regression was

performed using GraphPad Prism 6.02 to generate a calculated sigmoidal model of dose-response curves based on four parameter fit according to Motulsky and Christopoulos (2003). The relative inhibition was calculated as a response of treatment as follows: (mean value of control-value of test sample)/(mean value of control) and was represented as percentage relative to controls (Ehrenman et al., 2013, Labaied et al., 2011).

3.7 Quantitative real-time polymerase chain reaction (qPCR)

3.7.1 Gene transcription of cholesterol metabolism-related molecules

3.7.1.1 Target genes, primers and probes design

Primers and probes were designed targeting several host cell genes being involved in cholesterol metabolism. Overall, only coding sequences were used for the design of qPCR systems. To ensure exon-intron mapping of the amplicon, assembly analyses using the Ensembl (http://www.ensembl.org/) web page were employed to avoid false positive results due to undigested genomic DNA. Splice variants were also taken into account before choosing the best target sequence combination to be entered into the software designer for each assay (Bustin et al., 2009). Primers and probes were designed using Beacon Designer 7 software (Premier Biosoft) in combination with the Primer3 NCBI software (http://www.ncbi.nlm.nih.gov/tools/primer-blast/) considering melting temperature, self complementarity, heterodimer formation, hairpin formation, primer dimers and alternate splicing. *In silico*-primers, probes and amplification products were controlled for *Bos taurus* identity by BLAST (Altschul et al., 1990, at www.ncbi.nlm.nih.gov/BLAST/) and for homology to the closest species of the *Eimeriidae* genus, *Eimeria tenella,* to confirm the host transcription target, the correct sequence and to avoid false-positive pathogen-derived mRNA amplification. The designed primers and probes, due to their short nucleotide length, were accepted when exhibiting in less than 70 % similarity compared to *Eimeriidae*. According to Taubert et al (2006a,b), GAPDH was used as housekeeping gene. The sequences of primers and probes used for the experiments are listed in Table **3.1**.

Table 3.1. Sequences of primers and probes

Symbol	Name	Accession number	Amplicon length	Forward (5'→3')	Reverse (5'→3')	Probe (reporter 5'-3' quencher)
ACAT1	Acetyl-CoA acetyltransferase 1	NM_001046075.1	102	TCATATGGGCAACTGTGCTGA	CTGCTTTACTTCTGGTATAG	FAM-AGCATAAGTATCCTGTTCCTCTCGTG-BHQ1
ACAT2	Acetyl-CoA acetyltransferase 2	NM_001075549.1	194	AGCAGTGGTTCTTATGAA	AGGCTTCATTGATTTCAAA	FAM-ATCAACATCCTCCAGCGACCA-BHQ1
HMGCS1	3-hydroxy-3-methylglutaryl-CoA synthase 1	NM_001206578	197	CTACCTCAGTGCATTAGA	CTCTGTTCTGGTCATTAAG	HEX-AAGTCATTCAGCAACATCCGAGC-BHQ1
HMGCR	3-hydroxy-3-methylglutaryl-CoA reductase	NM_001105613.1	109	GCCATCAACTGGATAGAG	CCTCAATCATAGCCTCTG	FAM-TCTCTGACAACCTTGGCTGGAAT-BHQ1
SQLE	Squalene epoxidase	NM_001098061.1	132	CCCTTCTTCACCAGTAAA	CCCTTCAGCAATTTTCTC	HEX-AACAACAGTCATTCCTCCACCAGTA-BHQ1
OLR1	Oxidized low density lipoprotein/ (lectin-like) receptor 1	NM_174132.2	102	CGCCTACCTCTTCTTTAC	ACCACGTTCTTAAGGTTG	TET-TCGCTTCGGTCCAGAGTCATC-BHQ1
LDLR	Low density lipoprotein receptor	NM_001166530.1	96	CGCCTACCTCTTCTTTAC	ACCACGTTCTTAAGGTTG	FAM-TCGCTTCGGTCCAGAGTCATC-BHQ1
CH25H	Cholesterol 25-hydroxylase	NM_001075243.1	87	TTGGGTGTCTTTGACATG	CAGCCAGATGTTGACAAC	FAM-CGTCTTGCTGCTCCAGTGTC-BHQ1
SOAT1	Sterol-O-acyltransferase 1	NM_001034206.2	99	GCCCTCCTCATTCTCTTC	CCCAAAAGCATAAGACATGAG	FAM-AGCACCAGCCTTCCTTCATCA-BHQ1
GAPDH	Glyceraldehyde-3-phosphate dehydrogenase (Leutenegger et al., 2000)	AF022183	82	GCGACACTCACTCTTCTACCTTCGA	TCGTACCAGGAAATGAGCTTGAC	FAM-CTGGCATTGCCCTCAACGACCACTT–BHQ1

3.7.1.2 Generation of qPCR standards

Materials

1. 10X PerfeCTa qPCR FastMix (Quanta, MD, 733-2108)
2. 50 bp Generuler DNA molecular weight marker (Thermo Scientific, SM0373)
3. 6X gel loading buffer (Thermo Scientific, R0611)
4. Agarose (Roth, 3810.4) gel (1 % and 2 %)
5. Ethidium bromide (Etbr, Sigma-Aldrich, E7637), 5 µl in 100 ml TAE-buffer
6. Bam*HI* restriction enzyme (R0136S) and NEB buffer 3 [(B7003S), all New England Biolabs]
7. Colony PCR mixture: 25 µl total volume PCR reaction containing 2.5 µl of 10X PCR buffer (PeqLab), 2.5 µl $MgCl_2$ (25 mM), 0.5 µl dNTPs (10 mM peqGOLD dNTP-Set), 0.5 µl Taq polymerase (5 U FIREpol DNA Polymerase, Solis BioDyne), 1 µl of each primer [10 µM, SP6 (5'CATTTAGGTGACACTATAG3') and T7 (5'GTAATACGACTCACTATAG3')] and 17 µl dH_2O
8. Competent cells: NEB 10-β (New England Biolabs, C3020K)
9. Luria Bertani [(LB), Roth, X968.1] agar plates: LB-medium containing ampicillin (100 µg/ml), Xgal (40 ug/ml) and IPTG (0.1 mM)
10. pDrive-vector cloning kit (Qiagen, 231122)
11. peqGOLD gel extraction kit (PeqLab, 12-2501-02)
12. PeqGold plasmid miniprep kit (Peqlab, 12-6942-02)
13. TAE: 4.84 g Tris HCl (Roth) and 1.142 EDTA (Roth) adjusted to 1 L of ddH_2O, pH 8.0

Method

To verify whether the correct parts of the targeted genes showing correct length were amplified, control PCRs were performed using cDNA generated from uninfected BUVEC (see **3.7.1.6**). The qPCR conditions were as follows: hold at 95ºC for 10 min; 40 cycles at 95ºC for 10 s, 60ºC for 15 s and 72ºC for 30 s. Each sample was controlled for the molecular size via gel electrophoresis. Therefore, 10

µl of qPCR samples were mixed with 1-2 µl of 6X gel loading buffer and electrophoresed along with a 50 bp DNA molecular weight marker in a 2 % agarose gel at constant current (80 Volt, 30-45 min) in TAE buffer. The gel was stained with EtBr for 15 min and washed in dH_2O. The amplified product was visualized via UV light and illustrated by a documentation system (Intas, Goettingen, Germany). PCR products of the correct size were purified from the agarose gel using a gel extraction kit. Briefly, each DNA fragment of interest was excised from the gel. The gel piece was weighed and an equal volume of binding buffer was added. The mixture was incubated at 55ºC until the gel was completely solubilized. The solution was transferred to a DNA-binding column and centrifuged (10,000x*g*, 1 min). The flow-through was discarded and the column was washed with 750 µl washing buffer I and washing buffer II. Then 50 µl of elution buffer were added and the samples were centrifuged (10,000x*g*, 1 min). The flow-through containing the purified DNA was collected and used for cloning. Therefore, 5 µl of purified DNA were added to 5 µl of 2x ligation buffer and 1µl pDrive-vector. The mixture was incubated at 18ºC for 2-3 h and 10 µl thereof were added to 100 µl competent cells and incubated (30 min, on ice). The samples were heat-shocked for 2 min at 42ºC and immediately cooled on ice for at least 3 min. Then 600 µl of LB-medium devoid of ampicillin were added followed by incubation (37ºC, 45 min). The sample was centrifuged (1000x*g*, 3 min) and the pellet was cultivated in LB-plates containing Xgal and IPTG (overnight, 37ºC). Thereafter, positive individual bacteria colonies were selected and screened by conventional colony PCR. Briefly, a small amount of an individual colony was taken and mixed with 25 µl of PCR master mix. Cycling conditions of PCR was 5 min at 95^0C, 35 cycles of 30 s at 95ºC, 45 s at 47ºC, 45 s at 72ºC, and a final elongation step for 5 min at 72ºC. PCR-positive colonies containing plasmids carrying target genes were transferred to 5 ml of LB-medium and cultivated (overnight, 37ºC, under constant shaking). Plasmid-DNA extraction from overnight cultures was performed by using the peqGOLD plasmid miniprep kit according to the manufacturer's protocol. Briefly, overnight bacterial cultures were pelleted by centrifugation (10,000x*g*, 1 min). Then, 500 µl of solution

I/RNAse A were added per 5 ml culture pellet and cells were resuspended by gentle vortexing. 500 µl solution II and 750 µl of solution III were added and sample was centrifuged (10,000x*g*, 1 min). The supernatant was transferred to a DNA collumn and centrifuged (10,000x*g*, 1 min). The column was washed once with 500 µl washing buffer I and twice with 750 µl washing buffer II (10,000x*g*, 1 min). The plasmid-DNA was eluted with 50 µl of elution buffer (5,000x*g*, 5 min). The plasmid-DNA was stored at -20ºC until further use. The plasmids containing sequences of interest were linearized according to the enzyme manufacturer's instruction. To confirm plasmid digestion sites, CLC Sequence Viewer 5 (CLC bio, Qiagen) was utilized to draw a plasmid map. Since all systems designed showed similar maps, Bam*HI* was chosen for the linearization of all systems. The digestion solution contained 1 µg of isolated plasmid, 10 U restriction enzyme Bam*HI*, 10 µl of NEB buffer 3 and dH_2O adjusted to 50 µl total reaction volume. The solution was incubated (at 37ºC, 2 h). Succesful digestion was controlled by a 1 % agarose gel electrophoresis. All plasmids were sequenced employing SP6 and T7 primers flanking the multiple cloning site of pDrive vector to confirm the correct target gene sequence. Sequencing was performed by GATC Biotech AG (Germany). The identity of each amplicon was confirmed using ClustalW (http://www.ebi.ac.uk/Tools/msa/clustalw2/).

3.7.1.3 Analysis of qPCR efficiencies

Linearized plasmids containing target sequences were used to estimate amplification efficiencies of the PCR systems. A 100 % efficiency is defined as the doubling quantity of an amplicon during a PCR reaction's geometric phase (Pfaffl, 2001). The slopes of the standard curves generated by plasmid DNAs were used to estimate PCR efficiency of each system. To obtain these standard curves, amplification reactions covering 5 magnitude orders of 10 fold plasmid-DNA titrations were performed each in technical triplicates. The respective were slope-corrected utilizing the "slope correct" and "dynamic tab" options of the Rotor-Gene Q software (Rotor-Gene® Q User Manual, Qiagen). These steps reduced background fluorescences and technical replicates errors. The threshold

was manually defined and positioned within the linear logarithmic amplification phase of each target system. The formula used for efficiency correction was:

$$E= 10^{(-1/slope)} -1$$

Efficiency values are ideally taken into account for real-time PCR analysis (Pfaffl, 2001). Only if housekeeper efficiencies are above 90 % and are not significantly different to the amplification efficiencies of target genes the calculation may be performed using delta-delta-Ct methods (Livak and Schmittgen, 2001) since this method does not account for efficiency values corrections.

3.7.1.4 RNA preparation and cDNA synthesis

Materials

1. DNase I (Thermo scientific, EN0525)
2. On-column DNAse I digestion kit (Qiagen, 79254)
3. RNeasy isolation kit (Qiagen, 74104)
4. SuperScript® III First-Strand Synthesis System for RT-PCR (Life Technologies, 18080-051)
5. β-mercapthoethanol [(2-ME), Serva, 28625.01)]

3.7.1.5 Total RNA isolation and DNA digestion

Total RNA isolation was performed using the RNeasy kit according to manufacturer's protocol. Briefly, control and infected monolayers were lysed within the cell culture flasks by applying RLT lysis buffer (600 µl/25 cm^2 flask). After this step, lysed cells may either be stored at -80ºC or directly processed for total RNA isolation. For total RNA isolation, 600 µl of 70 % ethanol were added to the suspension, resuspended and transferred to the collumn. The samples were centrifuged (13,000x*g*, 1 min) and flow-throughs were discarded. Then the samples were washed with 500 µl buffer RW1 (13,000x*g*, 1 min). DNase solution (10 µl DNase I+70 µl buffer RDD of on-column DNase digestion kit) was added to the collumn and incubated (RT, 15 min). The samples were washed twice with 500 µl buffer RPE (13,000x*g*, 1 min). Total RNA elution was performed by adding 30-50 µl of DEPC-treated water to the collumn followed by centrifugation

(13,000x*g*, 1 min). Total RNAs were stored at -20ºC until further use. Examplary total RNA samples were controlled for their quality using Agilent bioanalyzer 2100 (Agilent Technologies, USA). Here, RNA integrity values (RIN numbers) of 8.5 were obtained for almost all samples. RNA concentrations were measured spectrophotometrically in terms of optical densities (OD) 260 nm and 280 nm. In order to guarantee absolute genomic DNA digestion, a second genomic DNA digestion step was performed. Therefore, 1 µg of total RNA was treated with 10 U DNase I in 1X DNAse reaction buffer (37ºC, 1 h). DNase was inactivated by heating the sample (65ºC, 10 min). The efficiency of genomic DNA digestion was controlled by including RT^--controls in each real-time PCR experiment.

3.7.1.6 cDNA synthesis

cDNA synthesis was performed using the SuperScript® III First-Strand Synthesis System according to manufacturer's protocol with slight modifications. For first-strand cDNA synthesis, the following constituents were mixed: 1 µg of DNAse-treated total RNA, 1 µl of 50 µM oligo d(T), 1 µl of 50 ng/µl hexamer primer, 1 µl of 10 mM dNTP mix and DEPC-treated water was adjusted to 10 µl total volume. The sample was incubated at 65ºC for 5 min and then immediately cooled on ice. For the second strand synthesis the following ingredient were added: 2 µl of 10x RT buffer, 1 µl 25 mM $MgCl_2$, 1 µl 0.1 M DTT, 1 µl RNaseOUT (40 U/µl) and 1 µl SuperScript III enzyme (200 U/µl). The sample was incubated at 50ºC for 60 min followed by a 85ºC-incubation for 15 min. Thereafter, the sample was treated with RNase H (40 U/sample, 37ºC, 20 min). Finally, nuclease-free dH_2O was adjusted to 200 µl total volume yielding a final concentration of 5 ng/µl cDNA.

3.7.1.7 Quantitative real-time polymerase chain reaction (qPCR) assay

Materials

1. Primers and probes as listed in Table **3.1.** (all were purchased from Biomers AG, Germany)
2. PerfeCta qPCR FastMix

Method

Real-time qPCR was performed in a 10 µl total volume containing 400 nM forward and reverse primers, 200 nM TaqMan probe, 10 ng cDNA and 5 µl PCR master mix. The reaction conditions for all systems were as follows: hold at 95ºC for 10 min, 40 cycles at 95ºC for 10 s, 60ºC for 15 s and 72ºC for 30 s. PCRs were performed utilizing an automated real-time PCR fluorometer (Rotor-Gene® Q, Qiagen, Hilden, Germany). Non-template controls (NTC) and RT^- reactions were included in each experiment. Cycle threshold (Ct) values of 40 were considered as non-significant amplification.

3.7.1.8 Data analysis

The qPCR data analysis was based on the ΔΔCt method and data were normalized to GAPDH results as housekeeping gene (Livak and Schmittgen, 2001, Schmittgen and Livak, 2008). Therefore, the following equation used was as follows:

$$\text{Fold change expression compared to control} = 2^{-\Delta\Delta Ct}$$

with:

$\Delta Ct\ control_{(control\ samples)} = Ct\ control_{housekeeping\ gene} - Ct\ control_{target\ gene}$

$\Delta Ct\ treated_{(test\ samples)} = Ct\ treated_{housekeeping\ gene} - Ct\ treated_{target\ gene}$

$\Delta\Delta Ct = \Delta Ct\ control_{(control\ samples)} - \Delta Ct\ treated_{(test\ samples)}$

3.7.2 qPCR-based E. bovis merozoite I quantification

Materials

1. 10X PCR buffer (PeqLab, 01-1000), diluted 1:10 in dH_2O
2. 10X PerfeCTa qPCR FastMix
3. Lysis buffer containing 0.32 M Sucrose, 1 % Triton X-100, 0.01 M Tris-Cl (pH 7.5) and 5 mM $MgCl_2$ (all Roth)
4. Proteinase K (Qiagen, 158920)

Method

To circumvent laborious manual *E. bovis* merozoite I counting, a quantitative real-time PCR for merozoite I quantification based on the single copy gene of *E. bovis* microneme protein 4 (Ebmic4, Lutz, 2008). The following primers and probes were designed using Beacon Designer 7 software (Premier Biosoft): forward primer was 5'CACAGAAAGCAAAAGACA3', reverse primer 5'GACCATTCTCCAAATTCC3', and probe 5'FAM-CGCAGTCAGTCTTCTCCTTCC-BHQ13'. For real-time PCRs, the following constituents were used: 5 µl DNA of merozoites I samples, 0.8 µl (400 nM final concentration) of each primer, 0.4 µl of probe (200 nM final concentration) and 10 µl PerFecta MasterMix in 20 µl total reaction volume. The PCR conditions were as follows: hold at 95ºC for 10 min; 40 cycles at 95ºC for 10 s, 60ºC for 15 s and 72ºC for 30 s. For PCR efficiency analyses, a plasmid containing Ebmic4-amplicon sequence was generated analogous to section **3.7.1.3**. Ebmic4 specific-efficiency of the qPCR was also estimated using *E. bovis* merozoite I DNA as template by following procedure: Supernatants containing freshly released merozoites I from infected monolayers were collected. Merozoites I were pelleted by centrifugation (600x*g*, 15 min) and counted in a Neubauer chamber. Serial dilutions of merozoites I were performed covering 6 magnitude orders of 10-fold (10^6-10). DNA was isolated by adding 200 µl of lysis buffer to each merozoite I pellet. Then, 100 µl 1X PCR buffer and 20 µl proteinase-K (20 mg/ml) were added and incubated (56ºC, 1 h). Proteinase K was heat-inactivated (95ºC, 10 min) and the samples were frozen at 20ºC until further use. All samples were processed as triplicates.

3.8 Immunoblotting

Materials

1. Acrylamide gel:
   a. **10 %**: 3.3 ml Rotiphore gel 30 % (Roth, 3037.2), 2.5 ml Tris 1.5 M pH 8.8, 50 µl SDS 20 % (all Roth), 4.1 ml dH_20, 5 µl TEMED (Bio-Rad, 161-0801), 70 µl 10 % APS (Sigma-Aldrich, A3678)

b. **4.5 %**: 0.75 ml Rotiphore gel 30 %, 1.25 ml Tris 0.5 M pH 6.8, 25 µl SDS 20 %, 2.95 ml dH_20, 5 µl TEMED, 25 µl 10 % APS

2. 10X Ponceau red: 2 g Ponceau S (Serva, 33429.01), 30 g trichloroacetic acid (Roth), 30 g sulfosalicylic acid (Roth)
3. 10X Tris buffer saline: 60.57 g Tris, 85 g NaCl, pH 7.4 (all Roth)
4. 5X SDS sample buffer: 10 % SDS, 12.5 % 2-mercaptoethanol (Serva, 28625.01), 25 % glycerol (Merck, Darmstadt), 25 mg bromphenolblue (Merck, Darmstadt), 150 mM Tris-HCL, pH 6.8 (unless stated, all Roth)
5. Amersham ECL plus kit (GE Healthcare, RPN2108)
6. Blocking buffer: 1X TBST containing 5 % low fat milk (Roth, T145.3)
7. Bradford protein assay (Bio-Rad, Muenchen)
8. BSA protein standard (Thermo Scientific, 23227), diluted in 1x PBS
9. Fiber pads (Bio-Rad)
10. Filter paper (Bio-Rad, 170-3966)
11. Immobilon® polyvinylidene difluoride (PVDF) membrane (Milliopore, Bedford, PR02531)
12. Kodak film (Sigma-Aldrich, Z370398)
13. Kodak GBX developer and replenisher (Sigma-Aldrich, P7042 and P7167)
14. PageRuler plus prestained protein ladder 10-250K (Thermo Scientific, 26619)
15. Primary antibodies: rabbit anti-human OLR1 (1:1000, Antibody online, USA, ABIN676988), rabbit anti-human CH25H (1:1000, Santa Cruz Biotechnology, sc-135228), rabbit anti-human SOAT1 (1:500, Antibody online, ABIN872876) and goat anti-human GAPDH (1:500, Santa Cruz Biotechnology, sc 20357). All antibodies are cross-reactive to bovine molecules.
16. Protease inhibitor cocktail (Sigma-Aldrich, P8340)
17. RIPA buffer: 50 mM Tris-HCl, pH 7.4, 1 % NP-40, 0.5 % Na-deoxycholate, 0.1 % SDS, 150 mM NaCl, 2 mM EDTA, 50 mM NaF (all Roth)
18. Running buffer: 0. 125 M Tris, 0.96 M Glycin, 0. 5 % SDS (all Roth)

19. Sondary antibodies: donkey anti-goat IgG-HRP (1:10,000, Santa Cruz Biotechnology, sc-2020) and goat anti-rabbit IgG-HRP (1:10,000, Santa Cruz Biotechnology, sc-2030)
20. Transfer buffer: 15 % methanol, 0.005 % SDS, 192 mM glycin, 25 M Tris (all Roth)
21. Washing buffer: 1X TBS 0.1 % Tween20 [(TBST), all Roth]

Method

Infected and non-infected BUVEC were washed in PBS to remove any medium traces, trypsinized (see **3.1.2**) and pelleted (600x*g*, 10 min). 200 µl of RIPA buffer containing 2 µl of protease inhibitor cocktail were added to the pelleted cells. Thereafter, the cells were sonicated (20 s, 5X) on ice and centrifuged (8000x*g*, 10 min, 4ºC). The protein contents of the supernatants were measured by Bradford assay (Bradford, 1976). Therefore, the Bradford buffer was equilibrated at RT. 150 µl of the protein standards representing 25, 20, 15, 10, 5, 2.5 and 1.25 µg/ml final concentrations and test samples were mixed with 150 µl of Bradford buffer (1:1) and incubated (RT, 5-10 min). The protein concentration was determined via 595 nm photometric reading in a Varioskan™ Flash Multimode Reader. The protein concentrations of the samples were obtained by interpolating photometric values to the linear regression curve of the standard protein. For western blot analyses, 100 µg of the test samples were heated in reducing 5X SDS sample buffer (10 min, 95ºC). The samples were processed by SDS-PAGE (120 V, 1 h) and transferred to PVDF membrane by the wet transfer method using mini Trans-Blot (Bio-Rad) systems (see **Fig. 3.1.**) applying 100 V at 4-8ºC for 1 h. Protein transfer efficiency was controlled by Ponceau red staining of the blots for 5 min. Thereafter, ponceau dye was washed off the membrane in dH_2O. The membrane was incubated in blocking buffer overnight at 4ºC. Then it was reacted with primary antibodies diluted in blocking buffer (2 h, RT). The membranes were washed thrice in TBST (RT, 15 min) and incubated with corresponding secondary antibodies (1 h, RT). The membranes were then washed thrice in TBST (RT, 15 min). Signals were detected by a chemiluminescence detection system according

to the manufacturer's instructions. Therefore, membranes were incubated in reaction buffer (solution A:B= 40:1, RT, 5 min) followed by film developing. Signal development were performed in the dark. Therefore, the kodak films were placed on the membrane and fixed in a casette for several minutes (5-15 min). Films were developed in developer solution for 1 min, washed in dH_2O for 30 sec and fixed in fixer solution for 30 sec. Protein sizes were controlled relative to the protein ladder of the prestained marker.

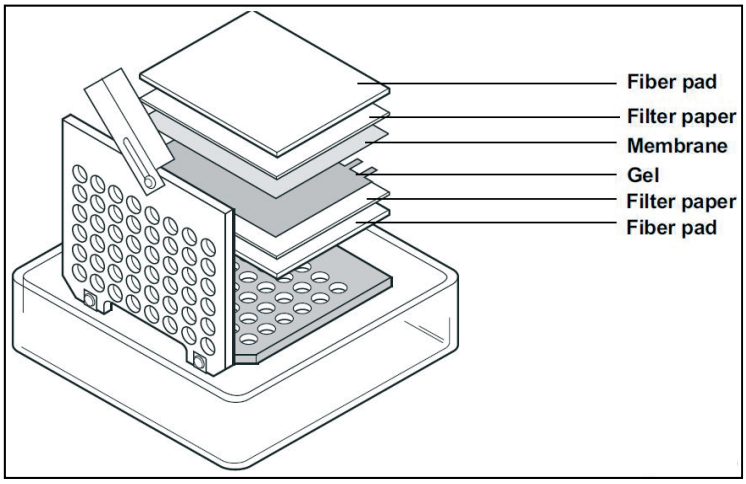

Fig. 3.1. Sandwich set-up for membrane protein transfer (Anonymous b,-).

3.9 Statistical analysis

All data presented in the results part of this study were statistically analysed by *t*-tests comparing treated and untreated groups using GraphPad Prism 6.02 software. The p-values of each experiment are noted in Appendix I.

4 RESULTS

4.1 Cholesterol and lipid droplet localization in free parasite stages and infected cells

4.1.1 *Cholesterol localization in E. bovis stages*

Filipin represents a commonly used tracer of cholesterol (Gimpl and Gehrig-Burger, 2007, Maxfield and Wustner, 2012) and was here used to detect non-esterified cholesterol in invasive stages and in *E. bovis*-infected cells.

Both investigated parasite stages, i. e. sporozoites and merozoites I, were intensively stained by filipin (**Fig. 4.1.**). The strongest reactions were detected at the apical part and in the outer membrane of these stages indicating a high cholesterol content of the apical complex and the pellicula (**Fig. 4.1.**). In addition, an intense staining was observed in the cytoplasm of sporozoites and merozoites I. These reactions may origin from intraparasitic organelle membranes since free cytoplasmatic cholesterol is generally described as toxic for cells (Tabas, 2002). However, the microscopic resolution did not allow for further detailed analyses. Unfortunately, filipin is a very fast bleaching compound hampering any laser-assisted experiments (e. g. confocal microscopy) that would have been of benefit for organelle identification.

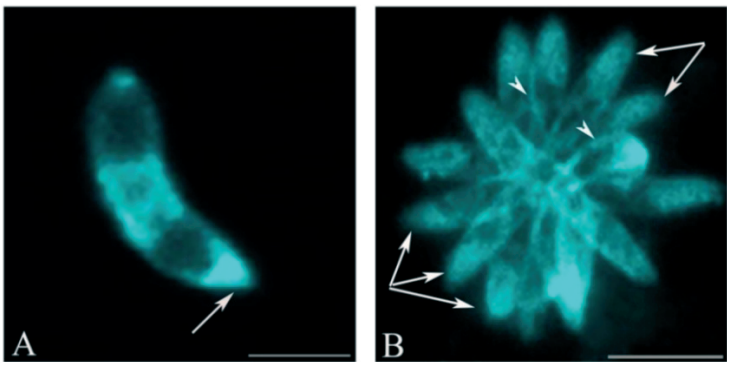

Fig. 4.1. Filipin staining of invasive *E. bovis* stages
E. bovis sporozoites (A) and merozoites I (B) were stained by filipin. Note the intense filipin-derived signals in the apical part of both stages (arrow; A, B). The arrow heads indicate reactions of the outer layers of merozoites I (B). Scale bars: 5 µm.

In *E. bovis*-infected host cells, cholesterol abundance significantly increased with ongoing macromeront formation (**Fig. 4.2.**).

One day after host cell infection, filipin-positive signals accumulated very close to the parasites intracellular position as illustrated in **Fig. 4.2.A**. Given that sporozoites always reside in a parasitophorus vacuole (PV), cholesterol signals may co-localize with the PV or even with the membrane of the PV (PVM). However, since the shape of the cholesterol accumulation site is not always typically roundish as it should be if only the PV or PVM was stained, other cell compartments may be involved in cholesterol accumulation, too.

Compared to non-infected control cells directly neighbouring infected host cells, the cholesterol abundance was significantly enhanced in immature- and mature-meronts (**Fig. 4.2.B, C**). As such, the cholesterol content of infected host cells increased with ongoing development and increasing macromeront sizes. As depicted in **Fig. 4.2.C**, cholesterol accumulation occurred within the immature meront itself occasionally showing a punctuated morphology. Whenever *E. bovis* macromeronts were multichambered, the inner septae also reacted with filipin indicating these membranes also to contain cholesterol molecules.

In mature *E. bovis* macromeronts the strongest reactions upon filipin-staining were observed in the outer layers of the infected host cells (**Fig. 4.2.D**). Owing to the enlargement of the host cell leading to a close position of PVM and host cell membrane, it cannot be concluded whether the signals originate merely from the parasite and its PVM or from the host cell membrane or both. In filipin-stained mature macromeronts, merozoites I could not be structurally identified although being visible in the phase contrast mode. Most probably, this was due to the strong signals of the outer membrane outshining the rather weak reactions of the merozoites I themselves.

Fig. 4.1.2. Filipin staining of *E. bovis* infected host cells
BUVEC were infected with *E. bovis* sporozoites and were monitored for cholesterol contents during *in vitro* infection: (A) 1 day p. i. (invaded sporozoites, arrows), (B) 8 days p. i. (early immature meront), (C) 14 days p. i. (immature meront), (D) 17 days p. i. (mature meront). Scale bars: 10 µm.

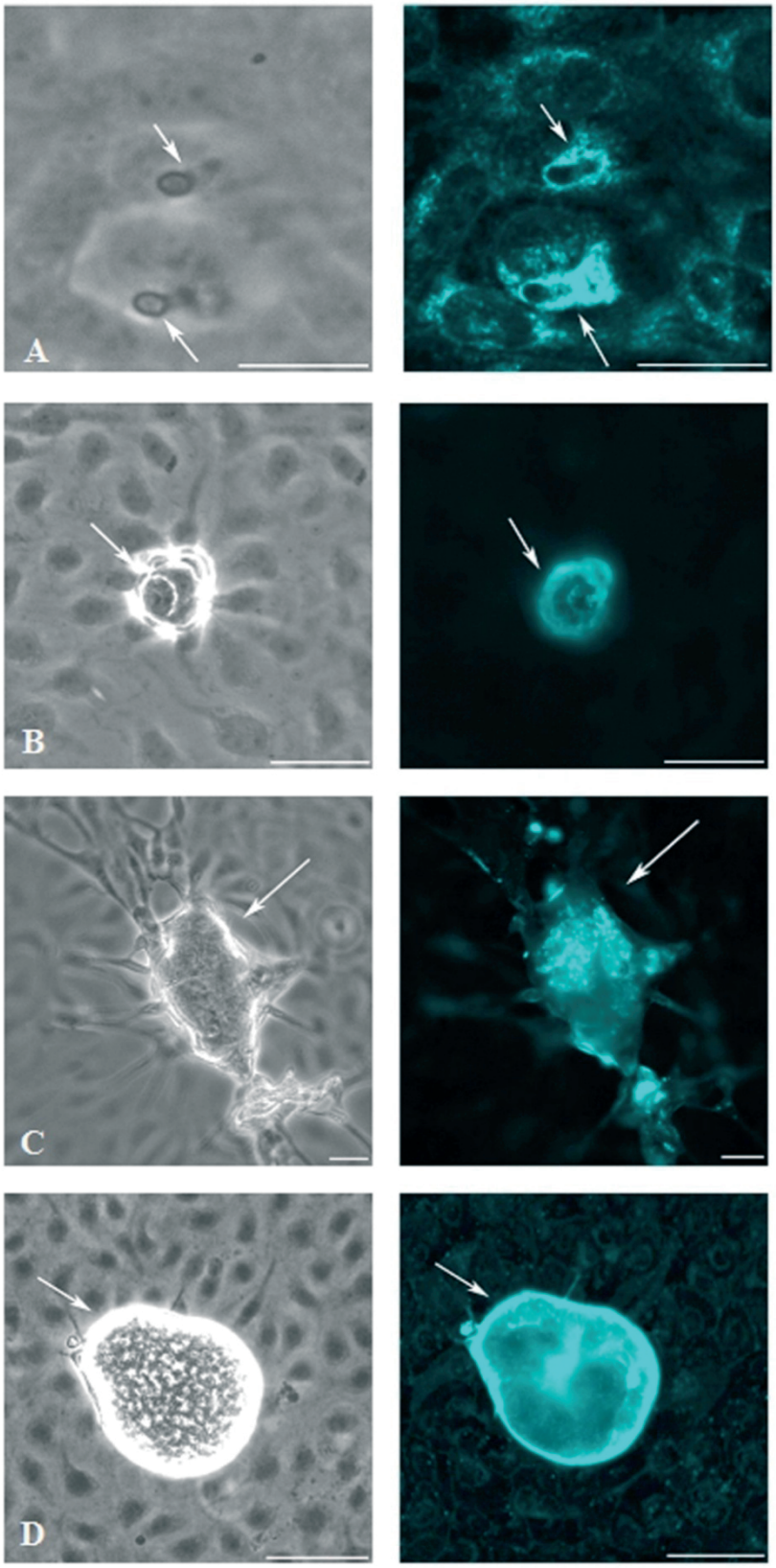
A
B
C
D

Filipin staining at day 1 p. i. revealed a considerable accumulation of cholesterol surrounding the invaded sporozoite (see above). However, from these results it cannot be concluded whether these molecules were host cell-derived or originated from the parasite stage itself. Therefore, rhodamin cholestanol was used to exclusively label host cell-derived molecules prior to sporozoite infection. As depicted in **Fig. 4.3.** a clear accumulation of cholesterol close to the parasite was detected after rhodamin cholestanol supplementation indicating that host cell cholesterol is recruited to the parasites site after invasion. Given that the sporozoite resides within a PV these molecule may also contribute to the formation of the PVM. However, the resolution of the current assays did not allow for this conclusion.

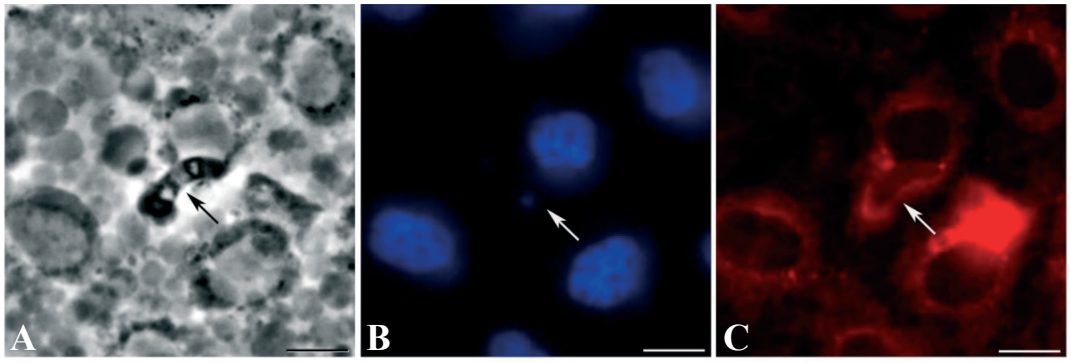

Fig. 4.3. Cholesterol distribution within *E. bovis*-infected BUVEC after rhodamin cholestanol labelling
BUVEC were labelled with rhodamin cholestanol-supplemented. Thereafter, they were infected with viable *E. bovis* sporozoites. 1 day p. i. infected cells were processed by fluorescence microscopy applying the TRITC filter setting. Scale bars: 10 µm.

4.1.2 *Dansyl-cholesterol incorporation into E. bovis stages*

In order to analyze whether free and intracellular stages of *E. bovis* are capable to incorporate cholesterol from an extracellular source, free sporozoites and intracellular meronts were pulse-labelled with dansyl-cholesterol, a fluorescent cholesterol analogue that is described to be comparably processed as non-modified cholesterol within the cell (Wiegand et al., 2003, Shrivastava et al., 2009).

The exposure of sporozoites to dansyl-cholesterol led to a rapid uptake of this tracer molecule and respective fluorescence patterns within these stages. Within the specimens, the reactions appeared concentrated in the apical part and, to a higher degree, in the refractile bodies of the sporozoite (**Fig. 4.4.B**). Given that dansyl-cholesterol is a non-esterified molecule and that these reaction patterns overlap with those of neutral lipid (bodipy 493/503) staining (see **Fig 4.6.B, C**), it appears likely to assume that dansyl-cholesterol was not only incorporated and transported to the apical complex but also converted to cholesteryl esters and deposited as such in the refractile bodies.

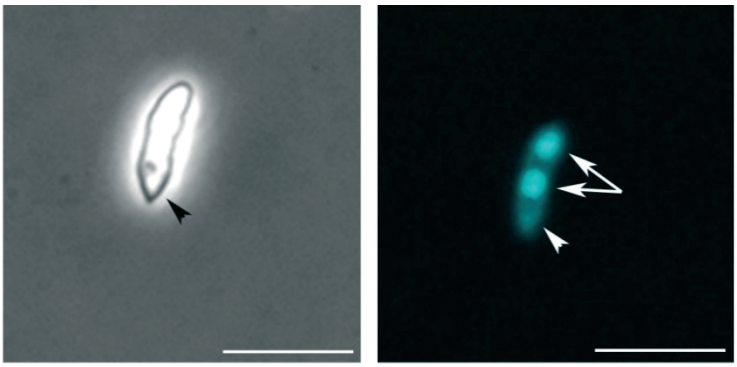

Fig. 4.4. Dansyl-cholesterol-labelling of *E. bovis* sporozoites
E. bovis sporozoites were stained with dansyl cholesterol-cyclodextrin complexes. Note the bright fluorescence of the refractile bodies of the sporozoite (arrows) and of the apical complex (arrow head). Scale bars: 20 μm.

Exogenously supplied dansyl-cholesterol was also incorporated in intracellularly situated meronts I as depicted in **Fig. 4.5.B**. The bright staining of lipid body-like structures within the infected host cell and, most probably, within the parasitic stage itself, implies that dansyl-cholesterol was processed analogous to non-modified cholesterol, i. e., it was esterified and stored in lipid droplets. The bright fluorescence of the meronts I after dansyl-cholesterol pulse-labelling (**Fig. 4.5.B**) confirmed an increase of cholesterol/cholesterylester abundance in infected cells when compared to non-infected controls.

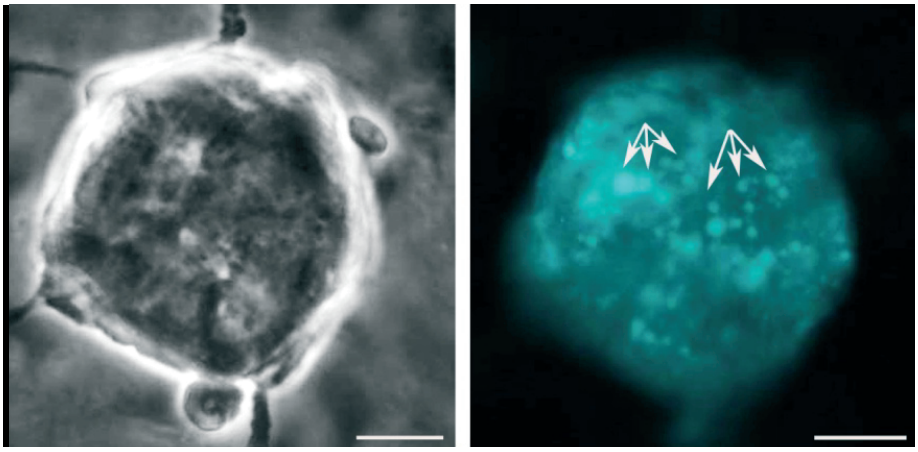

Fig. 4.5. Dansyl-cholesterol-labelling of *E. bovis* meronts I
Dansyl-cholesterol-cyclodextrin complexes were administered to *E. bovis*-infected host cells (15 days p. i.). Note the bright fluorescence of LD-like structures in a meront I-infected host cell (arrows). Scale bars: 20 µm.

4.1.3 *Lipid droplet (LD) formation in E. bovis stages*

Since excess intracellular concentrations of free cytoplasmatic cholesterol are toxic for cells, this molecule is generally converted intracellularly to cholesteryl esters which then are stored in LDs (Chang et al., 2006). LDs represent dynamic lipid storage organelles found in any cell type which needs rapidly mobilized lipids. Thus, LDs are not only enriched in cholesteryl esters but also in triacylglycerol and phospholipids (Mahlberg et al., 1990, van Meer, 2001). To monitor LD formation in invasive stages and infected host cells throughout the development of *E. bovis* macromeronts, three different stainings were here applied which all detect neutral lipids and are commonly used to detect LD formation within mammalian cells (Greenspan et al., 1985, Brown et al., 1988, Gocze and Freeman, 1994): Nile red® and bodipy 493/503 as fluorescent dyes and osmium tetroxide for bright field microscopy.

Sporozoites and merozoites I of *E. bovis* all showed an intense staining by Nile red®- and bodipy 493/503-dyes, clearly indicating a high content of neutral lipids within analyzed stages. However, using Nile red® we failed to demonstrate structurally defined LD-like structures within the cytoplasm of these stages, whilst bodipy 493/503 staining resulted in strong fluorescing globular bodies. In merozoites I and sporozoites LDs were situated in the cytoplasma and differed in

numbers per specimen (**Fig. 4.6.**). Overall, up to 8 LD-like structures were detected per stage. The strongest reactions upon Nile red® or bodipy 493/503 staining were found in the refractile bodies of the sporozoite stage (merozoites I do not contain any refractile bodies) (**Fig.4.6.B, C**) indicating the storage of neutral lipids within these apicomplexan organelles.

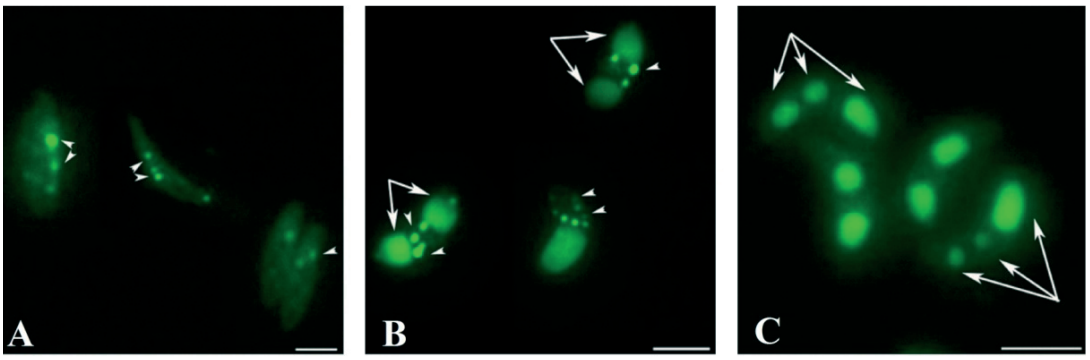

Fig. 4.6. Neutral lipid staining in *E. bovis* invasive stages
Merozoites I (A) and sporozoites (B) were stained with bodipy 493/503 and Nile red® (only sporozoites, C) to visualize neutral lipids and LDs. LDs are situated within the cytoplasm of both stages (A, B, arrow heads). In addition, the refractile bodies of the sporozoites strongly reacted with both stainings (arrows, B, C). Scale bars: 5 µm.

Given that bodipy 493/503 staining was superior to Nile red® if LDs were to be stained, we used the former staining to monitor LD formation in *E. bovis*-infected BUVEC. Soon after completing the invasion process, intracellular sporozoites seemed to lose the contents of their anterior refractile body since the fluorescence of these were clearly diminished when compared to free sporozoites (**Fig. 4.7.A**, arrows).

Compared to non-infected controls, a considerable enhancement of LD formation was observed with ongoing macromeront development showing the most significant accumulation of distinct LD-like structures in immature macromeronts (15-17 days p.i.). Here, differential distribution patterns of these organelles were observed since they were either homogeneously spread within the macromeront-carrying host cell (**Fig. 4.7. B, D**: macromeront at the left side) or found clustered in certain areas (**Fig. 4.7. C**). With maturation and merozoite I formation the fluorescence pattern changed from a spotty appearance illustrating single LDs to a rather cloudy and diffuse reaction indicating that lipid droplet contents were

almost totally exhausted or consumed for merozoite I formation (**Fig. 4.7. D**, macromeront at the right side).

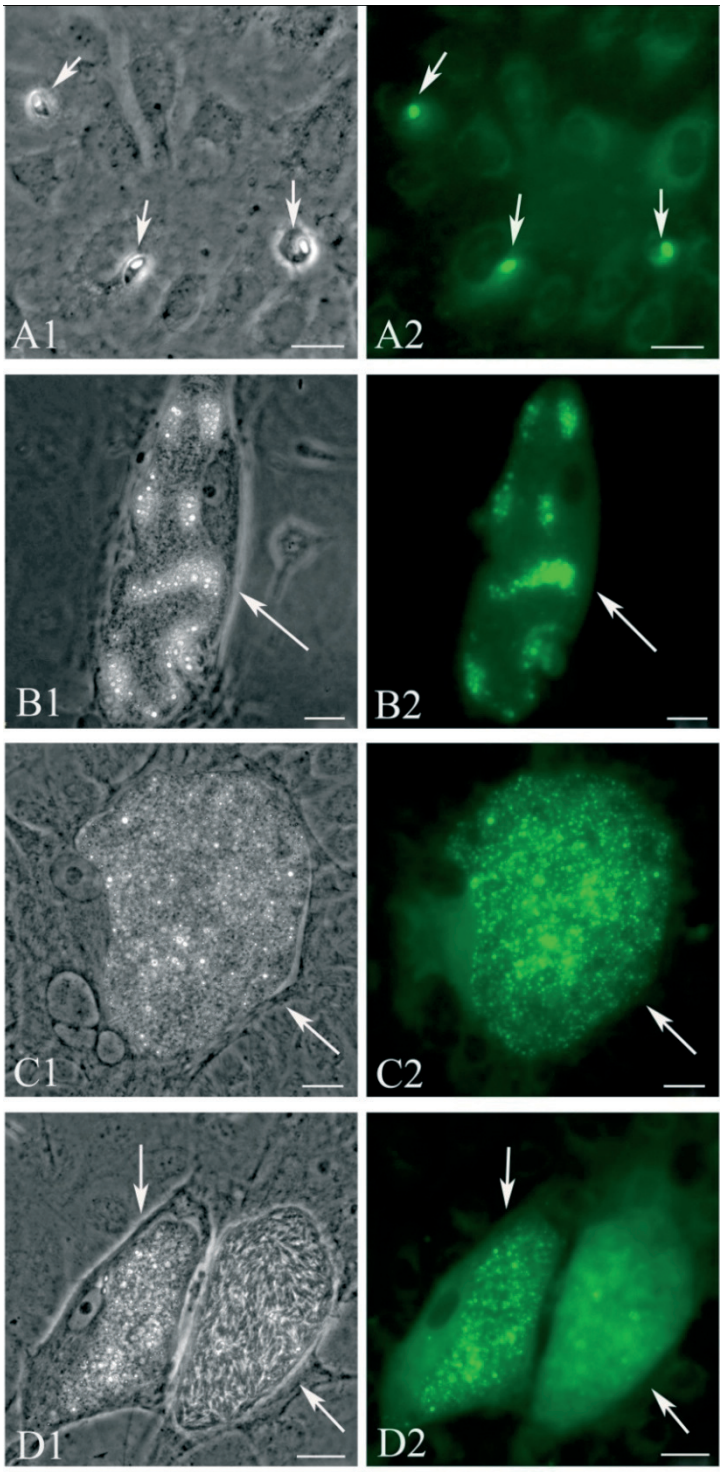

Fig. 4.7. Bodipy 493/503 staining of *E. bovis* infected host cells
BUVEC were infected with *E. bovis* sporozoites and were monitored for LD contents during *in vitro* infection: (A) 1 day p. i. (invaded sporozoites, arrows), (B-D) 17 days p. i. with homogeneously spread spotty (B), clustered (C) and cloudy (D) distribution of bodipy 493/503-positive reactions in meronts I. Scale bars: 20 µm.
A1, B1, C1, D1: phase contrast; A2, B2, C2, D2: bodipy 493/503 staining

Given that the fixation mode may alter LD integrity leading to dimmed LD appearance (DiDonato and Brasaemle, 2003), this study additionally used osmium tetroxide fixation which preserves lipid body structures. However, osmium tetroxide treatments led to similar results as bodipy 493/503 staining and thus confirmed the significant increase of LD abundance in *E. bovis* macromeront-carrying host cells (**Fig. 4.8.**).

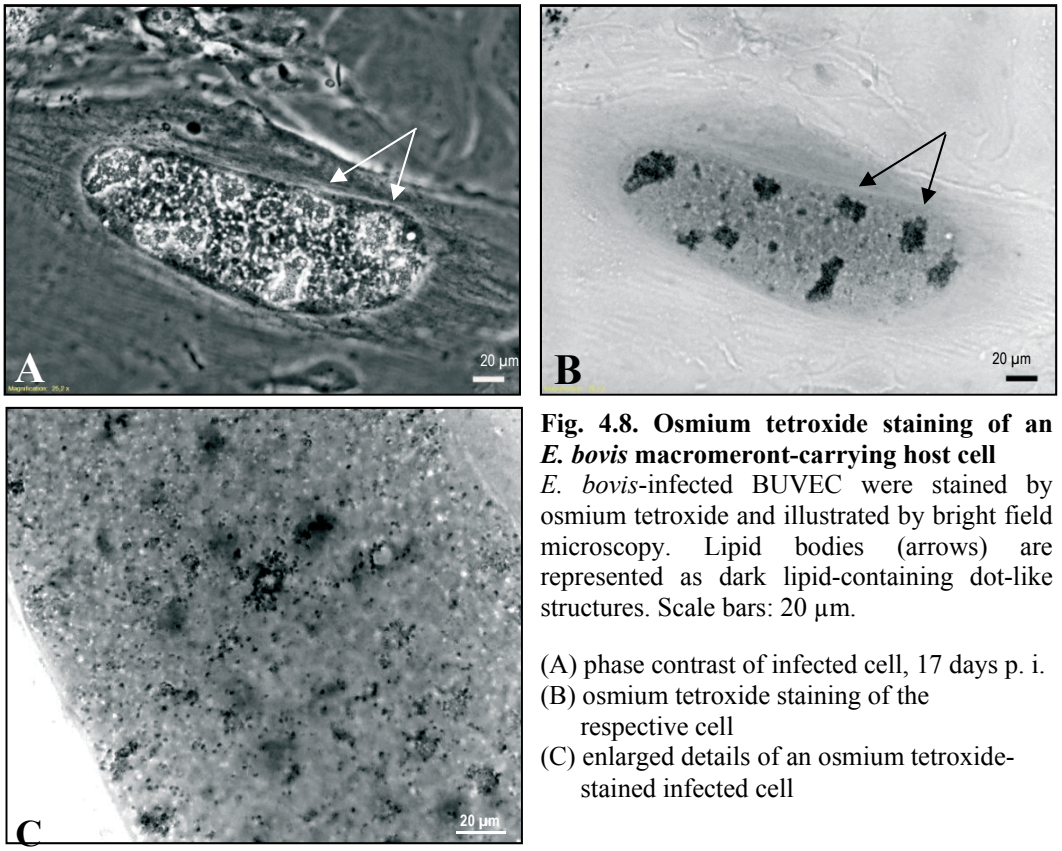

Fig. 4.8. Osmium tetroxide staining of an *E. bovis* macromeront-carrying host cell
E. bovis-infected BUVEC were stained by osmium tetroxide and illustrated by bright field microscopy. Lipid bodies (arrows) are represented as dark lipid-containing dot-like structures. Scale bars: 20 µm.

(A) phase contrast of infected cell, 17 days p. i.
(B) osmium tetroxide staining of the respective cell
(C) enlarged details of an osmium tetroxide-stained infected cell

In order to better define LDs position, structure and size within *E. bovis*-infected cells we extended our experiments by confocal microscopy applying bodipy 493/503 staining. Analyses of host cells 17 days after infection revealed the presence of brightly fluorescing LDs throughout the meront I corpus since they were detected in each layer (Z-stack) of the specimen (**Fig. 4.9.A-C**). LDs showed classical globular shapes but were of differing sizes. Whilst most LDs were rather small (< 1 µm), some of them revealed a size of up to 5 µm in diameter. The simultaneous staining of the LDs (bodipy 493/503) and nuclei (DAPI) showed the

makromeronts to be densely filled with lipid sources and developing merozoites I (**Fig. 4.9. D**).

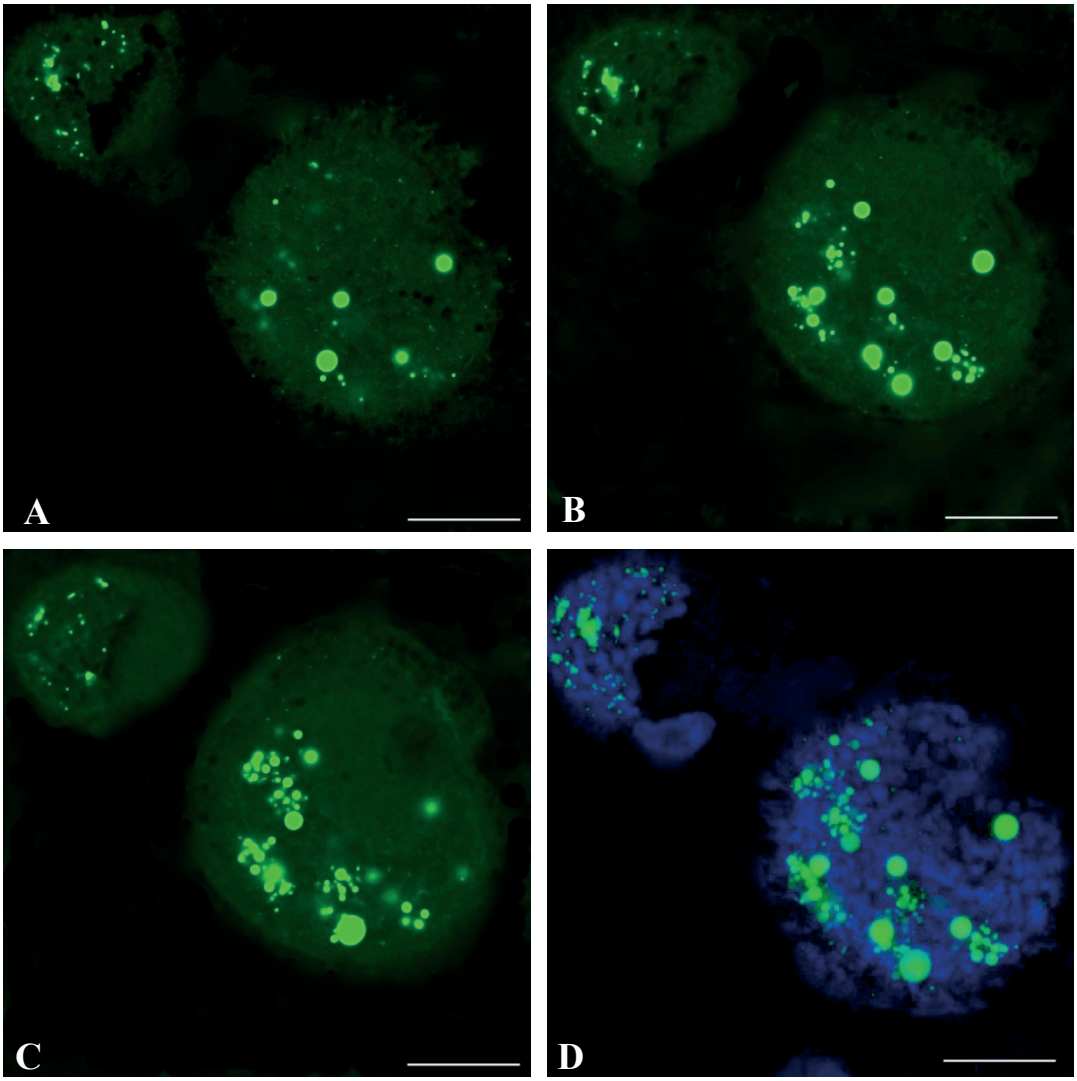

Fig. 4.9. Bodipy 493/503 staining of an *E. bovis* macromeront-carrying BUVEC
Bodipy 493/503- (green= lipid droplets) and DAPI- (blue= nucleus) stained *E. bovis*-infected BUVEC (17 days p. i.) were analyzed via confocal microscopy. **A-C** represent single Z-stacks of one bodipy 493/503-stained infected host cell, **D** shows an overlay of all stacks after bodipy 493/503- and DAPI-stainings. Note numerous nuclei of developing merozoites I (D, blue) and large globular LD-like structures (green). Scale bars: 20 µm.

4.2.Quantification of cholesterol and lipid droplet (LD) contents in *E. bovis*-infected host cells

4.2.1. Cholesterol accumulation in E. bovis-infected host cells

To confirm the qualitative findings of cholesterol accumulation in *E. bovis* infected host cells (see **4.2**), total cellular cholesterol quantification of infected cells was performed by using an enzyme-based fluorometric assay (Amplex Red® Cholesterol Assay). In this commercially available assay free and esterified forms of cholesterol were equally detected. However, the use of the provided solvent failed since the total lipid extracts were not properly dissolved in this agent. Thus, the method had to be adapted and the solvent was replaced by isopropanol-NP40 according to Robinet et al. (2010). Given that the solvent isopropanol-NP40 contained a certain level of residual peroxidase activity resulting in rather high background noises using the Amplex Red® Cholesterol Assay, we applied catalase treatments to each sample in order to inactivate peroxidase activity prior to be processed for cholesterol measurements. Overall, catalase treatments of isopropanol-NP40 significantly reduced background reactions resulting in a r^2 value of 0.99 for the standard curve (**Fig. 4.10.**).

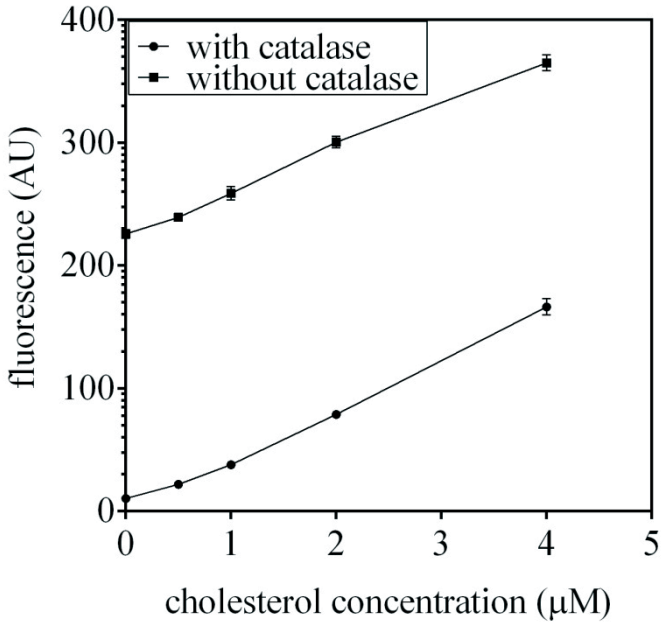

Fig. 4.10. Cholesterol quantification of catalase pre-treated samples
Cholesterol standard was dissolved at different concentrations (0.5, 1, 2, 4 µM) in catalase-treated or non-treated isopropanol-NP40 and quantified using the Amplex Red® Cholesterol Assay.

Cholesterol quantification in total lipid extracts revealed a significant increase of cholesterol abundance in *E. bovis*-infected host cells over time when compared to non-infected controls (**Fig. 4.11.**). Thus, significant differences were detected beginning with 4 days p. i. up to 17 days p. i. (4 days p.i: $p < 0.01$; 8 days p.i: $p < 0.01$; 17 days p.i: $p < 0.01$), although the infection rates were rather low in times of meront I maturation (17 days p. i., 20-30% infection rate). Given that the cholesterol content of sporozoites (here the individual infection dose of 5×10^5 sporozoites was analyzed) was rather low (**Fig. 4.11.**), the changes of host cellular cholesterol content did not originate from invading stages and resulted from infection-triggered alteration of the cholesterol metabolism.

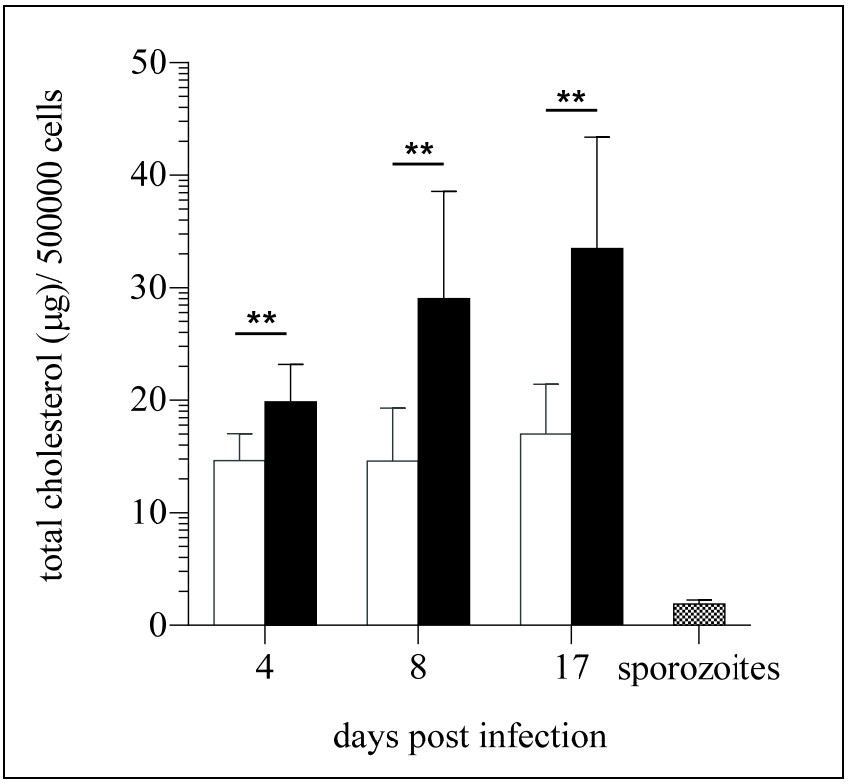

Fig. 4.11. Total cholesterol abundance in *E. bovis*-infected host cells
The total cholesterol abundance was estimated in *E. bovis*-infected BUVEC (black bars) and in non-infected controls (white bars) using the Amplex Red® Cholesterol Assay following total lipid extraction. The data represent means ± SD of 7 different BUVEC isolates.

4.2.2 *Lipid droplet (LD) accumulation in E. bovis-infected host cells*

To verify LD accumulation previously observed in *E. bovis*-infected host cells (see **4.1.3.**) we established a flow cytometry-based assay allowing for LD quantification in *E. bovis*-infected cell layers and in non-infected controls by measuring bodipy 493/503-derived fluorescence signals.

The LD abundance in *E. bovis*-infected BUVEC was significantly enhanced over time during macromeront formation resulting in highly significant values ($p \leq 0.0001$) for days 17 and 21 p.i., respectively. These results corroborated our previous qualitative observations on bodipy 493/503 and osmium tetroxide-stained host cells (see **4.1.3.**).

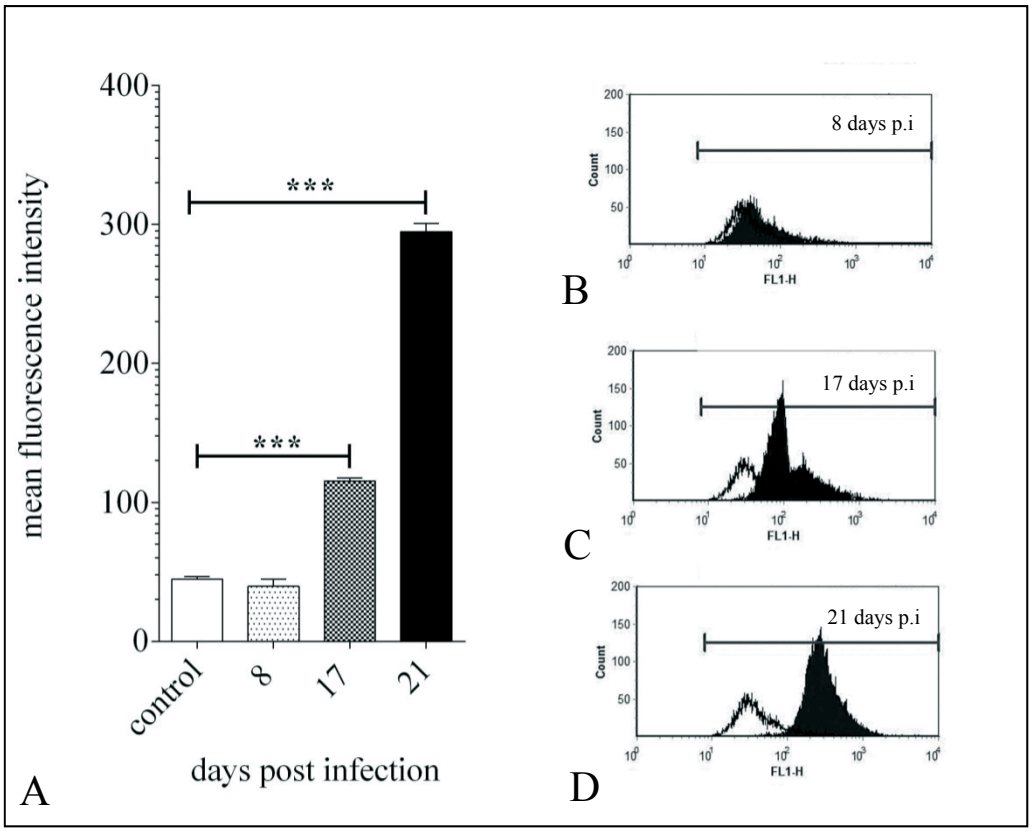

Figure 4.12. Lipid droplet abundance in *E. bovis*-infected host cells
Eimeria bovis-infected BUVEC were stained with bodipy 493/503 to trace LDs and analyzed at different time points p. i. (8, 17, 21 days p. i.) via flow cytometry. Infected cells were assigned according to their size and granularity. **(A)** Means and standard deviations of three isolates, **(B-C)** exemplary illustration of histograms of infected (black) and non-infected (white) BUVEC on days 8, 17 and 21 p. i., respectively.

4.3 Influence of cholesterol and lipid droplet (LD) enrichment on *E. bovis* development *in vitro*

4.3.1 *Effects of cholesterol supplementation on macromeront development*

To assess the effects of exogenously supplied cholesterol on *E. bovis* macromeront development, free sterols (cholesterol and desmosterol) were administered to cell cultures. Desmosterol is a cholesterol intermediate precursor and can replace cholesterol function in sustaining cell proliferation (Rodriguez-Acebes et al., 2009). To avoid intracellular crystallization and cytotoxicity (Xu et al., 2005), low concentrations (5 µM) of these substituents were applied.

Whilst infection rates and macromeront sizes were not significantly altered by cholesterol or desmosterol supplementation (**Fig. 4.13.A**), a significant beneficial effect ($p \leq 0.05$) was observed on merozoite I production leading to enhanced offspring generation in both, cholesterol- and desmosterol-treated host cells (**Fig. 4.13.B**).

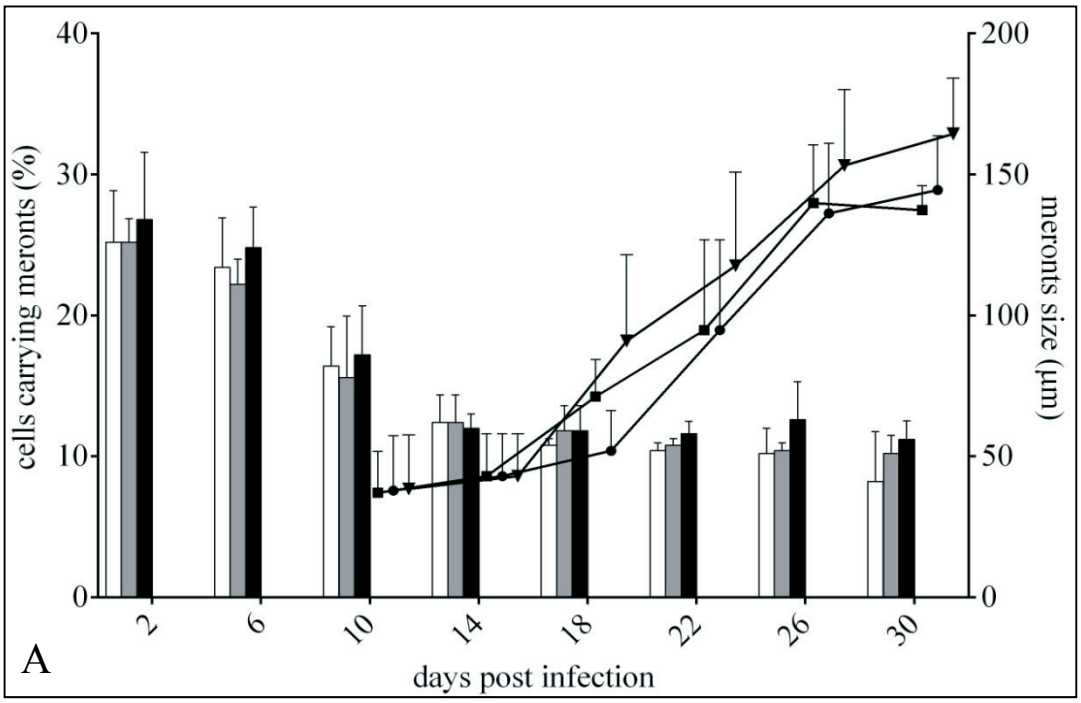

to be continued

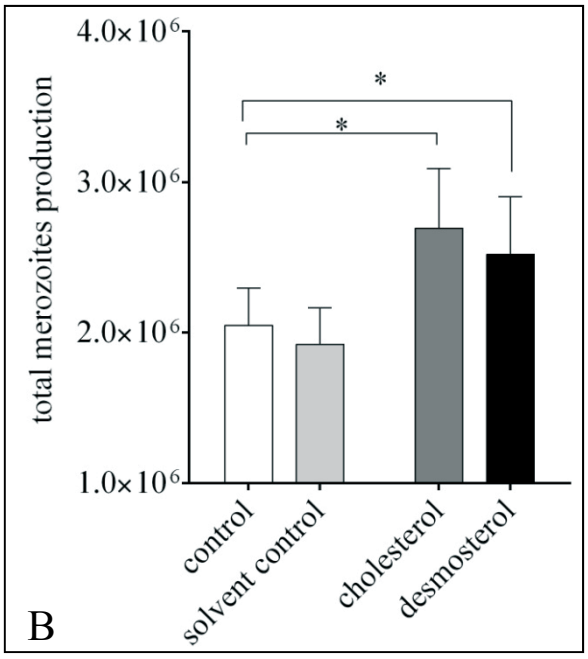

Fig. 4.13. Effects of cholesterol and desmosterol supplementation on *E. bovis in vitro* development
E. bovis-infected BUVEC were cultivated in non-supplemented (= controls) and cholesterol- or desmosterol-enriched medium. The effects of cholesterol and desmosterol supplementation on macromeront development **(A)** were assessed microscopically by estimating the rate of macromeront-carrying host cells (black bars: cultures treated with 5 µM cholesterol; grey bars: cultures treated with 5 µM desmosterol, white bars: controls) and by measuring the sizes of developing meronts (circles: cultures treated with 5 µM desmosterol; triangles: cultures treated with 5 µM cholesterol; quarders: controls). The effects on merozoite I production **(B)** were quantified using an Ebminc4-based qPCR (see **3.7.2**) after 30 days p. i.

4.3.2 *Effects of cholesterol depletion on E. bovis development in vitro*

The invasion of host cells by other apicomplexan parasites is reported as an active process requiring both, host cell- and parasite-derived cholesterol (Coppens and Joiner, 2003, Pacheco-Soares and De Souza, 2000). To assess the role of host cell- and parasite-derived cholesterol in the initial infection phase, *E. bovis* invasion assays were performed by alternatively using either cholesterol-depleted sporozoites or cholesterol-depleted host cells. As depicted in **Fig. 4.14.**, the most significant effects ($p \leq 0.0001$) were achieved by sporozoite cholesterol depletion since 91.1% less sporozoites invaded host cells compared to non-treated controls, although sporozoites remained vital after cholesterol depletion [as estimated via the trypane blue exclusion test (data not shown)]. Additionally, a significant

reduction of intracellular parasites of approximately 51% was observed when cholesterol-depleted host cells were used ($p \leq 0.01$).

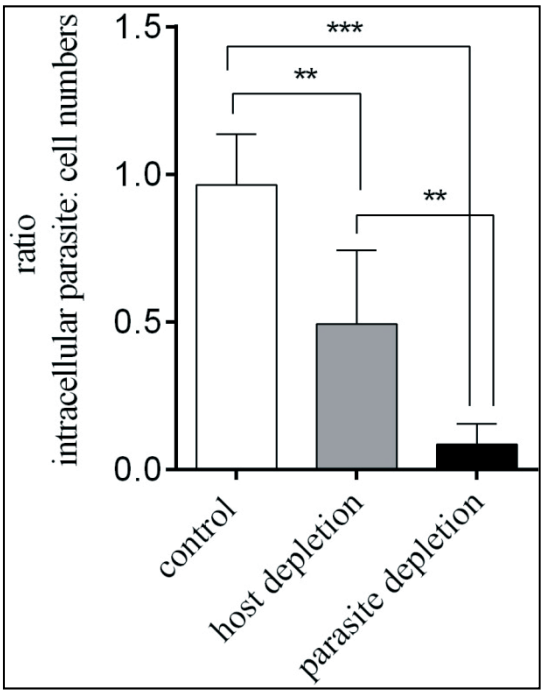

Fig. 4.14. Effect of host cell and sporozoite cholesterol depletion on initial *E. bovis* infection rates
Sporozoites of *E. bovis* (grey bar) or BUVEC (black bar) were depleted in cholesterol via MBCD treatment prior to host cell infection. Non-treated BUVEC were infected with non-depleted sporozoites and served as negative controls (white bar). Data represent means ± SD of five BUVEC isolates.

4.3.3 *Effects of increased host cellular lipid droplet disposability on E. bovis merozoite I production*

Given that LDs play a pivotal role in *E. bovis in vitro* development, we here assessed the effects of an artificially enhanced abundance of LDs in host cells. Oleic acid is a well-known inducer of LD formation in several types of mammalian cells (Martin and Parton, 2011). Since endothelial host cells generally react rather sensitive upon any stimulants and as oleic acid treatments were reported as toxic for human umbilical vein endothelial cells (HUVEC, Hua-Hong et al., 2010), preliminary cytotoxicity tests (MTT assays) were performed to identify oleic acid concentrations which increased LD formation but did not damage BUVECs.

MTT tests showed that BUVEC are very sensitive for oleic acid treatments since a high proportion BUVEC died even when low concentrations of oleic acid were applied (**Fig. 4.15.**). Thus, the application of 400 µM oleic acid, which is often used for cellular LD induction (Anonymous a,-), led to almost total cell death. LD generation in BUVEC was also controlled by bodipy 493/503 staining showing that long-term (24 h) treatments resulted in larger LDs than short term incubations (1 h, **Fig. 4.16.A, B**). Given that 2.5 µM oleic acid treatment induced a significant increase of (small) LD formation (**Fig. 4.16.C**), a combination of short-pulse induction by a relative mild dose (1 h, 50 µM) and maintenance in 2.5 µM oleic acid was chosen for *E. bovis*-related experiments.

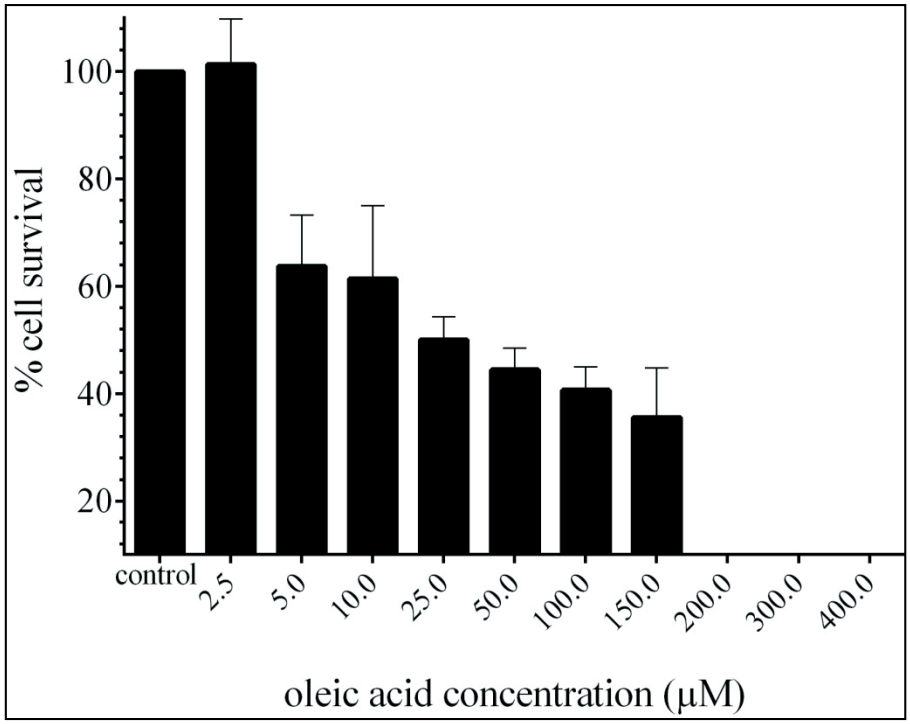

Fig. 4.15. MTT assay of oleic acid-treated BUVEC
BUVEC were exposed for 24 h to different concentration of oleic acid supplemented in the cell culture medium before being processed for MTT test. Means ± SD of triplicates.

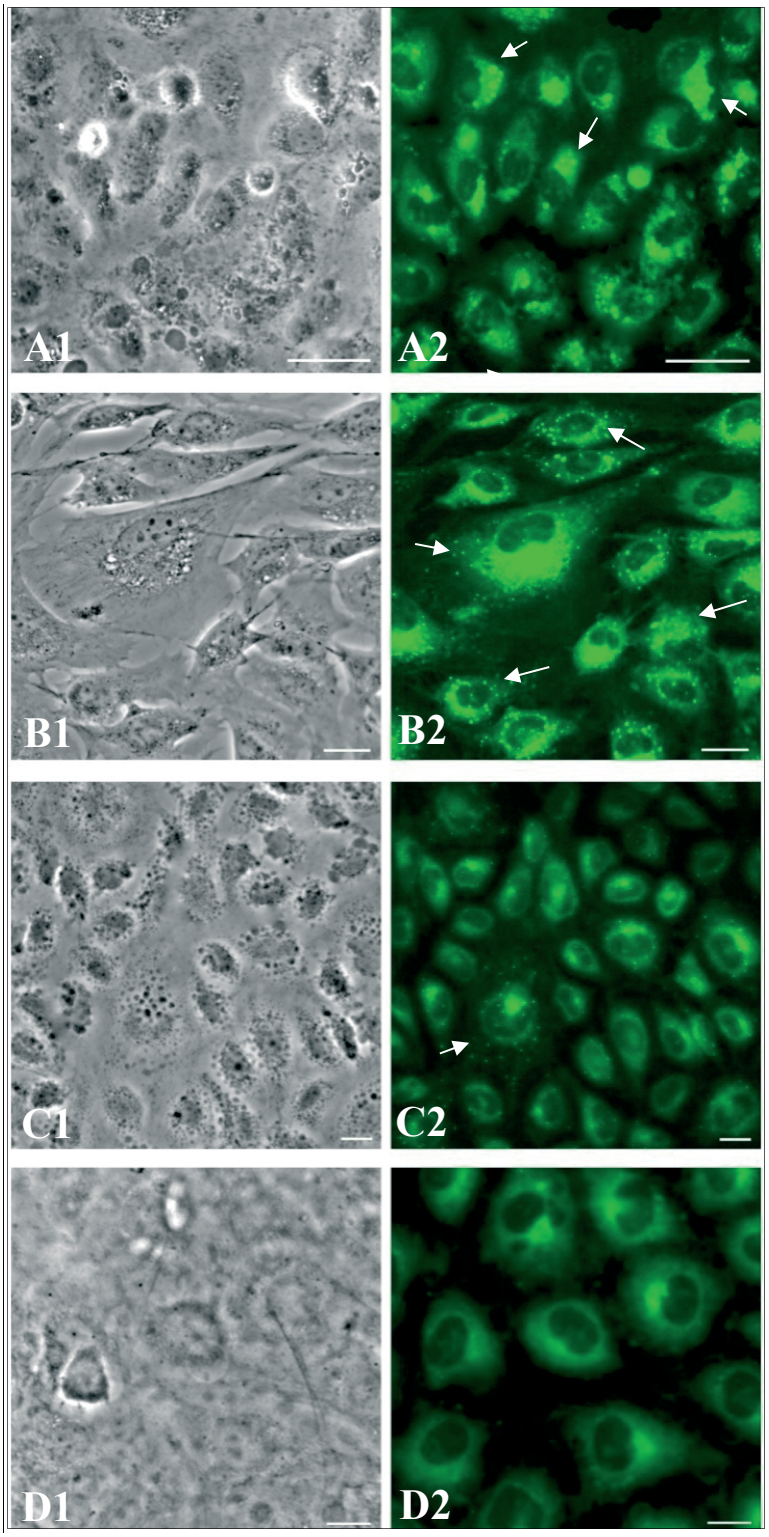

Fig. 4. 16. Effects of oleic acid treatments on LD formation in BUVEC
BUVEC were treated with oleic acid and stained by bodipy 493/503 to visualize LD formation.
(A): treatment with 50 µM oleic acid overnight, note large LDs (arrows).
(B): treatment with 50 µM oleic acid for 1 h, note small-sized LDs (arrows).
(C): treatment with 2.5 µM oleic acid overnight incubation
(D): non-treated controls
Scale bars: 20 µm, images at left side: phase contrast, at right side: bodipy 493/503 staining (green)

Analyses on *E. bovis* merozoite I production in oleic acid-treated BUVEC confirmed the key role of LDs in parasite proliferation. Thus, significant beneficial effects of oleic acid treatments on merozoite I production were observed over time of *in vitro* cultivation (**Fig. 4.17.A**). Referring to the total merozoite I production, a significant (**Fig. 4.17.B**), 4.7 ± 2.9 fold increase of offspring production was estimated.

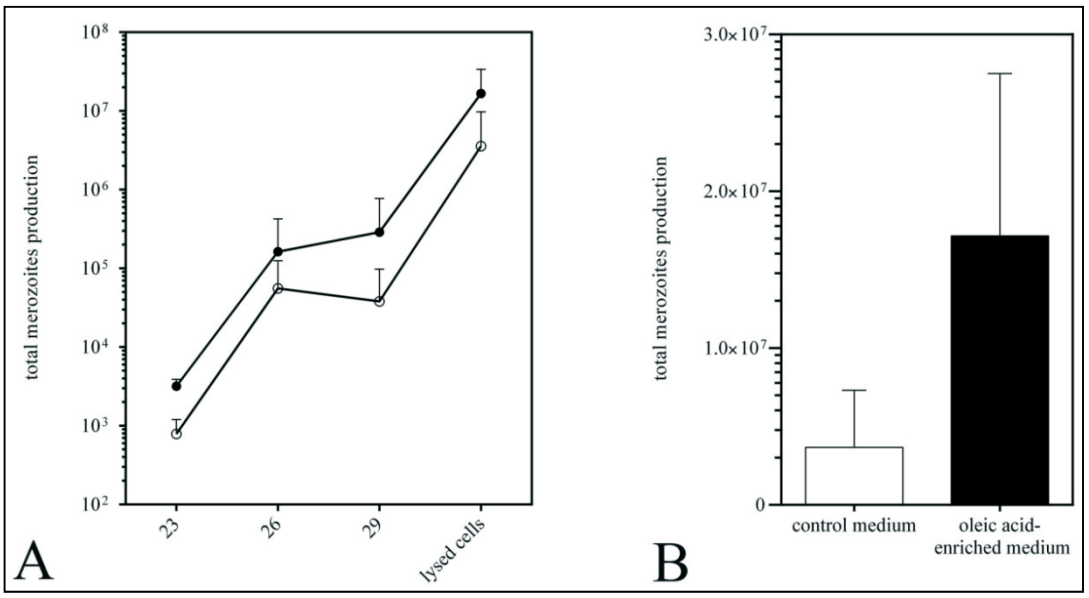

Fig. 4.17. Effects of oleic acid treatments on *E. bovis* merozoite I production
E. bovis-infected BUVEC were were cultured in oleic acid-enriched medium (A, B, black circles/column). Cultures in non-supplemented medium were used for controls (A, B, white circles/column). At different time points p. i. the numbers of merozoite I present in cell culture supernatants were quantified applying an Ebmic-specific qPCR (see **3.7.2**). **(A)** merozoite I production over time (oleic acid-treated cells: black circles, non-treated controls: open circles), **(B)** total merozoite I production in treated (black bar) and non-treated (white bar) BUVEC.

4.4 Involvement of LDL in *E. bovis* macromeront development *in vitro*

4.4.1 *Binding of LDL and acetylated LDL (acLDL) on parasite-infected host cells*

To assess whether LDL binding to the cell surface is altered in infected host cells, bodipy-labelled LDL was supplemented for short terms to *in vitro* cultures that had previously been starved in LDL-free medium. LDL binding was illustrated via fluorescence microscopy and quantified using FACS technology.

Utilizing confocal and conventional fluorescence microscopy a considerable increase of LDL binding to the surface of *E. bovis*-infected cells was demonstrated (**Fig. 4.18.**). Reactions varied from rather defined areas of intense spotty fluorescence (**Fig. 4.18.A**) to more homogeneously distributed bodipy-LDL-positive signals (**Fig. 4.18.B**) in the outer layer of infected BUVEC.

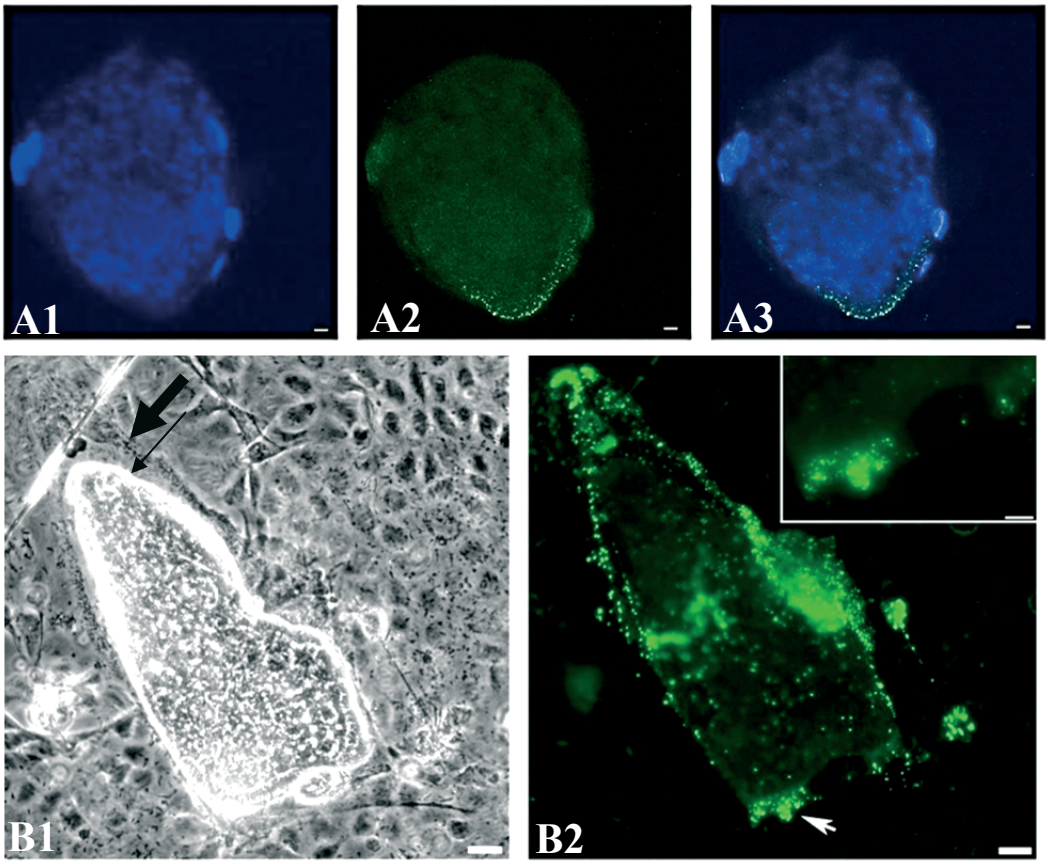

Fig. 4.18. LDL binding on *E. bovis*-infected host cells
E. bovis-infected BUVEC (17 days p. i.) were starved in LDL-free medium, exposed to bodipy-LDL, fixed and analysed using confocal (A1-A3) or conventional (B1-B2) fluorescence microscopy (scale bars: 20 µm).
thick arrow: host-cell membrane; thin arrow: meront.
blue: DNA-staining via DAPI; green: bodipy-LDL; grey: phase contrast

Prolonged supplementation of bodipy-LDL for more than 5 h resulted in bodipy-positive signals in different localizations within infected cells (**Fig. 4.19**.). Thus, analyses of single sections of Z-stacks identified these reactions to be located at both areas, i. e., the surface and the inside of the *E. bovis* macromeront-carrying cell indicating a certain degree of bodipy-LDL up-take within the macromeront.

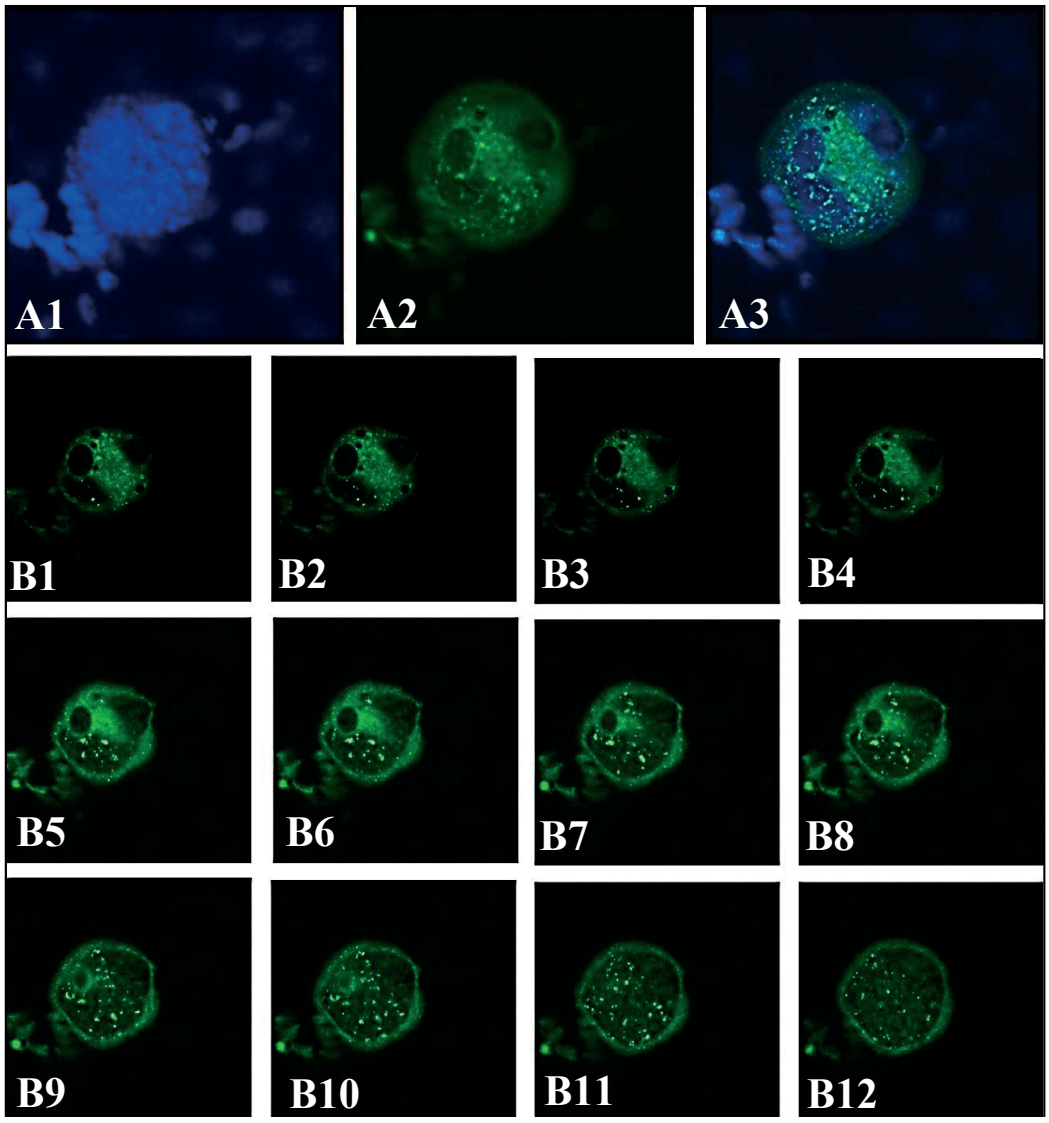

Fig. 4.19. LDL binding and up-take in *E. bovis*-infected host cells
E. bovis-infected BUVEC (17 days p. i.) were starved in LDL-free medium, exposed to bodipy-LDL for 5 h, fixed and analysed by confocal fluorescence microscopy.
A1-3: DAPI, bodipy-LDL, and merge of a Z-Stack, respectively.
B1-12: single sections of bodipy-LDL staining

The LDL binding assays were extended to FACS analysis to obtain quantitative data. Indeed, a significant increase of bodipy-LDL binding was detected in infected cells when compared to non-infected controls ($p < 0.0001$, **Fig. 20**.). Overall, a 37.5-fold enhancement was measured. However, it has to be kept in mind that these reactions may not exclusively reflect surface-bound LDL but may also originate from a small proportion of internalized LDL.

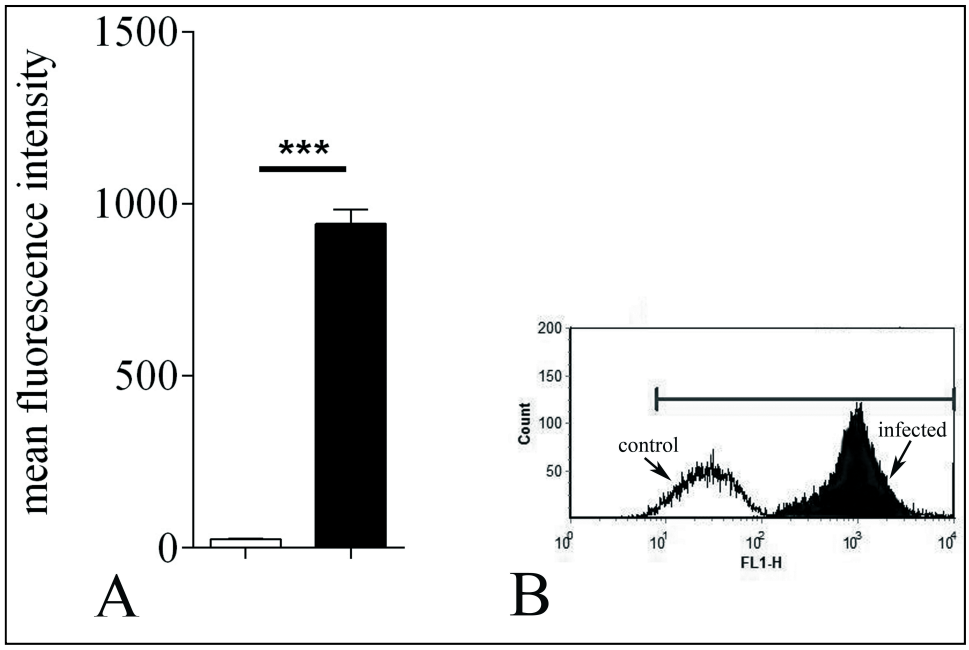

Fig. 4.20. Quantitative assessment of LDL binding to *E. bovis*-infected BUVEC
E. bovis-infected (17 days p. i.; black bar/pannel) and non-infected (white bar/pannel) BUVEC were starved in LDL-free medium, exposed to bodipy-LDL, fixed and analysed by flow cytometry. **(A)** means of three different BUVEC isolates in triplicate, **(B)** exemplary histogram.

Whilst most cell types are able to incorporate non-modified LDL via the LDLR pathway, only endothelial cells and macrophages have the capacity to internalize acetylated LDL (acLDL) via so-called scavenger receptors (Goldstein et al., 1979, Voyta et al., 1984). Consequently, acLDL up-take is routinely used for primary endothelial cell characterization (Voyta et al., 1984). Since the high demand for cholesterol in macromeront-carrying cells may also be met by modified LDL derivates, LDL binding assays were further extended to acLDL molecules. Short term supplementation of *in vitro* cultures with acLDL resulted in strong surface

reactions of *E. bovis*-infected host cells (**Fig. 4.21**.) indicating an increased binding of acLDL in these cells.

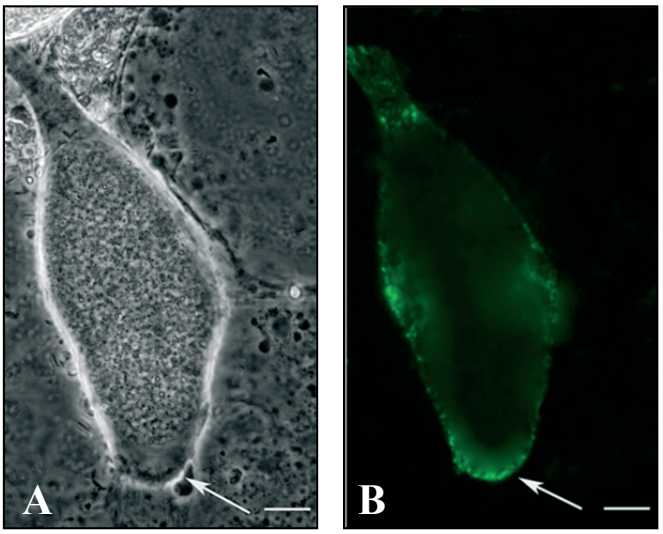

Fig. 4.21. acLDL binding on *E. bovis*-infected host cells
E. bovis-infected BUVEC (17 days p. i.) were starved in LDL-free medium, exposed to bodipy-acLDL, fixed and analysed using conventional fluorescence microscopy (scale bars: 20 µm). (A) phase contrast, (B) bodipy-acLDL-based green fluorescence

In agreement, FACS-based quantification confirmed a significant ($p < 0.0001$) enhancement of acLDL binding on *E. bovis*-infected host cells (5.2-fold, **Fig. 4.22.**). Overall, the relative increase was lower than that induced by non-modified LDL.

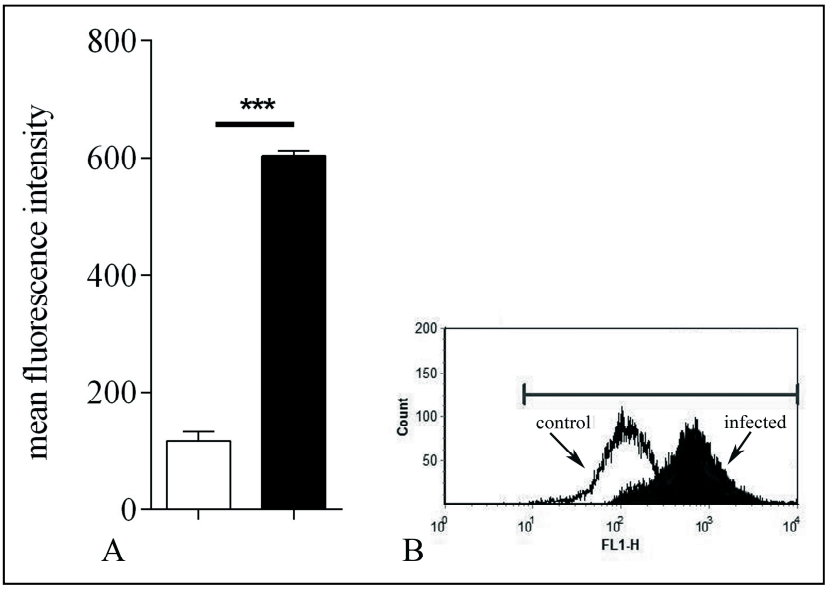

Fig. 4.22. Quantitative assessment of acLDL binding to *E. bovis*-infected BUVEC
E. bovis-infected (17 days p. i.; black bar/pannel) and non-infected (white bar/pannel) BUVEC were starved in LDL-free medium, exposed to bodipy-acLDL, fixed and analysed by flow cytometry. **(A)** means of three different BUVEC isolates in triplicate, **(B)** exemplary histogram

4.4.2 *Surface LDL receptor (LDLR) expression on E. bovis-infected host cells*

LDL binding assays indicated an increased binding of LDL to *E. bovis*-infected cells. To estimate whether these reactions originated from enhanced surface LDLR expression, a flow cytometry-based assay was established utilizing an LDLR-specific antibody and tested on *E. bovis*-infected BUVEC at 17 days p. i.

As expected, the data revealed a significant ($p < 0.0001$), infection-induced increase of LDLR surface expression (1.92 fold) in macromeront-carrying host cells. These results indirectly confirmed the data obtained via LDL binding assays.

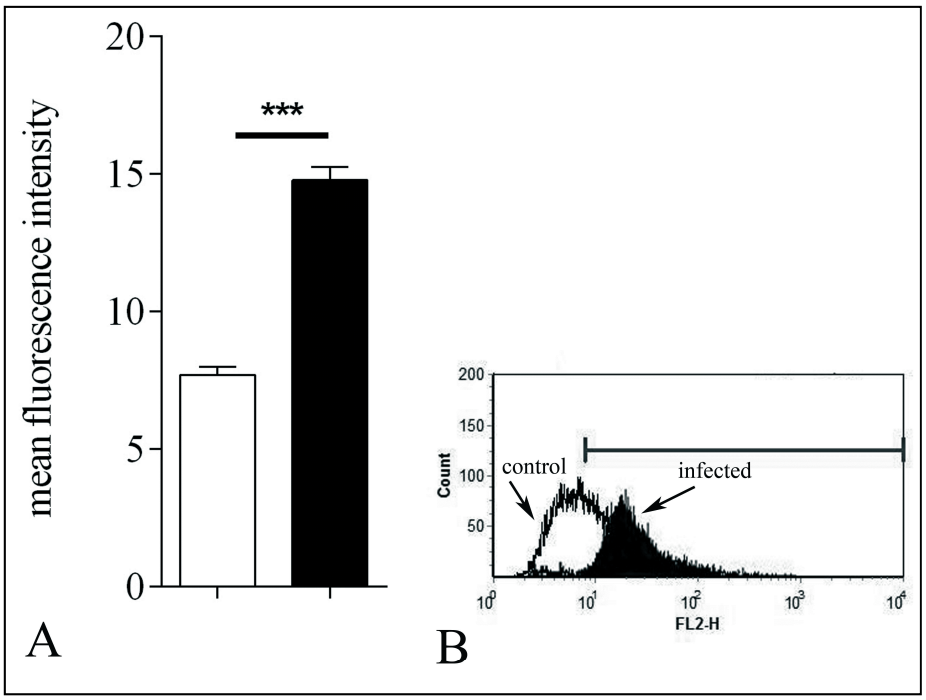

Fig. 4.23. LDLR surface expression on *E. bovis*-infected host cells
E. bovis-infected BUVEC (17 days p. i.) were reacted with primary antibodies directed against LDLR and respective conjugates and processed via flow cytometry. (A) means ± SD of three BUVEC isolates, (B) exemplary histogram.

4.4.3 *Effects of LDL enrichment on E. bovis in vitro development*

Given that LDL binding and LDLR surface expression is enhanced in *E. bovis*-infected host cells, we here investigated whether exogenous LDL supplementation would be of benefit for *E. bovis* macromeront development *in vitro*. Treated and

control BUVEC showed equal infection rates (25.2-25.4 %). Indeed, excess LDL stimulated macromeront growth. Thus, slightly increased macromeront sizes and rates were observed (**Fig. 4.24.A**). In addition, a significant ($p < 0.01$) effect of LDL enrichment on the total merozoite I production was observed (**Fig. 4.24.B**) resulting in a 1.54-fold enhancement of offspring synthesis most probably owing to an earlier maturation and release of merozoites I (**Fig. 4.24.A**).

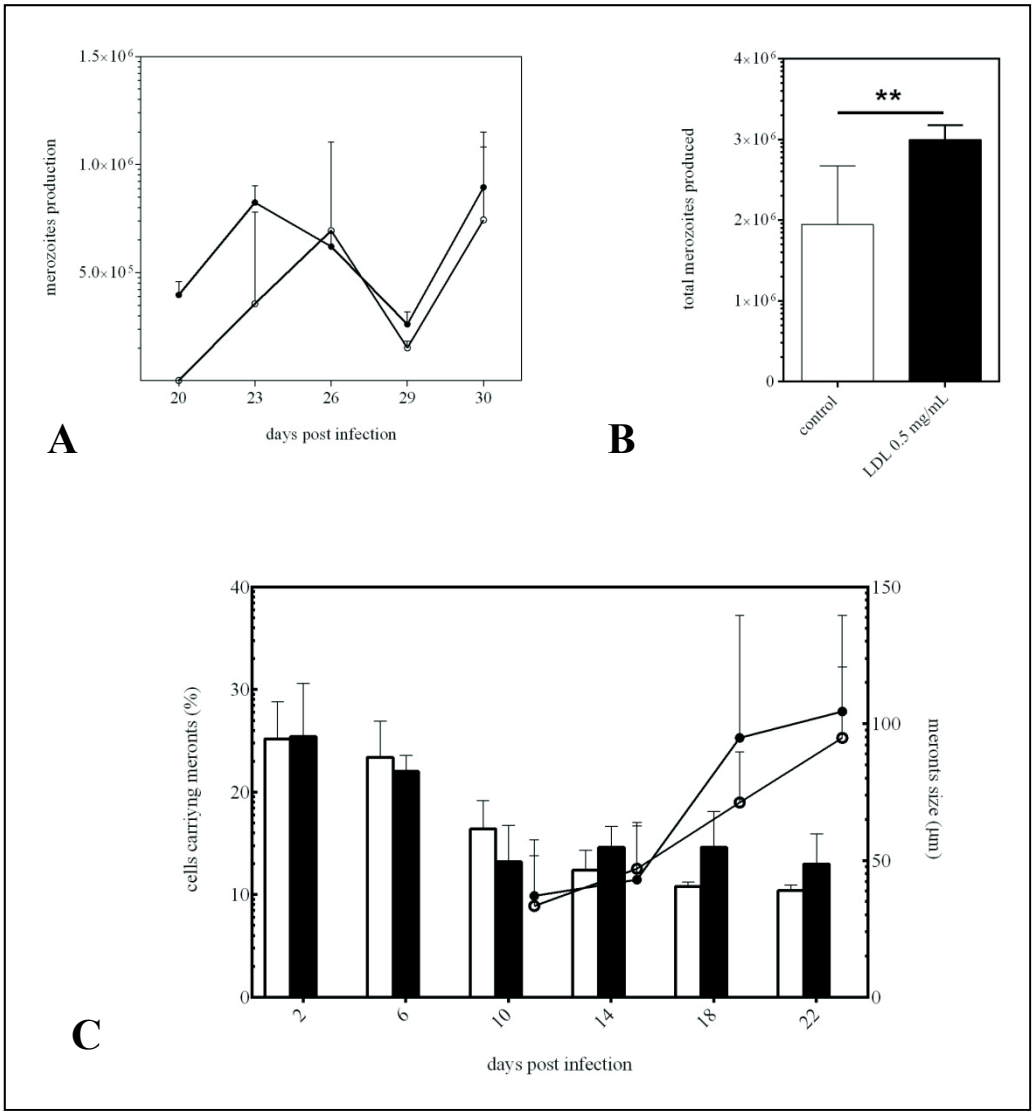

Fig. 4.24. Effect of LDL supplementation on *E. bovis in vitro* development
E. bovis-infected BUVEC were cultivated in non-supplemented (controls = white bars or open circles) and LDL-enriched (black bars or circles) medium. The effects of LDL supplementation on merozoite I production over time **(A)** and in total **(B)** were quantified using an Ebmic4-based qPCR (see **3.7.2**) after 30 days p. i. The effects on macromeront development **(C)** were assessed microscopically by estimating the rate of macromeront-carrying host cells and by measuring the sizes of developing meront stages. Arithmetic means and SD of five BUVEC isolates.

4.5 Gene transcription and protein expression of cholesterol metabolism-related molecules in *E. bovis*-infected host cells

4.5.1 *Establishment and validation of qPCR systems*

To calculate real-time qPCR efficiencies for each target gene, titration assays were performed covering at least 5 magnitudes orders of 10-fold dilutions of technical triplicates using respective plasmid DNA (**Fig. 4.25.A**). Using efficiency plots the efficiency of each system was estimated by plotting Ct values against plasmid DNA concentrations (**Fig. 4.25.B**). Overall, the Ct values ranged from 10-30. The calculated qPCR efficiencies for each system ranged from 0.93-1.08 (see **Table. 4.1.)**. Since all qPCR systems exceeded an efficiency value of 0.9, respective assays were analyzed by the delta-delta Ct method (Livak and Schmittgen, 2001, Schmittgen and Livak, 2008).

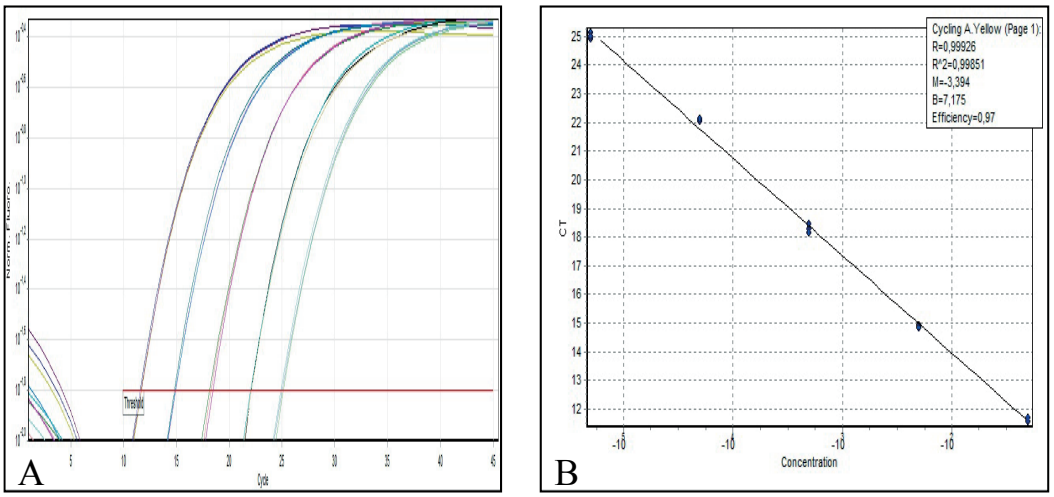

Fig. 4.25. Exemplary amplification (A) and efficiency (B) plot of titrational assays on the OLR1 qPCR system
OLR1-plasmid-DNA titrations covering 5 magnitude orders of 10 fold dilutions were processed by realtime qPCR. Data were analyzed for amplification efficiency and illustrated by an amplification (A) and efficiency (B) plot.

Table 4.1. qPCR efficiencies

Target gene	qPCR efficiency
OLR1	0.97
LDLR	1.00
HMGCS1	0.93
HMGCR	0.94
SQLE	0.93
CH25H	1.00
SOAT1	0.93
ACAT1	0.95
ACAT2	1.08
GAPDH	0.98

Since the quality of the RNA is crucial for achieving meaningful and reproducible gene expression data, exemplary RNA samples were analyzed for integrity and purity in an Agilent bioanalyzer (exemplary illustration in **Fig. 4.26.**). All RNA samples tested achieved RIN values of > 8.5 indicating good RNA qualities (Fleige et al., 2006).

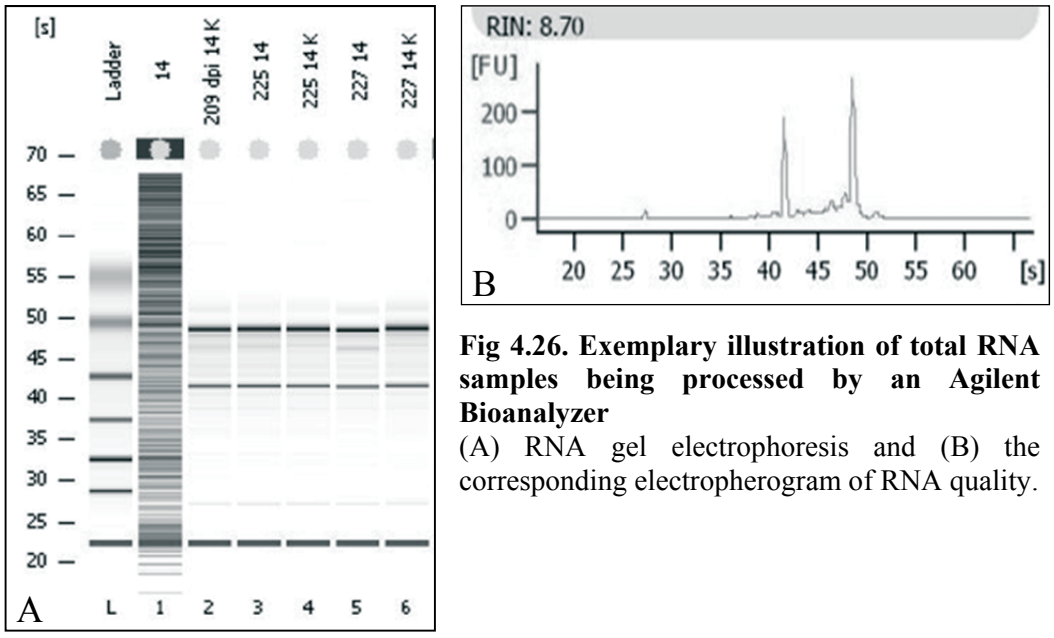

Fig 4.26. Exemplary illustration of total RNA samples being processed by an Agilent Bioanalyzer
(A) RNA gel electrophoresis and (B) the corresponding electropherogram of RNA quality.

4.5.2 *Transcriptional profiling of different molecules relevant for host cholesterol metabolism in E. bovis-infected BUVEC*

Host cell *de novo* biosynthesis of cholesterol is a multistep metabolic pathway involving more than 30 enzymatic reactions (see **Fig. 4.27.**). In these experiments transcriptional profiles of several relevant molecules were analyzed during *E. bovis* macromeront formation *in vitro*.

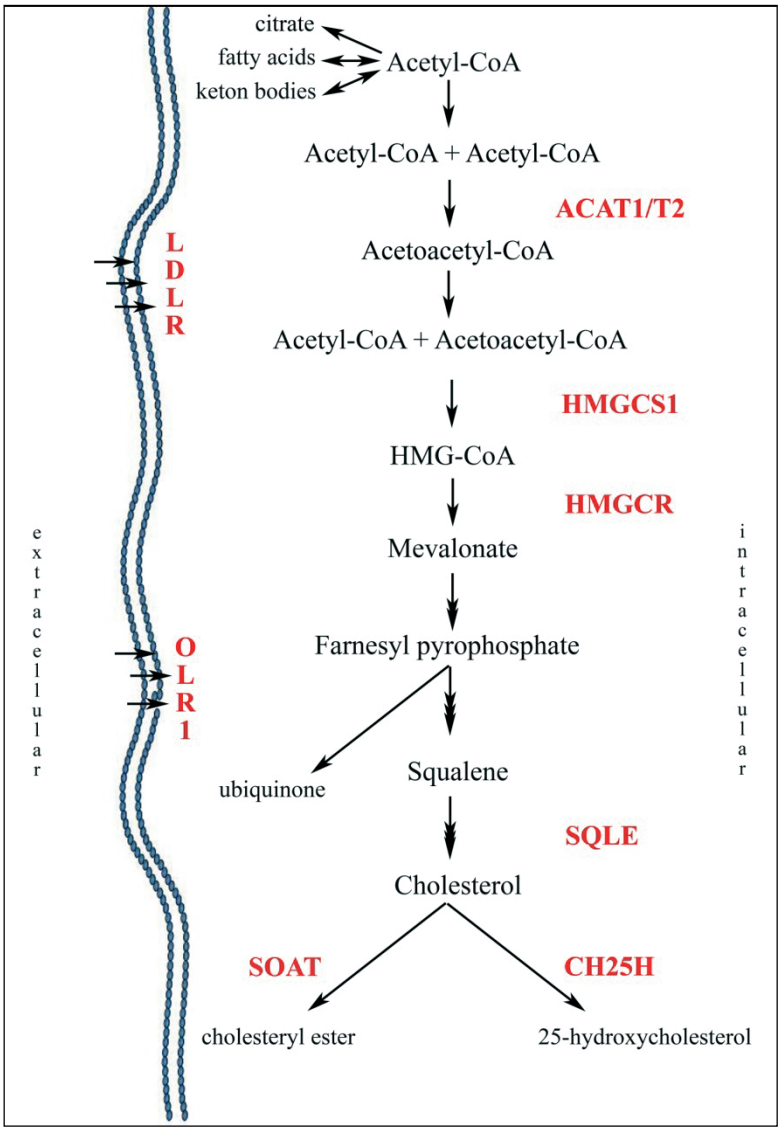

Fig. 4.27. Host cell intracellular *de novo* synthesis and uptake of cholesterol via extracellular lipid sources and indication of molecules of interest in this investigation
Modified according to Goldstein and Brown (1990), Vance and Vance (2004), Ikonen (2008).

For the formation of acetoacetyl-CoA representing an important substrate of the mevalonate biosynthesis pathway, ACAT1/ACAT2 activities are needed (Vance and Vance, 2004). Gene transcription profiles of *E. bovis*-infected BUVEC in times of macromeront formation revealed the highest and significant upregulation ($p < 0.01$) for both molecules at 17 days p. i. indicating a high demand of acetoacetyl-CoA when merozoites I are to be formed (**Fig. 4.28**.). Overall, the up-regulation of ACAT1 gene transcripts (11.03 ± 2.53-fold) was higher than that of ACAT2 (4.41 ± 2.7-fold).

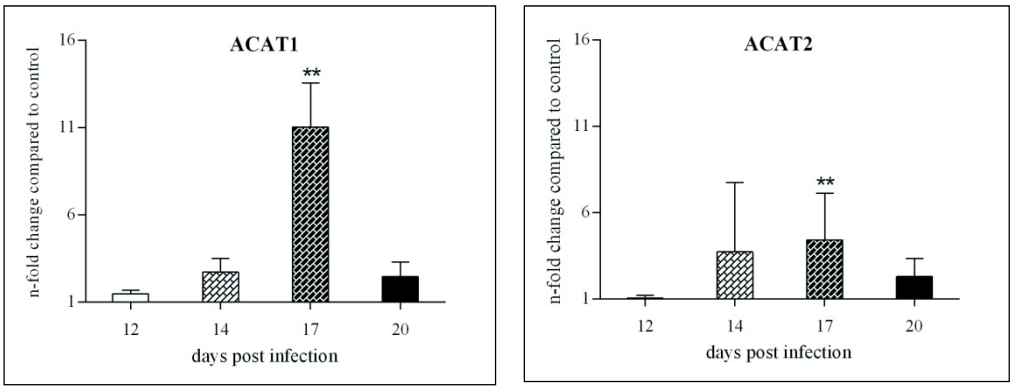

Fig. 4.28. Transcriptional pattern of the ACAT1 and ACAT2 genes during *E. bovis* macromeront formation *in vitro*
E. bovis-infected BUVEC were analyzed for ACAT1 and ACAT2 gene transcription at different time points of macromeront formation (12, 14, 17 and 20 days p. i.) applying realtime qPCR. Data represent means of three BUVEC isolates ± SD.

The initial steps of the mevalonate pathway are catalyzed by HMGCS1 promoting the formation of 3-hydroxy-3-methylglutaryl-CoA (HMG-CoA), and by HMGCR which is described as rate-limiting step of this pathway triggering mevalonate formation. Mevalonate is an essential intermediate for the biosynthesis of both, sterols and non-sterol isoprenoids which are critical for eukaryotic cell growth and proliferation (Goldstein and Brown, 1990). In contrast, SQLE-mediated squalene fomation represents the key step for cholesterol production (Buhaescu and Izzedine, 2007, Goldstein and Brown, 1990).

The gene transcriptions of HMGCS1, HMGCR and SQLE were all found to be up-regulated during *E. bovis* macromeront formation (**Fig. 4.29.**). Significant reactions were detected at 17 and 20 days p. i. for all three molecules analyzed

(HMGCS1: $p < 0.05$, HMGCR and SQLE: $p < 0.01$) and additionally for SQLE at 20 days p. i. ($p < 0.05$) (**Fig. 4.29.**). These data explicitly indicate that *E. bovis* macromeront development interfers with the host cell *de novo* synthesis via the mevalonate biosynthesis pathway. Given that all molecules were equally found up-regulated, these reactions may mirror the strong need of the parasite for excess cholesterol synthesis.

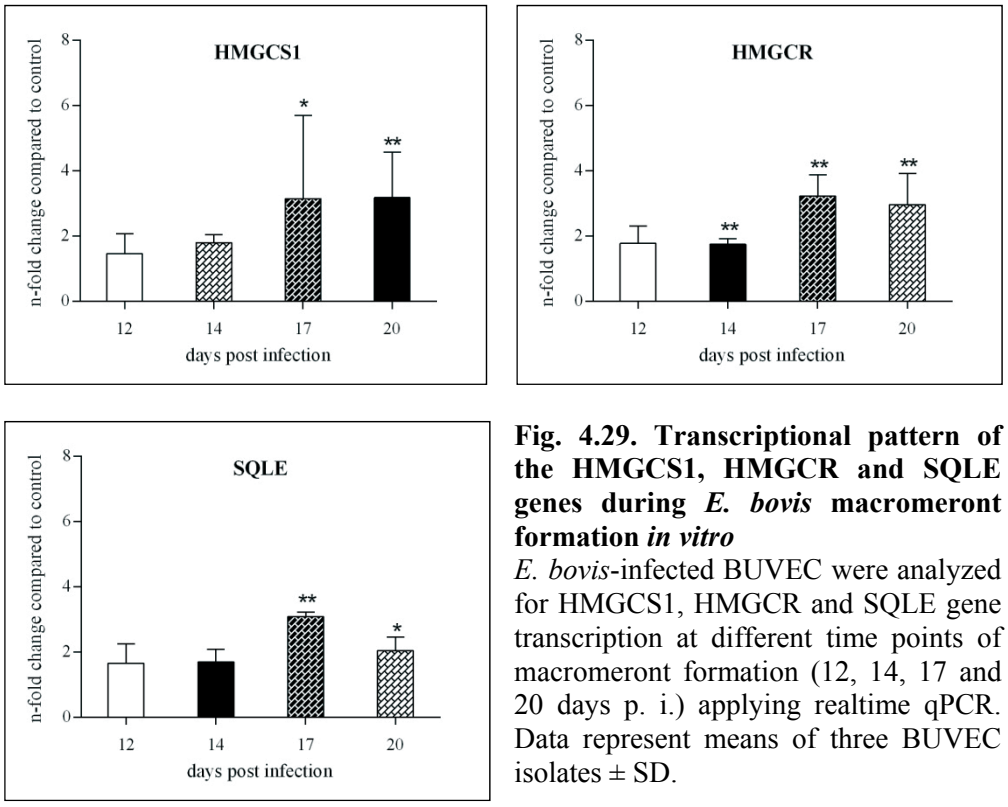

Fig. 4.29. Transcriptional pattern of the HMGCS1, HMGCR and SQLE genes during *E. bovis* macromeront formation *in vitro*
E. bovis-infected BUVEC were analyzed for HMGCS1, HMGCR and SQLE gene transcription at different time points of macromeront formation (12, 14, 17 and 20 days p. i.) applying realtime qPCR. Data represent means of three BUVEC isolates ± SD.

Following *de novo* synthesis, cholesterol may either be recycled to the membranes or be detoxified [excess of free cholesterol molecules is toxic for eukaryotic cells, (Tabas, 2002)] via further enzymatic steps. Therefore it is rapidly esterified by SOAT1 or hydroxylized via CH25H (for review see Ikonen, 2008).

Analyses on *E. bovis*-infected BUVEC revealed that both pathways of cholesterol processing were up-regulated at times of macromeront formation (**Fig. 4.30**.). Thus, SOAT1 gene transcripts were found significantly increased for 3.31- and 10.2-fold at 14 and 17 days p.i. (both $p < 0.01$), respectively, when compared to

non-infected controls. Since cholesteryl esters are stored in LD, these results indirectly confirmed the data on enhanced LD genesis in *E. bovis*-infected host cells (see **4.2.2**). The overall strongest up-regulation of all gene transcripts tested was measured for CH25H (**Fig. 4.30**.). Hence, significant enhancements of gene transcription were detected at days 14, 17 and 20 p. i. ($p < 0.0001$, $p < 0.0001$, $p < 0.01$, respectively) suggesting a crucial role of 25-hydroxycholesterol (25-HCH) synthesis in the development of *E. bovis* macromeronts.

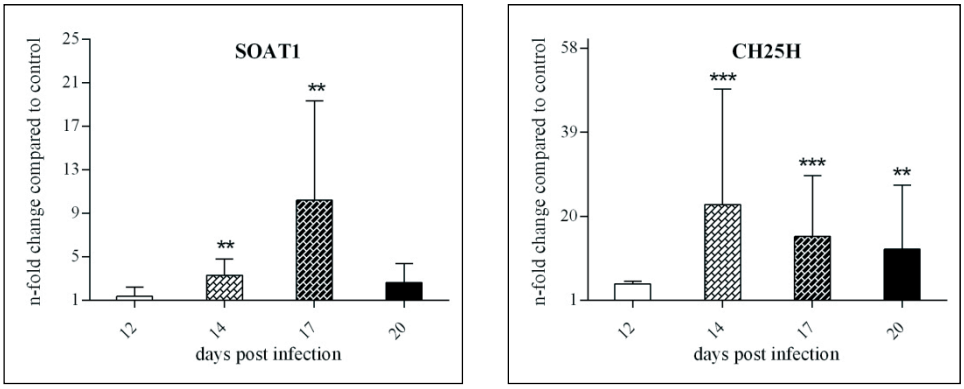

Fig. 4.30. Transcriptional pattern of the SOAT1 and CH25H genes during *E. bovis* macromeront formation *in vitro*
E. bovis-infected BUVEC were analyzed for SOAT1 and CH25H gene transcription at different time points of macromeront formation (12, 14, 17 and 20 days p. i.) applying realtime qPCR. Data represent means of three BUVEC isolates ± SD.

Besides being synthesized via the mevalonate pathway, cholesterol is also incorporated by cells from exogenous sources via LDL (Brown and Goldstein, 1986). LDL-mediated cholesterol internalization is a receptor-dependent process involving LDLR (present on most cell types) or scavenger receptors, which are restricted to certain mammalian cell types (Twigg et al., 2012). Analyzing LDLR and OLR1, we accounted for two molecules being known to be involved in the receptor-mediated pathway.

Transcriptional profiling of LDLR and OLR1 in *E. bovis*-infected host cells showed significantly enhanced mRNA levels for both molecules (**Fig. 4.31.**). Compared to non-infected controls, significant reactions were detected for LDLR at 12 and 17 days p. i. (both $p < 0.01$, respectively) reaching an up to 9.49-fold

increase. OLR1 gene transcripts were significantly enhanced during the entire period of investigation, i. e. throughout total meront I formation (12, 17 and 20 days p. i.: $p < 0.01$, 14 days p. i.: $p < 0.5$, **Fig. 4.31**.) reaching an average of up to 7-fold increase in *E. bovis* infected cells.

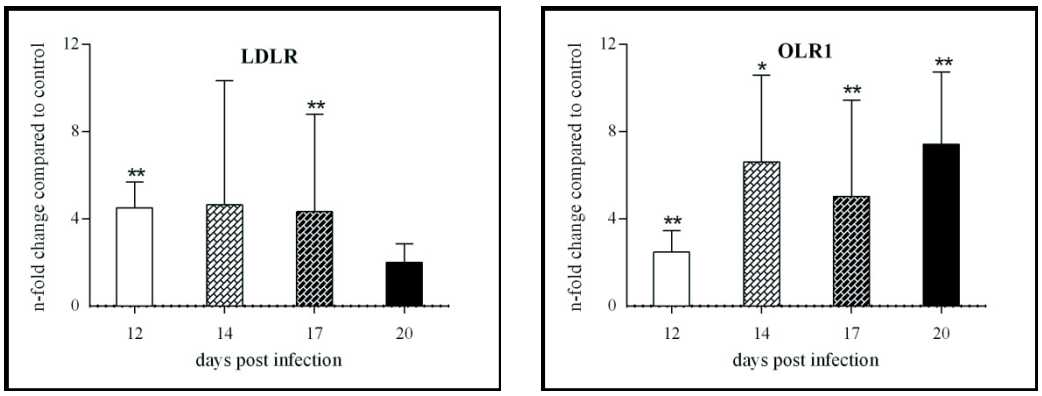

Fig. 4.31. Transcriptional pattern of the LDLR and OLR1 genes during *E. bovis* macromeront formation *in vitro*
E. bovis-infected BUVEC were analyzed for LDLR and OLR1 gene transcription at different time points of meront I formation (12, 14, 17 and 20 days p. i.) applying realtime qPCR. Data represent means of three BUVEC isolates ± SD.

Overall, the gene transcription data strongly suggest that *E. bovis* expoits both mechanisms of cholesterol acquisition, i. e., host cell *de novo* synthesis and receptor-mediated internalization of extracellular lipid sources.

4.5.3 *Protein expression of ACAT1, CH25H, OLR1 and SOAT1 in E. bovis-infected BUVEC*

To confirm the transcriptional data on protein level, the expression levels of ACAT1, CH25H, OLR1 and SOAT1 were determined via semiquantitative Westernblot analysis in *E. bovis*-infected BUVEC and in non-infected control cells in parallel. Therefore, the date of maximum gene transcript up-regulation (17 days p. i.) was chosen. Given that only a limited panel of commercial antibodies is available in the bovine system, we had to restrict our analyses on ACAT1, CH25H, OLR1 and SOAT1. As illustrated in **Fig. 4.32.** ACAT1, CH25H, OLR1 and SOAT1 protein expressions were all found up-regulated in *E. bovis*-infected BUVEC at times of meront I formation confirming previous transcriptional data (see **4.5.2**). The most prominent signals were observed for CH25H, which is also in agreement with gene transcription profiles. It is worth noting, that ACAT1, CH25H and SOAT1 were expressed at a low level in non-infected cells, whilst OLR1 showed strong signals already in the controls indicating a general high abundance of this scavenger receptor in the endothelial cell type.

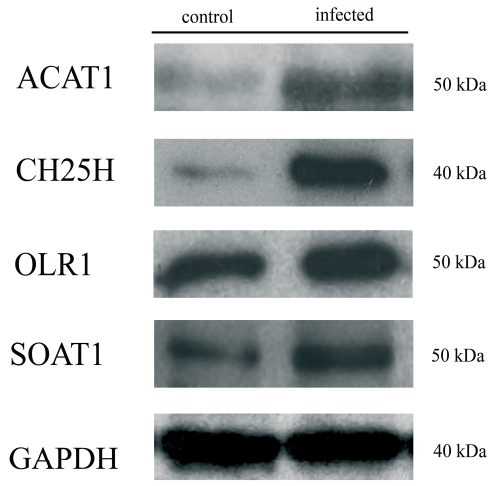

Fig. 4.32. ACAT1, CH25H, OLR1 and SOAT1 expression in *E. bovis*-infected cells
E. bovis-infected BUVEC (17 days p. i., n = 3) were harvested for total protein isolation and processed by Western blot analysis applying primary antibodies directed against ACAT1, CH25H, OLR1 and SOAT1. Figure shows an expemplary Western blots of ACAT1, CH25H, OLR1 and SOAT1 expression.

4.6 Inhibition of *E. bovis in vitro* development by interference with the mevalonate biosynthesis pathways and fatty acid synthesis

4.6.1 *Evaluation of adequate inhibitor concentrations*

Given that primary endothelial cells generally react very sensitive and do not tolerate common inhibitor concentrations, we here performed cytotoxicity assays for each inhibitor (lovastatin, zaragozic acid, CI976 and C75). As depicted in **Fig. 4.33**. high mortality rates were induced in BUVEC by concentrations ranging from 200 to 12.5 µM irrespective of the type of inhibitor. Whilst a concenctration of 6.25 µM of zaragozic acid, CI976 and C75 treatments induced little cell death in BUVEC, lovastatin concentrations had to be lowered to 1.58 µM to achieve comparable effects (**Fig. 4.33.C**). Considering these results, the following inhibitor concentrations were chosen for *E. bovis*-related inhibition experiments: 1 µM for lovastatin and 5 µM for zaragozic acid, CI976 and C75 treatments.

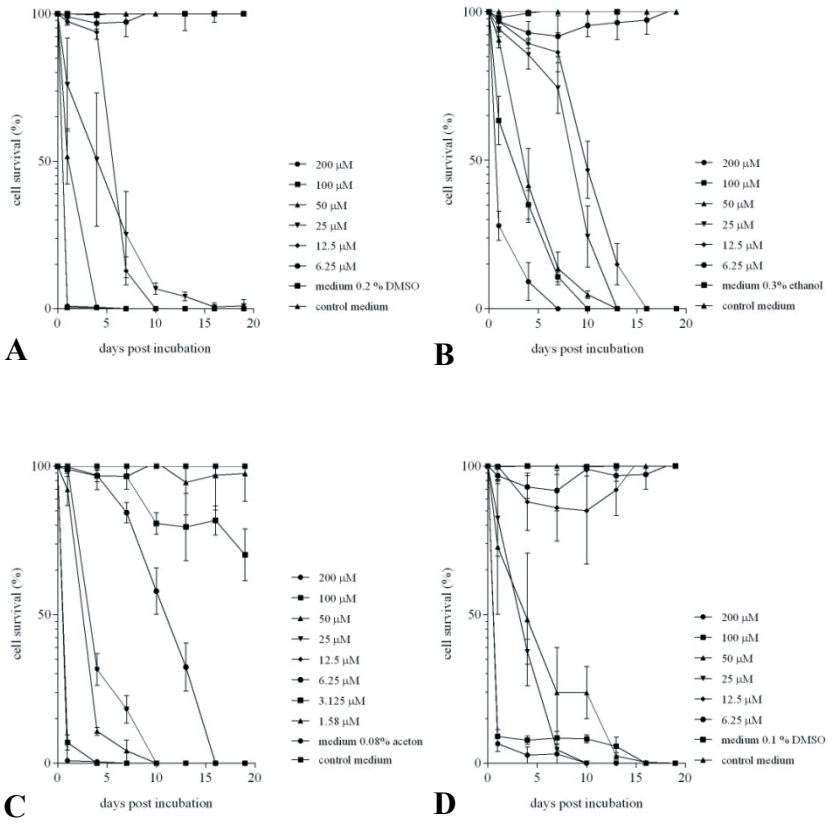

Fig. 4.33. Cytotoxicity of CI976 (A), zaragozic acid (B), lovastatin (C) and C75 (D) for BUVEC

BUVEC were treated with different concentrations of lovastatin, zaragozic acid, CI976 and C75 for indicated days before being processed for MTT test.

4.6.2 *Establishment of Ebmic4-based qPCR for merozoites I quantification*

To avoid laborious manual counting of offspring production, an Ebmic4-based realtime qPCR was established for merozoite I quantification. Therefore, efficiency and sensitivity analyses were performed. To calculate the qPCR efficiency, titration assays were performed covering at least 6 magnitudes orders of 10-fold dilutions of DNA derived from manually pre-counted merozoites I (ranging from 1.6 x 10^6 - 1.6 x 10^1 specimens) and of plasmid DNA (**Fig. 4.34**.). The efficiency of the Ebmic4-PCR system was estimated by plotting Ct values against DNA concentrations (**Fig. 4.34**.).

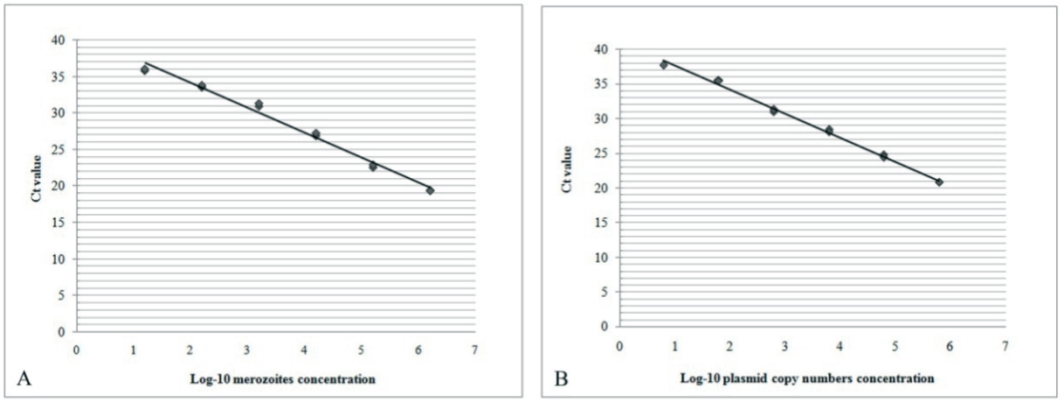

Fig. 4.34. Efficiency plots of the Ebmic4-specific qPCR system
Merozoite I (A) and Ebmic4 plasmid (B) DNA titrations covering 6 magnitude orders of 10 fold dilutions were processed by Ebmic4-specific realtime qPCR. Data were analyzed for amplification efficiency and illustrated by efficiency plots.

For both sample types the Ebmic4-based qPCR proved high efficiency. Thus, PCR efficiencies ranged from 0.99 to 1.11 (r^2: 0.97-0.99) when using plasmid DNA as template and from 0.93-1.03 (r^2: 0.98-0.99) when merozoite I DNA was tested. Addionally, the Ebmic4-based PCR system showed a high sensitivity since at least 6 plasmids and 2 merozoites I were detected in a 5 µl-sized sample (this volume was generally applied per reaction in respective PCR experiments).

Furthermore, the reproducibility of the standard curves was good as tested by three independent titration experiments using merozoite I DNA (**Fig. 4.35.A**). In general, a titration of merozoite I DNA was included in each PCR experiment as

standard. As depicted in **Fig. 4.35.C**, the Ct values of randomly chosen, culture-derived test samples fitted well to those of the standard curve and allowed for reliable merozoite I quantification.

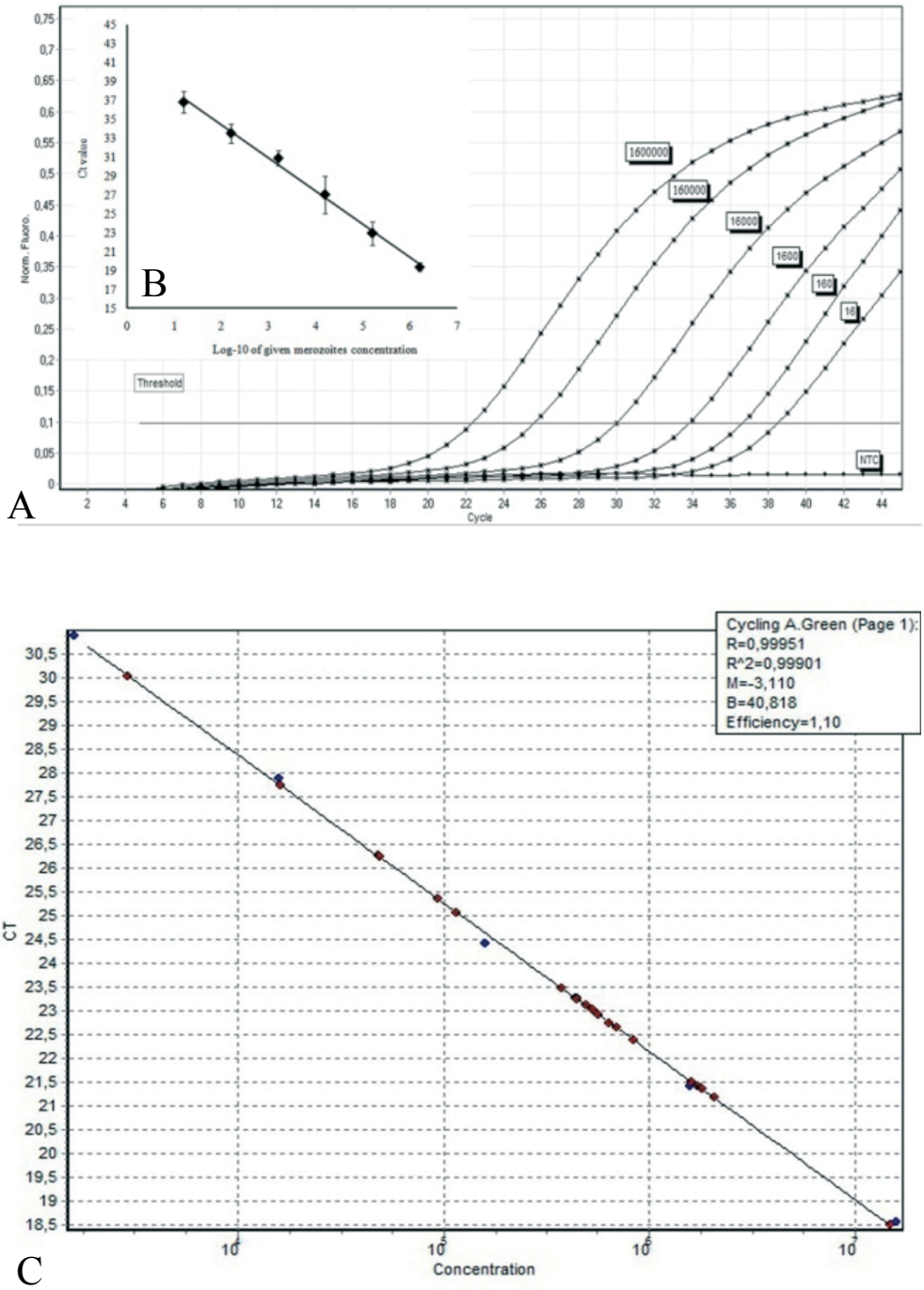

Fig. 4.35. Merozoite I-based standard curve amplification and reproducibility and offspring quantification in test samples
(A) Amplification plot of 10-fold dilutions of merozoites I ranging from 1.6 x 10^6-1.6 x 10^1 specimens, **(B)** Ct values of three independent titration experiments plotted against merozoite numbers, **(C)** Comparative plot of Ct values of exemplary test samples (red quarders) plotted on standard Ct values (blue quarders).

4.6.3 *Inhibition of HMGCoA reductase*

Lovastatin treatments of *E. bovis*-infected BUVEC exhibited significant effects on both, the rate and the size of developing macromeronts (**Fig. 4.36.**). As such, the rate of cells carrying developing macromeronts was significantly lower in treated cultures compared to non-treated ones at most time point tested (10, 26 and 30 days p.i.: $p < 0.01$; 14, 18 and 22 days p. i.: $p < 0.0001$, **Fig. 4.36.**) indicating an arrest of development and degradation of *E. bovis* meronts (for illustration see **Fig. 4.36.B**). In fact, the rate of meront carrying host cells was below 2 % at 30 days p. i. compared to 8.2 % in the controls (**Fig. 4.36.**). Also the growth of meronts was arrested by lovastatin treatments and, consequently, the meront sizes did not improve any further towards the end of the incubation period (14 days p.i.: $p < 0.05$; 22 days p.i: $p < 0.01$; 18, 26 and 30 days p.i.: $p < 0.0001$, **Fig. 4.36.**).

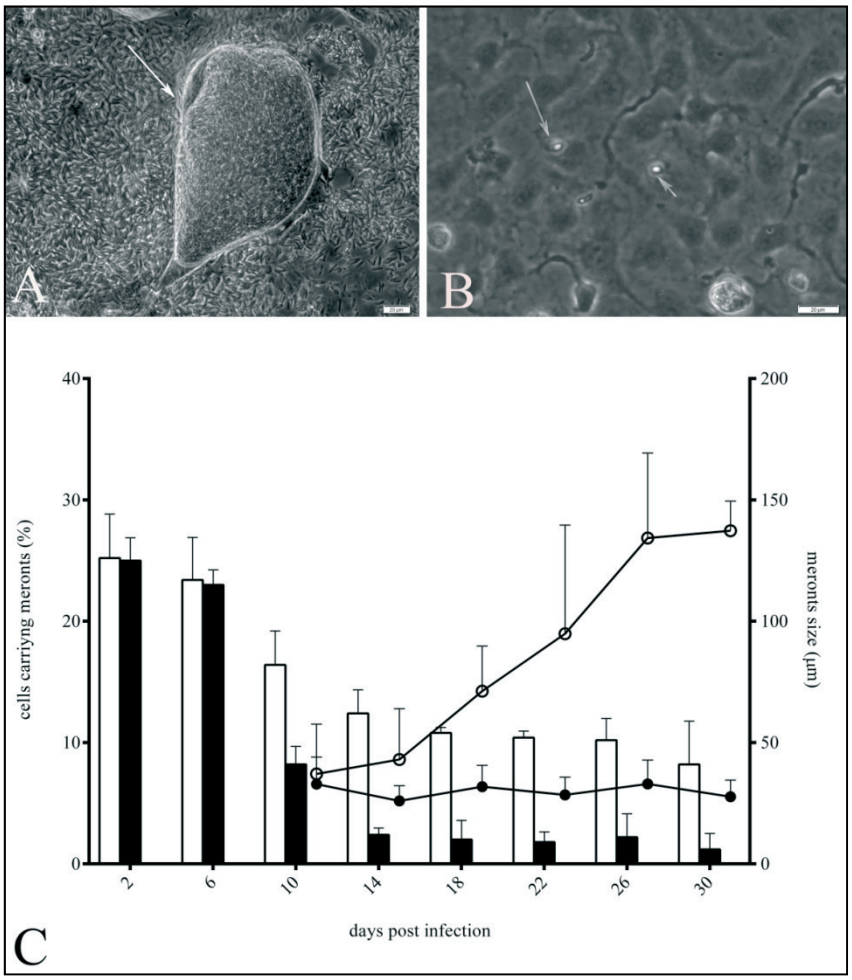

Fig. 4.36. *E. bovis* macromeront development in lovastatin-treated BUVEC cultures
E. bovis-infected BUVEC (n = 5) were treated with lovastatin (1 µM) from 1 day p. i. onwards (B) and compared to non-treated *E. bovis*-infected cultures (A). The effects of treatment (C) were assessed microscopically by estimating the rate of macromeront-carrying host cells (black bars: lovastatin-treated infected cells, white bars: non-treated infected controls) and by measuring the size of developing macromeronts (black circles: treated cultures, open circles: controls). (A) and (B) show exemplary illustrations of non-treated and treated *E. bovis*-infected (17 days p. i.) BUVEC, respectively. Scale bars: 20 µm.

In addition, lovastatin treatments effectively inhibited the *E. bovis* merozoite I production (**Fig. 4.37.**). These effects were dose-dependent since increasing concentrations of lovastatin showed enhanced effects on parasite replication (**Fig. 4.37.A**). Thus, significant effects were determined at lovastatin concentrations of ≥ 0.05 µM (0.05 µM: $p < 0.05$, 0.1 µM: $p < 0.01$, 0.5 µM and 1 µM: $p < 0.0001$). Compared to non-treated controls, a reduction of 99.6 ± 0.1% of total merozoite I production was achieved via lovastatin (1 µM) treatment. Based on the inhibition of merozoite production an IC_{50} of 0.1 µM ($r^2 = 0.9$) was calculated for lovastatin treatments (**Fig. 4.37.B**).

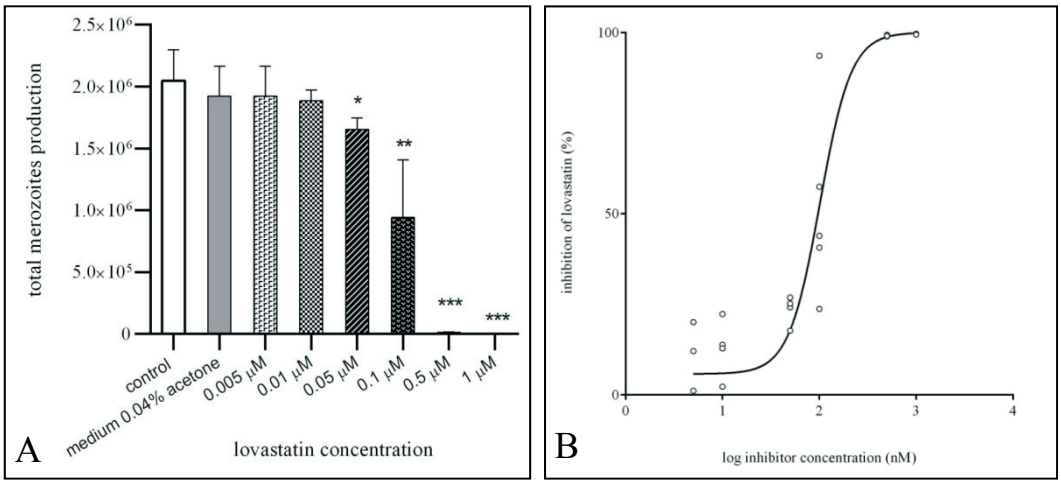

Fig.4.37. Effects of lovastatin treatment on the merozoite I production
E. bovis-infected BUVEC (n = 5) were treated with different doses of lovastatin and assessed for merozoite I production (A) using Ebmic4-based qPCR (see **3.7.2.**). To calculate the IC_{50} of lovastatin treatment, inhibitor doses were plotted against the respective reduction of merozoite I production (relative to non-treated, *E. bovis*-infected cultures).

4.6.4 *Inhibition of squalene synthase*

Treatments of *E. bovis*-infected BUVEC with zaragozic acid also resulted in a significant reduction of the rates of host cells carrying developing macromeronts and in significantly decreased macromeront sizes (**Fig. 4.38.**) underlining the key role of the cellular *de novo* cholesterol biosynthesis for successful parasite replication. The overall effects of zaragozic acid supplementation appeared less prominent than those induced by lovastatin treatment. Thus, the enlargement of developing macromeronts moderately improved with ongoing *in vitro* culture and significant differences in comparison to non-treated controls were achieved only towards the end of macromeront maturation from 26 days p. i. onwards (26 days p.i.: $p < 0.0001$; 30 days p. i.: $p < 0.01$, **Fig. 4.38.**). In addition, zaragozic acid treatment had less dramatic effects on infection rates at the meront stage than lovastatin treatments (14, 18 and 26 days p.i.: $p < 0.01$; 22 days p.i.: $p < 0.0001$, **Fig. 4.37.**). Nevertheless, we observed a significant inhibition of macromeront formation and clear detrimental effects on macromeront development as visualized by meront shrinkage and blebbing (for illustration, see **Fig. 4.38.B**).

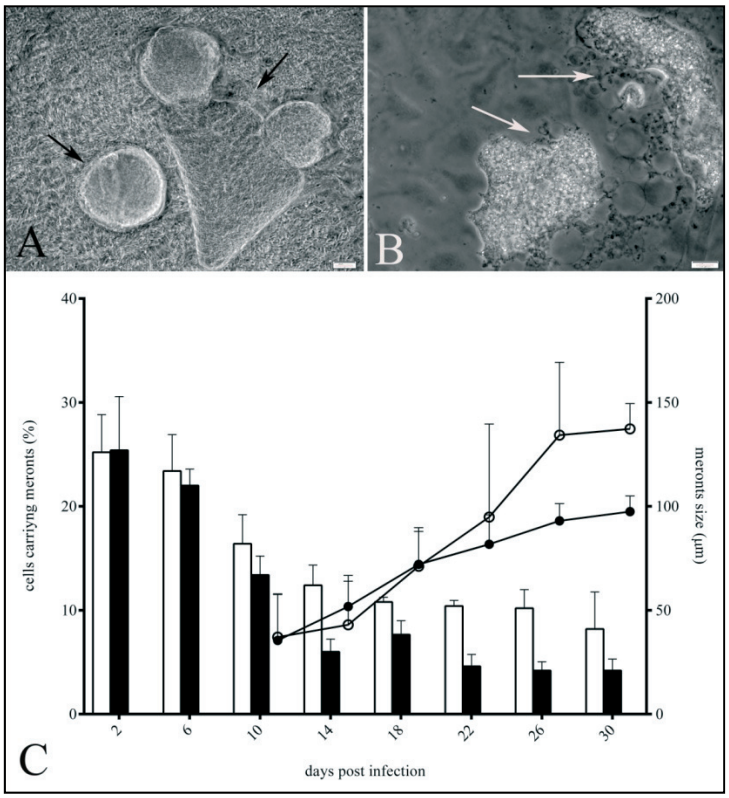

Fig. 4.38. *E. bovis* macromeront development in zaragozic acid-treated BUVEC cultures
E. bovis-infected BUVEC (n = 5) were treated with zaragozic acid (5 µM) from 1 day p. i. onwards (B) and compared to non-treated *E. bovis*-infected cultures (A). The effects of treatment (C) were assessed microscopically by estimating the rate of macromeront-carrying host cells (black bars: zaragozic acid -treated infected cells, white bars: non-treated infected controls) and by measuring the size of developing meronts (black circles: treated cultures, open circles: controls). (A) and (B) show exemplary illustrations of non-treated and treated (note strong degradation as indicated by arrows) *E. bovis*-infected (17 days p. i.) BUVEC, respectively. Scale bars: 20 µm (A) and 10 µm (B).

In addition, the total merozoite I production of infected host cells was significantly inhibited in zaragozic acid treated cultures (**Fig. 39.B**). This effect proved to be dose-dependent (2.5 µM: $p < 0.01$; 5 µM:$p < 0.0001$) and resulted in a 70.2 ± 11.6% reduction, when zaragozic acid was applied at 5 µM final concentration (**Fig. 39.B**). Based on the inhibition of merozoite I production we calculated an IC_{50} of 3.32 µM (r^2= 0.96) for zaragozic acid treatment.

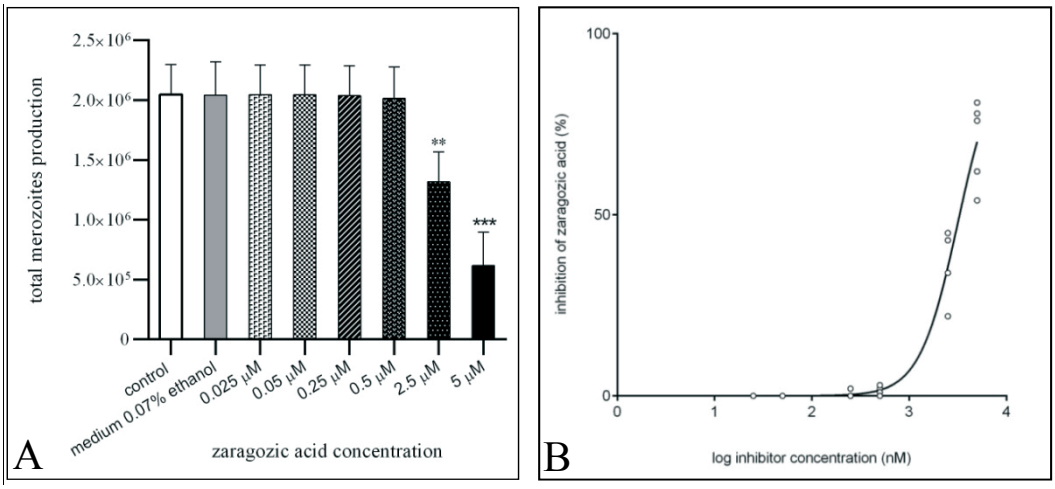

Fig. 4.39. Effect of zaragozic acid treatment on the merozoite I production
E. bovis-infected BUVEC (n = 5) were treated with different doses of zaragozic acid and assessed for merozoite I production (A) using Ebmic4-based qPCR (see **3.7.2**). To calculate the IC_{50} of zaragozic acid treatment, inhibitor doses were were plotted against the respective reduction of merozoite I production (relative to non-treated, *E. bovis*-infected cultures).

4.6.5 *Inhibition of acyl-CoA cholesterol acyltransferase*

Treatments with CI976 were applied to inhibit cholesterol esterification within infected host cells via blockage of acyl-CoA cholesterol acyltransferase. We here chose two different time points of treatment onset with 1 and 10 days p. i. in order to affect both, trophozoite and macromeront formation.

Overall, both CI976 treatments led to an arrest of parasite development (treatment since 1 day p.i.= 10 and 14 days p.i.: $p < 0.01$; 18, 22, 26 and 30 days p. i.: $p < 0.0001$; treatment started from 10 days p.i.= 18 and 22 days p.i: $p < 0.01$; 26 and 30 days p.i.: $p < 0.0001$, **Fig. 4.40.**) since no significant development or macromeront growth was observed throughout the investigation period compared to control monolayers (for illustration see **Fig. 4.40.B, C**). When treatment started at 1 day p. i. sporozoites failed to develop any further and occasionally showed an untypically enlarged, round-shaped PV being accompanied by a cashew-shaped distorsion of the host cell nucleus (**Fig. 4.40.C**). In macromeronts being arrested in their development via CI976 treatment beginning at 10 days p. i., we consistently observed persistent round-shaped bodies within the macromeronts (**Fig. 4.40.B**) that may be considered as remaining refractile bodies of the parasite and, as such, are not visible in non-treated controls. Besides macromeront formation, CI976 treatments effectively inhibited merozoite I production in a dose-dependent manner (5 µM, 2.5 µM and 0.5 µM: $p < 0.0001$; 0.25 µM: $p < 0.01$; 0.05 µM: $p < 0.05$, **Fig. 4.42.**). Thus, increasing concentrations of CI976 led to a significant diminishment of parasite proliferation. Based on the inhibition of merozoite I production we calculated an IC_{50} of 0.34 µM (r^2= 0.98) for CI976 treatment.

Fig. 4.40. *E. bovis* macromeront development in CI976-treated BUVEC cultures
E. bovis-infected BUVEC (n = 5) were treated with CI976 (5 µM) from day 1 (C) or 10 (B) p. i. onwards and compared to non-treated *E. bovis*-infected cultures (A). The effects of treatment (D) were assessed microscopically by estimating the rate of macromeront-carrying host cells (black bars: day 1 p. i. onwards, grey bars: 10 day 1 p. i. onwards, white bars: controls) and by measuring the size of developing meronts (black triangles: day 1 p. i. onwards, black circles: 10 day 1 p. i. onwards, white circles: controls). A-C show exemplary illustrations of non-treated and treated (B: from 1 day p. i. and C: from 10 days p.i. onwards) *E. bovis*-infected (17 days p. i.) BUVEC, respectively. Scale bars: 20 µm.

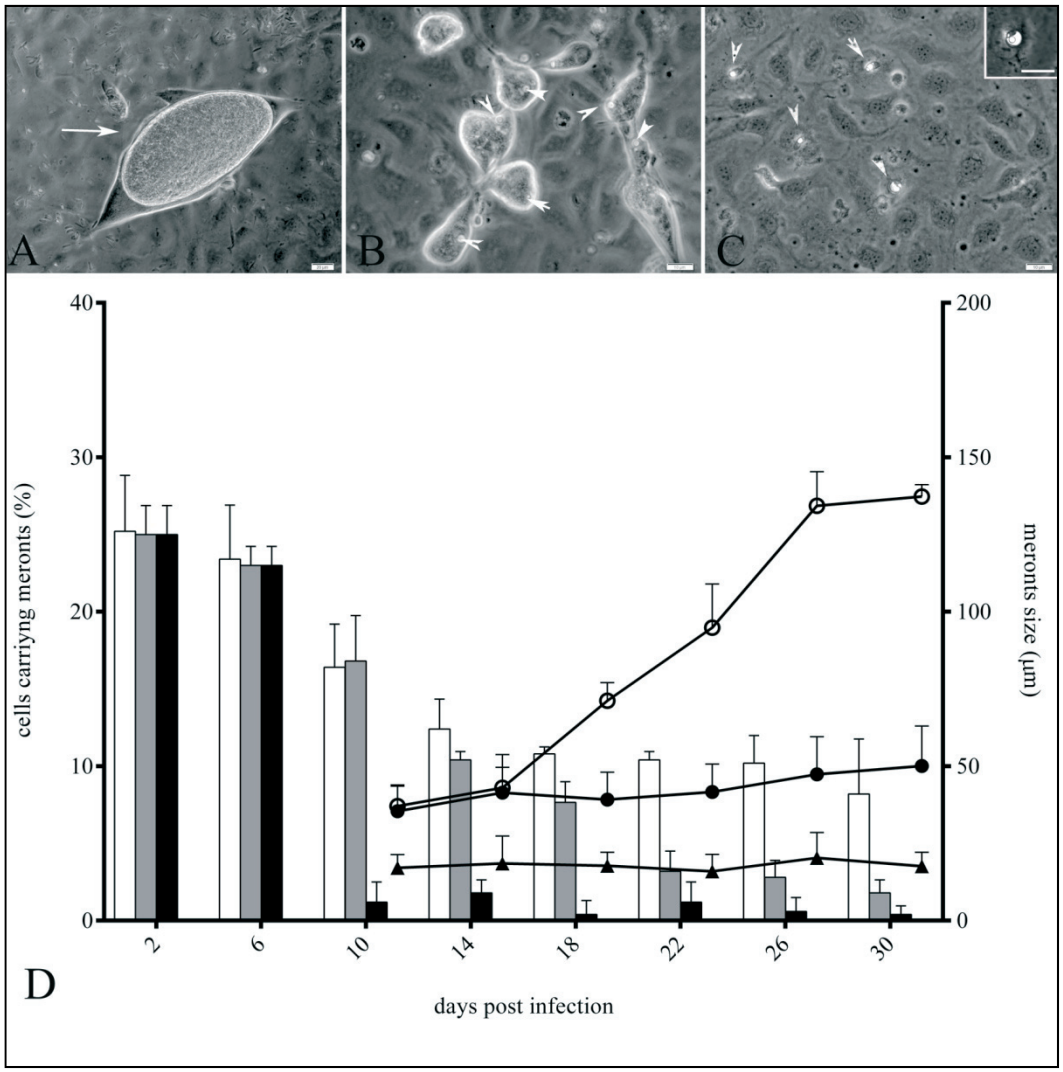

Inhibition of macromeront maturation via CI976 treatment coincided with reduced LD/neutral lipid (NL) deposition in infected host cells as confirmed by Nile red staining (**Fig. 4.41**.). Thus, non-treated *E. bovis*-infected host cells showed significantly increasing accumulation of LD-/NL-rich areas ($p < 0.0001$) with ongoing *in vitro* macromeront growth (**Fig. 4.41.D**). In contrast, CI976 treatments led to an immediate abrogation of LD/neutral lipid deposition irrespective of the onset of CI976 supplementation. In addition, throughout treatment, LD/NL deposition did not recover and remained on the same low level (**Fig. 4.41.D**). Microscopic analyses revealed a spotty appearance of LD-/NL-rich areas within infected control host cells carrying mature meronts (**Fig. 4.41.A**), whilst in treated

ones the reaction pattern were more homogeneous in immature meronts (**Fig. 4.41.B**) or were restricted to the refractile bodies of intracellular sporozoites (**Fig. 4.41.C**), all being arrested in their development when treatment was applied at 1 or 10 days p. i., respectively.

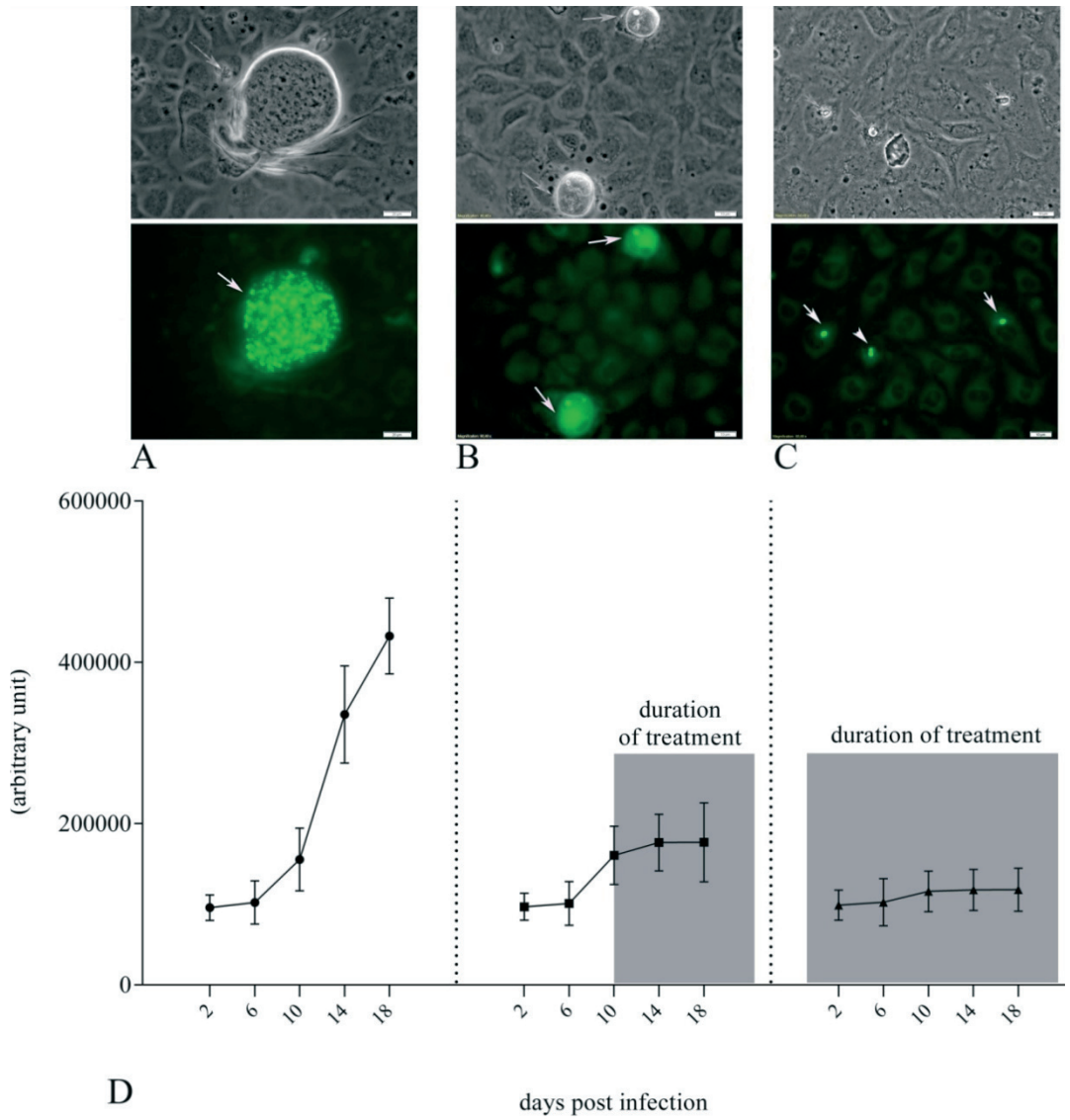

Fig. 4.41. Effects of CI976 treatments on lipid droplet (LD) deposition in *E. bovis* infected host cells
E. bovis-infected BUVEC were treated with CI976 (5 µM) from days 1 and 10 p. i. onwards. At different time points after infection (2, 4, 6, 10, 14, 18 days p. i.), cells were stained with Nile red for LD detection (for illustration see **A**: non-treated controls, 18 days p. i.; **B**: infected cells treated with CI976 from 10 days p. i. onwards, 18 days p. i.; **C**: infected cells treated with CI976 from 1 days p. i. onwards, 18 days p. i.). The amount of LDs (**D**) was estimated on single cell level via software-assisted measurements of fluorescence intensities in 10 cells per infected sample.

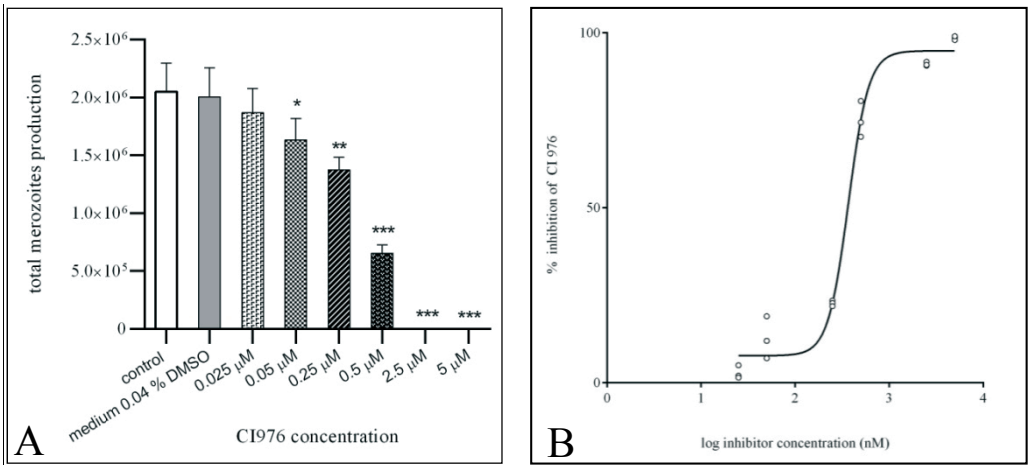

Fig. 4.42. Effects of CI976 treatment on the merozoite I production
E. bovis-infected BUVEC (n = 5) were treated with different doses of CI976 and assessed for merozoite I production (A) using Ebmic4-based qPCR (see **3.7.2.**). To calculate the IC_{50} of CI976 treatment, inhibitor doses were plotted against the respective reduction of merozoite I production (B) (relative to non-treated, *E. bovis*-infected cultures).

4.6.6 *Inhibition of fatty acid synthase*

The compound C75 blocks fatty acid synthesis thereby interacting indirectly with cholesteryl ester synthesis. Overall, the C75-treatment of *E. bovis*-infected host cells resulted in a significantly reduced parasite growth as estimated by macromeront sizes (10, 14 and 22 days p. i.: $p < 0.01$; 18, 26 and 30 days p. i: $p < 0.0001$, **Fig. 4.43**.). However, although this effect was earlier observed than in zaragozic acid treatments (**Fig. 4.38**.), the sizes slightly recovered beginning with 22 days p. i. but did not reach the values of the non-treated controls. Furthermore, the rate of cells carrying developing macromeronts was significantly lower in treated cultures when compared to non-treated ones from 18 days p. i. onwards (18, 22 and 26 days p.i.: $p < 0.01$, **Fig. 4.43**.) indicating macromeront degradation. Accordingly, microscopic analyses revealed a strong vacuolization of the macromeronts (**Fig. 4.43.B**).

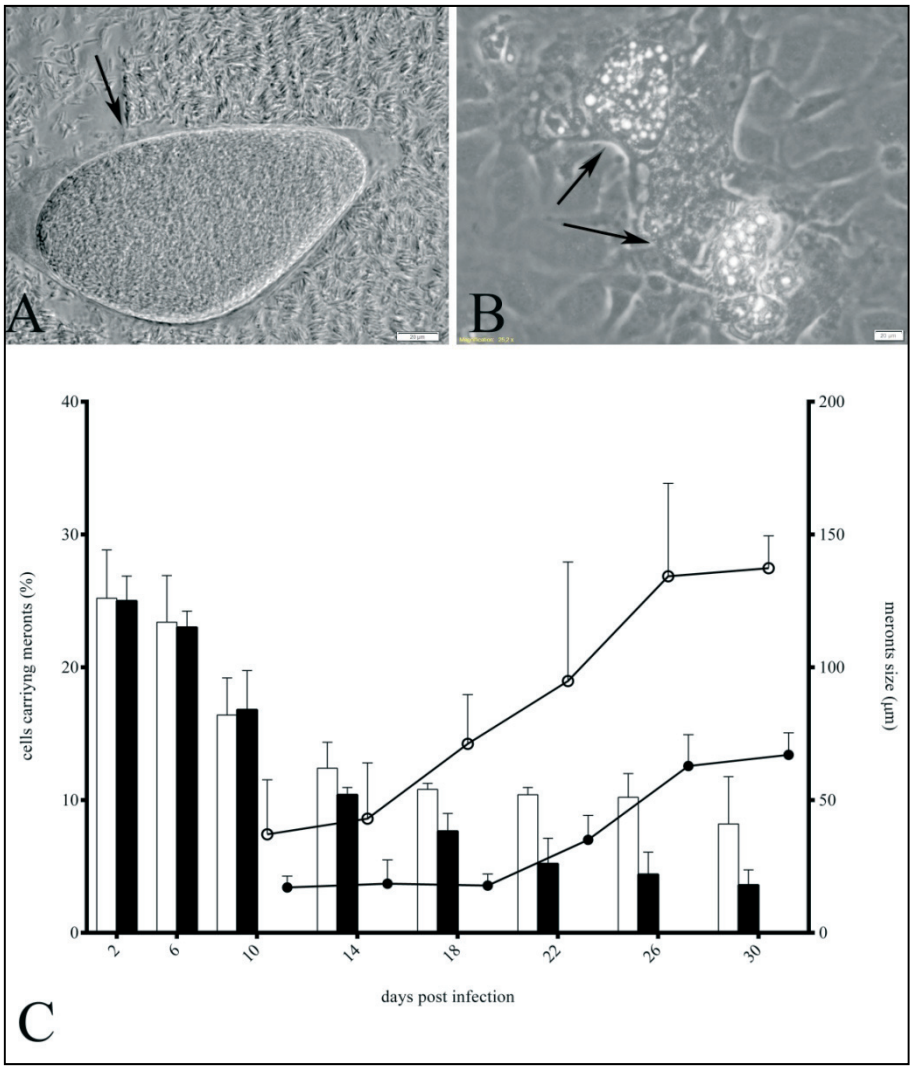

Fig. 4.43. *E. bovis* macromeront development in C75-treated BUVEC cultures *E. bovis*-infected BUVEC (n = 5) were treated with C75 (5 µM) from 1 day p. i. onwards (B) and compared to non-treated *E. bovis*-infected cultures (A). The effects of treatment (C) were assessed microscopically by estimating the rate of macromeront-carrying host cells (black bars: C75-treated infected cells, white bars: non-treated infected controls) and by measuring the size of developing meronts (black circles: treated cultures, open circles: controls). (A) and (B) show exemplary illustrations of non-treated and C75-treated (note strong vacuolization as indicated by arrows) *E. bovis*-infected (17 days p. i.) BUVEC, respectively. Scale bars: 20 µm.

In addition, C75 treatments effectively inhibited merozoite I production in a dose-dependent manner (**Fig. 4.44.**). Thus, increasing concentrations of C75 led to a significant diminishment of parasite proliferation (5 and 2.5 µM: $p < 0.0001$; 0.5 µM: $p < 0.01$; 0.25 µM: $p < 0.05$). The C75 treatments resulted in a marked reduction of merozoite I production (84.6 ± 5.32%), when being applied at 5 µM final concentration. Based on the inhibition of merozoite I production we calculated an IC_{50} of 1.28 µM ($r^2 = 0.97$) for C75 treatment.

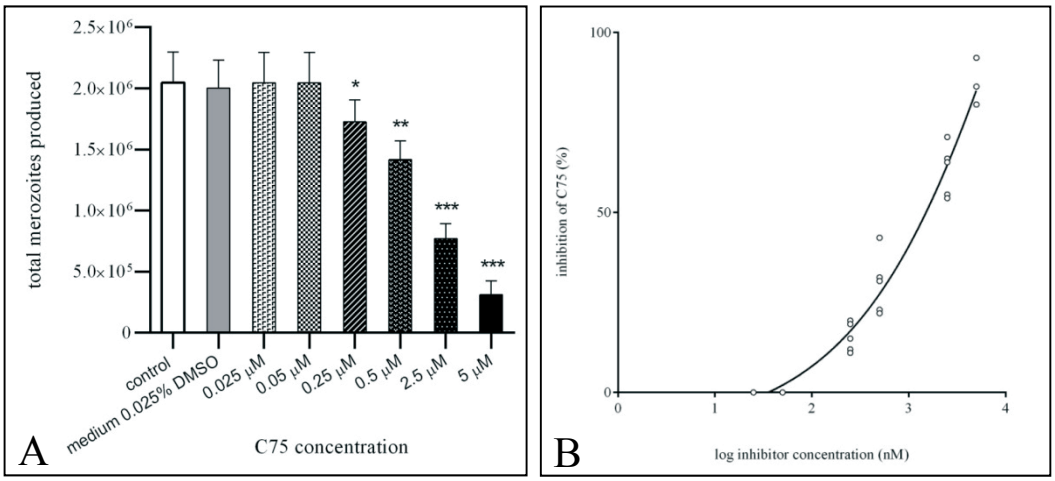

Fig. 4.44. Effects of C75 treatment on the merozoite I production
E. bovis-infected BUVEC (n = 5) were treated with different doses of C75 and assessed for merozoite I production (A) using Ebmic4-based qPCR (see **3.7.2.**). To calculate the IC_{50} of C75 treatment, inhibitor doses were plotted against the respective reduction of merozoite I production (B) (relative to non-treated, *E. bovis*-infected cultures).

Overall, all compounds tested in this investigation showed significant efficacies against *E. bovis* when estimated on the level of merozoite I production inhibition. The comparison of the dose-effect-curves and respective IC_{50} values revealed lovastatin as the most effective compound, being followed by CI976, C75 and zaragozic acid.

5 Discussion

5.1 Free cholesterol and lipid droplets accumulate in *E. bovis*-infected host cells and reveal as key factors of parasite replication

Within the first merogony, *E. bovis* forms macromeronts in lymphatic endothelial host cells. During this developmental phase, the host cell is heavily enlarged since intracellular mature macromeronts may account for up to 400 µm (Hammond et al., 1946, Hammond et al., 1966) inducing a 10-15-fold aggrandisement of the host cell. Additionally, more than 120,000 merozoites I may be formed (Hammond et al., 1946). These developmental features all bear an enormous demand for cholesterol. Overall, cholesterol is needed for three main reasons: *i*) the massive enlargement of the host cell membrane, *ii*) the formation and enlargement of the PV and *iii*) the formation of large numbers of merozoites I.

5.1.1 *Free cholesterol accumulation in parasite stages*

In order to reveal free cholesterol existence and distribution within *E. bovis* stages filipin staining was used. Filipin forms a complex with free 3′-OH-groups of cholesterol and is routinely used as a tracer for free cholesterol (Gimpl and Gehrig-Burger, 2011). For this purpose it has also been applied for some other apicomplexan parasites, such as *Plasmodium yoelii*, *T. gondii* or *C. parvum* (Coppens and Joiner, 2003, Labaied et al., 2011, Ehrenman et al., 2013).

In the case of *E. bovis*, sporozoites and merozoites I were intensively labelled in their apical part and in their outer membrane, indicating that cholesterol is not homogenously distributed within the parasite but predominantly occurs within the apical complex and the pellicle. In contrast to *P. yoelii* free sporozoites lacking filipin staining (Labaied et al., 2011), this is in line with tachyzoites of *T. gondii*, where cholesterol is enriched in the anterior apical complex exhibiting a high cholesterol/phospholipid ratio of 1.5/1 (Foussard et al., 1991b). Within this complex, cholesterol appears to accumulate in the rhoptries. Thus, the cholesterol/phopholipid ratio in these organelles was higher than in the total

tachyzoite (Foussard et al., 1991b). In agreement, rhoptry-enriched fractions of purified *T. gondii* tachyzoites also identified cholesterol as the most abundant lipid component (Besteiro et al., 2008). However, *T. gondii* rhoptries do not appear to function as cholesterol-storing organelles since filipin-derived reactions originated mainly from the basal bulbous portions of rhoptry membranes whilst their lumen was free of cholesterol (Coppens and Joiner, 2003). Furthermore, by considering the apical organelle distribution, the signals in *E. bovis* stages may additionally have originated from dense granules since these organelles have also been reported as filipin-positive in *T. gondii* tachyzoites (Coppens and Joiner, 2003). Unfortunately, laser-assisted fluorescence-based microscopic analyses allowing for higher resolution and thereby for organelle identification cannot be performed using filipin-stained samples owing to the fast bleaching of this compound. Nevertheless, the reaction pattern of *E. bovis* merozoites I were rather similar to those of newly egressed tachyzoites of *T. gondii* which exhibit prominent filipin signals in the nascent apical complex and in the remaining residual body of the mother cell (Coppens et al., 2000).

The outer membrane of *E. bovis* sporozoites and merozoites I also reacted with filipin indicating free cholesterol to be located in the pellicula. Overall, these reactions were consistant but rather weak when compared to the signals of the apical region suggesting rather low contents of free cholesterol in the pellicle. In line with these findings, tachyzoites of *T. gondii* exhibited similar reaction patterns (Coppens and Joiner, 2003) and purified pellicles of tachyzoites showed low free cholesterol contents since the cholesterol/phospholipid ratios were rather low (0.2-0.36), indicating a high level of fluidity of these membranes (Foussard et al., 1991a, b). Furthermore, filipin-derived fluorescence of *E. bovis* sporozoite and merozoite I outer membranes appeared rather heterogenous suggesting areas of cholesterol-rich microdomains as generally observed in the eukaryotic system (Albert, 2008). In agreement, transmission electron microscopic analyses showed discontinued filipin/sterol complexes in the parasite plasma membrane and inner membrane complex of *T. gondii* tachyzoite pellicles (Coppens and Joiner, 2003).

After host cell invasion, *E. bovis* sporozoites are generally located close to the host cell nucleus. One day after infection, an intense filipin labelling was observed in the area directly surrounding newly invaded sporozoites. Owing to insufficient microscopic resolution it cannot be concluded whether these reactions origin from the PV space, the PVM or from host cell-derived organelles, such as mitochondria or lysosomes which are known to be recruited in high numbers close to the PV in the case of *T. gondii* (Sinai and Joiner, 2001, Coppens et al., 2006) or *E. bovis* (C. Hermosilla, personnel observation). However, the occasionally hackly, non-circular appearence of filipin-positive areas surrounding the sporozoite rather argues against a sole PV origin.

As intracellular stage, *E. bovis* resides within its obligatory PV. In general, the PV lumen of coccidians is filled with electron dense material, intravacuolar tubules and structures extending from the PV membrane (Dubremetz and Elsner, 1979). The PV enlarges with ongoing development and often surpasses the original size of the host cell (Beyer et al., 2002, Entzeroth et al., 1998, Hermosilla et al., 2002, Ruiz et al., 2010). *E. bovis* macromeronts exhibit differential morphologies in *in vitro* cultures (Hermosilla et al., 2002). Some macromeronts contain several septae that may originate from PVM protrusions. In the current experiments both, the PV and meront-derived septae exhibited strong filipin staining in developing macromeronts. In principle, this is in accordance to findings on *T. gondii* showing that the PVM contains cholesterol (Coppens and Joiner, 2003). In addition, the PV of *P. yoelli, P. berghei* and *C. parvum* merozoite membranes revealed filipin-positive reactions (Labaied et al., 2011, Ehrenman et al., 2013). However, it has to be kept in mind that in contrast to TEM-based findings of clearly defined organelles and membranes bearing filipin-derived signals in the case of *T. gondii* (Coppens and Joiner, 2003), a clear distinguishment between the host cell membrane, PVM, PV space or even the inner part of the developing macromeront can not be performed based on the current experiments. Nevertheless, it is undoubted that enhanced levels of free cholesterol are detected in infected host cells compared to non-infected controls. Furthermore, the total intensities of

filipin signals per host cell representing free cholesterol accumulation appeared to increase with the ongoing *E. bovis* macromeront maturation process leading to the most intense reactions in fully mature macromeronts. It is tempting to speculate that this phenomenon directly mirrors the parasites need for cholesterol for the PV enlargement and numerous offspring assembly. Quantitative analyses on cholesterol contents (free + esterified form) ascertained the general phenomenon of cholesterol accumulation in *E. bovis*-infected host cells and quantitatively confirmed the qualitative impression of increasing cholesterol deposition paralleling ongoing macromeront maturation. Given that the parasite is in need of cholesterol for successful development, we used cholesterol- and desmosterol- (a cholesterol precursor) supplemented cell culture medium to enrich host cells prior to and throughout infection. In accordance to *T. gondii* (Coppens et al., 2000), excess exogenous cholesterol resulted in significantly enhanced offspring production confirming the key role of high cholesterol abundance for successful *E. bovis* macromeront development.

Pulse-labelling analyses using the fluorescent cholesterol analogue dansyl cholesterol demonstrated the capacity of *E. bovis* sporozoites to incorporate and distribute free cholesterol to diverse compartments, i. e., to the plasma membrane, the apical complex and to the refractile bodies. Since refractile bodies have previously been shown to lack free sterols by filipin staining, these data suggested that *E. bovis* may use free sterols either as substrate to form cholesteryl esters or directly integrate them in several membraneous structures. Even more evidence of differential parasite-driven cholesterol utilization was shown by pulse-labelling experiments of meront-carrying host cells where fluorescence was clearly detected in LD-like structures indicating that dansyl-cholesterol served as substrate for cholesteryl ester formation and subsequent deposition in LDs. These data are in accordance to findings in *T. gondii*-infected cells showing that NBD-cholesterol was inserted into tachyzoite membranes but was also modified and found in LD-like cytoplasmic structures (Charron and Sibley, 2002). In contrast, in *P. yoelii* and *P. berghei*-infected hepatocytes NBD-cholesterol occurred the developing

schizonts (Labaied et al., 2011) but was not utilized for cholesteryl ester production (Nawabi et al., 2003, Palacpac et al., 2004, Vielemeyer et al., 2004).

Intracellular life of *E. bovis* sporozoites begins with active host cell invasion. To assess the role of cholesterol in the initial phase of intracellular parasitism, host cell-or parasite-derived cholesterol was depleted by MBCD treatments prior to infections and the effects on subsequent infection rates were observed. Indeed, host cell cholesterol depletion resulted in significantly reduced infection rates when compared to non-treated control cells indicating a certain role of host cell-derived cholesterol in parasite invasion and intracellular establishment. Thus, in line with other apicomplexa (Suss-Toby et al., 1996, Lauer et al., 2000, Coppens et al., 2003, Sinai, 2008) host cell-derived cholesterol may be involved in *E. bovis* PV formation. Indeed, we could show that by exclusively labelling host cell cholesterol with rhodamin cholestanol prior to infection, cholesterol of host cell origin was detected in close proximity to the sporozoite, most probably within the PV. In agreement, other studies showed that host cell cholesterol or cholesterol-rich domains of host cells (lipid rafts) are important for intracellular establishment of several parasites. Thus, cellular lipid raft alteration reduced *T. gondii* invasion in macrophages and epithelial cells (Cruz et al., 2013) and MBCD treatments of fibroblast also diminished *T. gondii* invasion (Coppens and Joiner, 2003). Furthermore, *Plasmodium* merozoites were shown to integrate lipids derived from the erythrocyte membrane into the nascent PV (Ward et al., 1993) and MBCD-treated Vero and HeLa cell lines revealed less succeptible for *T. cruzi* invasion (Fernandes et al., 2007). Cholesterol depletion from macrophage plasma membranes via MBCD also resulted in a significant reduction in the extent of leishmanial infection (Pucadyil et al., 2004).

E. bovis sporozoite cholesterol depletion also had a significant impact on active parasite host cell invasion. Referring to subsequent infection rates, the effects of parasite depletion accounted even higher than those of host cell depletion although sporozoite viability was not affected by MBCD treatment. Given that MBCD treatments do not only alter plasma membrane cholesterol contents but

may also affect cholesterol present at endocellular membranes (Zidovetzki and Levitan, 2007), respective treatments of sporozoites may have altered the membrane integrity of organelles which are required for gliding motility and invasion, such as micronemes or rhoptries. Since rhoptries are known to contribute to PV formation (Nichols et al., 1983, Porchet-Hennere and Nicolas, 1983, Carruthers and Sibley, 1997) and have been reported to contain cholesterol (Besteiro et al., 2008), Coppens and Joiner (2003) investigated the role of rhoptry cholesterol in PV formation and showed that these molecules are not necessary for PVM formation whilst host cell plasma membrane-derived cholesterol is incorporated into the forming PVM during invasion. In contrast, it rather seems to be involved in membrane plasticity and protein translocation during the invasion process (Besteiro et al., 2008, Ngo et al., 2004).

5.1.2 *Lipid droplet formation in parasite stages and infected host cells*

To account for neutral lipids, *E. bovis* free stages were stained by Nile Red, osmium tretroxide and bodipy 493/503. Respective reaction patterns differed entirely from those induced by filipin staining suggesting a differential distribution of free cholesterol and neutral lipids in *E. bovis* sporozoites and merozoites I. Thus, neutral lipids exclusively occurred in the refractile bodies of sporozoites (merozoites generally lack refractile bodies) and in cytosolic LD-like structures of sporozoites and merozoites I. This is in line with observations on *E. tenella* sporozoites (Lemgruber and Lupetti, 2012, de Venevelles et al., 2006) and with reports on LDs in the cytoplasm of *T. gondii* tachyzoites (Coppens et al., 2000, Sonda et al., 2001, Charron and Sibley, 2002). As described for *T. gondii* tachyzoites, containing 1-4 LDs per cell (Coppens et al., 2000, Sonda et al., 2001), *E. bovis* sporozoites and merozoites I-derived LDs also differed in their numbers accounting for up to 8 LDs per specimen. Given that the parasite expresses LDs itself, it is likely to assume that these organelles play a role in parasite lipid homeostasis. The fact that intracellular *C. parvum* merozoites form large cytosolic LDs in response to excess LDL in the cell culture medium (Ehrenmann et al., 2013) confirms that coccidian parasites principally are equipped to store lipids

and that they may benefit from lipid super abundance by actively forming new or larger LDs.

Neutral lipid/LD abundance also revealed as key factor in *E. bovis* intracellular stages. Overall, a striking stage-dependent increase of LD formation was observed throughout macromeront development. Shortly after invasion, the refractile bodies of the sporozoites still showed strong Nile Red/bodipy 493/503 staining but, interestingly, the numbers of refractile bodies per intracellular parasite stage were reduced, i. e., only the posterior refractile body seemed to persist in infected cells. This is in line with other authors describing that, after sporozoite invasion, the anterior refractile body may either be divided into several small refractile bodies or the anterior refractile body might fuse with the posterior refractile body (Roberts and Hammond, 1970, Hammond et al., 1970, Dubremetz and Elsner, 1979). So far, the reason for refractile body disappearance is not known, however, it may be related to the parasites needs for lipids even in the early phase of development.

The induction of LD formation in *E. bovis*-infected host cells revealed as a stage-dependent process since beginning with parasite proliferation, a striking enhancement of LD formation occurred in infected host cells. This is in principle in line with reports on *P. falciparum*-infected erythrocytes which also reported on a stage-dependent increase of LDs (Vielemeyer et al., 2004, Nawabi et al., 2003, Palacpac et al., 2004). Interestingly, the maximum LD generation in *E. bovis*-infected host cells is observed in late immature meronts, i. e., at times when merozoites I are about to be formed. In contrast, in mature macromeronts carrying fully developed merozoites I, structurally defined LDs were hardly observed, suggesting that LD contents were almost totally consumed for merozoite I formation. Given that lipids were incorporated in newly developed merozoites I, a more homogeneous but bright fluorescence of the total mature macromeront occured which corresponded to the more homogeneous reactions found in single merozoites I. Bodipy 493/503 and osmium tetroxide stainings of infected host cells additionally revealed that LDs may be differentially distributed within the

parasite stage since they were either homogeneously spread or clustered in certain areas of the macromeronts. So far, the meaning of this observation is not clear. LD dense regions may overlap with areas of merozoite I budding, however, these phenomena have to be further analysed to allow for any assumption.

Confocal analyses revealed considerable variations of LD sizes in meront-carrying host cells, ranging from submicrometer diameters to large sizes of ≥ 5 µm (these estimations rather have to be interpreted as approximations since absolute measurements were not performed). Accordingly, "gigantic" LDs of up to 4 µm size were described in *T. cruzi*-infected host cells (Melo et al., 2006). Interestingly, Melo et al. (2006) found maximum LD sizes in irradiated macrophages which allowed for higher parasite burdens and offspring production, i. e., a situation that obviously parallels that of *E. bovis* replication. However, differing sizes are a common finding in these organelles (Melo et al., 2011) and are either based on enhanced localized lipid synthesis (Kuerschner et al., 2008) or on LD fusion (Olofsson et al., 2009).

Confocal analyses also revealed that LDs are mainly equally distributed throughout the macromeront body. Given that the developing macromeront pushes host cellular contents aside owing to its enormous size (see **Fig. 4.7.C**) and since LDs were detected in almost each Z-stack layer, it could be demonstrated that LDs indeed originated from the parasite itself.

Significant quantitative differences in bodipy 493/503-stained infected BUVEC were measured using FACS analyses confirming recent microscopic observations. Thus, significantly enhanced reactions were detected in immature meronts but even higher signals were found in mature macromeronts. Since FACS analysis merely measures fluorescence intensities and does not account for homogeneous or structured distributions, this is in line with the microscopic observations.

Infection-induced enhancement of LD abundance in infected host cells has also been reported for other protozoan parasites. Thus, acute infections with *T. cruzi* significantly induced LD formation in macrophages *in vivo* (Melo et al., 2003,

2006). Abundant LDs were also reported for *T. gondii*-, *P. berghei*- or *P. falciparum*-infected host cells (Rodriguez-Acosta et al., 1998, Vielemeyer et al., 2004, Jackson et al., 2004, Coppens, 2006, Gomes et al., 2014). However, the degree of LD enhancement in those cases was not at all comparable to *E. bovis* infections. Whilst in *T. cruzi*-infected macrophages the numbers of LDs increased from 2 in controls to a maximum of 18 in infected cells (Melo et al., 2003), in *T. gondii*-infected skeletal muscle cells from 4 to ~16 LDs in infected cells (Gomes et al., 2014) and in *P. falciparum*-infected erythrocytes to ≥ 10 LDs (Vielemeyer et al., 2004), LD numbers in immature *E. bovis* meronts revealed vastly higher (but uncountable owing to the thickness of the specimens). The striking dimension of *E. bovis*-triggered upregulation of LD formation obviously reflects the enormous demand for lipids for offspring production counting much higher in *E. bovis* than in any other here mentioned parasite. Furthermore, it is noteworthy that, in most cases, the above mentioned authors reported on enhanced numbers of LDs in the cytoplasm of respective host cells, whilst in the case of *E. bovis* macromeronts LD-like structures were definitively situated within the parasite stage itself.

Details on the LD formation process and the precise function of these organelles within parasitic stages are scarce. Especially in the case of *E. bovis* it remains to be elucidated whether LDs are formed by the parasite itself of whether they may be internalized from the host cell compartment. In the case of *T. gondii*-infected skeletal muscle cells increasingly formed LDs were observed in direct contact with the PVM, the vacuolar matrix and the parasite membrane and the authors speculate that recuited LDs directly deliver their contents to the PV (Gomes et al., 2014).

T. gondii-derived LDs contain cholesteryl esters (Charron and Sibley, 2002, Nishikawa et al., 2005, Lige et al., 2013) whilst these are absent in LDs of *Plasmodium*-infected cells (Jackson et al., 2004, Nawabi et al., 2003, Palacpac et al., 2004). Thus, NBD-labelled cholesterol is incorporated into intracellular *T. gondii* membranes and is also metabolized to cholesteryl esters as observed by

thin layer chromatography (Charron and Sibley, 2002). The fact that host cell SOAT1 is clearly upregulated in *E. bovis*-infected BUVEC at times of enhanced LD formation may argue for the storage of cholesteryl esters in these organelles. Interestingly, *T. gondii* is reported to express parasite-own SOAT-like molecules (Nishikawa et al., 2005, Lige et al., 2013), which may contribute to LD-derived cholesteryl ester storage. In the case of *E. tenella*, there is evidence of several peptides isolated from refractile bodies which are homologous to acyl-CoA synthases (de Venevelles et al., 2006). Furthermore, a sterol O-acyltransferase was predicted in the *E. tenella* genome (Bushkin et al., 2013) indicating that also *Eimeria* species may have the capacity to actively form cholesteryl esters by themselves and to store these molecules in LDs. Given that dansyl-cholesterol- (which is not esterified) derived signals occur in free sporozoite refractile bodies, which are devoid of free cholesterol as determined by the lack of filipin staining, rather argues for the existence of enzymes that metabolize free cholesterol to biochemical neutral forms, such as cholesteryl esters, in *E. bovis* stages. Referring to the facts mentioned above, it is tempting to assume that *E. bovis* is also equipped with parasite-derived SOAT-like molecules which contribute to LD formation. However, this item should be adressed in future studies.

The precise function of LDs in *E. bovis* macromeront development has not been defined yet. Assuming that the parasite has a high demand for lipids, it appears most likely that the large abundance of LD contents is consumed for the considerable enlargement of the host cell membrane, for the formation and enlargement of the PV and, probably most importantly, for the formation of large numbers of merozoites I. Accordingly, morphologically defined LDs disappear in macromeronts when mature merozoites I have been formed and parasite development fails when fatty acid synthesis as well as cholesterol synthesis or esterification is chemically blocked via inhibitors. Thus, the lipid storage capacity appears the most prominent function of LDs in *E. bovis*-infected cells and enhancement of LD formation may mirror the nutritional needs of the parasite. To analyze the actual role of LDs as “feeder organelles”, we took advantage of

artificial LD enhancement via oleic acid treatments of host cells prior to *E. bovis* infection and throughout intracellular development. The treatment of eukaryotic cells with oleic acid is a well-known tool for the stimulation of cytosolic LD formation and is often used as positive control in LD-related experiments (Seo et al., 2001). Indeed, oleic acid-triggered induction of LD formation significantly improved parasite proliferative capacities, since a 7-fold up-regulation of offspring production was observed when compared to non-induced host cells. These data clearly strengthen the assumption of LDs mainly functioning as lipid storage and "feeder" organelles in *E. bovis* macromeronts.

LDs have been described as very active and dynamic inclusion bodies (Martin and Parton, 2006, Fujimoto et al., 2008, Farese and Walther, 2009, Murphy et al., 2009, Olofsson et al., 2009, Fujimoto and Parton, 2011, Jungst et al., 2013) that are also involved in innate immune reactions of inflammatory leukocytes (d'Avila et al., 2008, Melo et al., 2006). Thus, nascent lipid bodies, the formation of which can be induced by different immunoactive stimuli, such as eicosanoids, chemokines, cytokines (eotaxin/RANTES, IL-5, IL16) or fatty acids, are reported as sites of enzyme localization (such as cyclooxygenase, prostaglandin E_2 synthase or leukotriene C_4 synthase), eicosanoid production, as well as cytokine storage (reviewed in Bozza et al., 2007). Whilst the production of PGE_2 was positively correlated with enhanced LD formation in *T. cruzi*-infected macrophages (Melo et al., 2003), no data on LD-produced immunomodulatory molecules are available on *Eimeria*-infected host cells and, in consequence, immunoreactive functions of *E. bovis*-induced LD should also be considered and further analyzed in future experiments.

5.2 *E. bovis* up-regulates both host cell cholesterol *de novo* synthesis and LDL-mediated uptake

5.2.1 *Up-regulation of the mevalonate biosynthesis pathway and of host cellular cholesterol processing by E. bovis infections*

Gene transcription profiling of *E. bovis*-infected endothelial host cells showed that all molecules being involved in the mevalonate biosynthesis pathway (HMGCR, HMGCS1, SQLE) or in the formation of early substrates for this pathway (ACAT1, 2) where predominantly found up-regulated in times of merozoite I formation (17 days p. i.) indicating a significant induction of host cell *de novo* synthesis to satisfy the parasites demand for high cholesterol abundance. Accordingly, an enhancement of ACAT1 was also confirmed on the protein level at 17 days p. i. However, it has to be noticed that actual enzymatic activities of these enzymes were not estimated. Thus, the current results may not necessarily mirror respective biochemical activities of the host cells. Nevertheless, HMGCS1 and SQLE inhibition studies clearly confirmed the relevance of cholesterol *de novo* synthesis in *E. bovis*-infected host cells (see **4.6**). In *T. gondii*-infected host cells the data on mevalonate biosynthesis pathway induction are somewhat conflicting. Whilst Coppens et al. (2000) negated any involvement of cholesterol *de novo* synthesis to satisfy the parasites need for cholesterol, other authors (Martins-Duarte et al., 2006, Blader et al., 2001, Nishikawa et al., 2011) presented data indicating that host cholesterol synthesis does indeed contribute to the growth of intracellular *T. gondii*. Thus, the gene transcriptions of HMGS1, HMGCR and SQLE genes were found up-regulated in times of tachyzoite formation (Blader et al., 2001) and blockage of HMGCR or SQLE inhibited *T. gondii* growth (Martins-Duarte et al., 2006, Nishikawa et al., 2011). However, given that different host cell types were used in these investigations, the different outcomes may rely on cell-type specific utilization of different pathways of cholesterol acquisition. In the case of *E. bovis*, the current data clearly argue for an up-regulation of the mevalonate biosynthesis pathway to promote parasite replication.

Gene transcription profiling also suggested enhanced cholesterol modification on the level of esterification and hydroxylation in *E. bovis*-infected host cells. Thus, SOAT1 and CH25H gene transcripts were significantly up-regulated at times of macromeront formation, paralleling those of molecules being involved in host cell *de novo* synthesis. In eukaryotic cells, excess cellular cholesterol is toxic and therefore *de novo* synthesis must be tightly regulated and coupled to pathways that enable removal of cholesterol (for review see Ikonen, 2008). Given that excess free cholesterol is indeed synthesized in infected host cells, it appears likely that these molecules are further processed e. g. by esterification and oxidation. In line with these assumptions a significantly enhanced LD formation was observed, representing the site of cholesteryl ester storage (see **4.2.2.**). In line with other apicomplexan parasites (Sonda et al., 2001, Nishikawa et al., 2005) the key role of cholesterol esterification in *E. bovis*-infected host cells was furthermore confirmed by SOAT inhibition experiments as showed in chapter **4.6.5**.

The overall predominant up-regulation of gene transcripts and proteins concerned CH25H (up to 52.69-fold increase) suggesting enhanced 25-OH-cholesterol (25-OHC) synthesis in *E. bovis*-infected host cells since the formation of different oxysterols is specifically mediated by different enzymes (Brown and Jessup, 2009). Again, it has to be mentioned that gene transcription and protein expression analyses do not necessarily reflect cellular enzyme activities. However, preliminary results on biochemical measurements of 25-OHC end product confirmed significantly enhanced concentrations of this molecule, but not of other oxysterols, such as 24-OHC or 27-OHC, in *E. bovis*-infected host cells (A. Taubert, unpublished data). Furthermore, these data are in line with previous studies on *E. bovis*-mediated host cell transcriptome alterations (Taubert et al., 2010).

Oxysterols are typically present in cells in minor amounts [(approximately 1:1000 compared to cholesterol, (Ikonen, 2008)] and in general exhibit different functions in eukaryotic cells. Thus, they may act as immunomodulators since they induce the synthesis of inflammatory cytokines such as tumor necrosis factor,

chemokines and adhesion molecules and alter B-, T- and dentritic cell functions (Spann & Glass, 2013, Poli et al., 2013). Furthermore they are described as regulators of the cholesterol metabolism by blocking the expression of genes involved in cholesterol synthesis via modulating the sequestration of cholesterol regulatory elements [(SREBPs), for review see Brown and Jessup, 2009]. In addition, they regulate the degradation of HMGCR, the rate-limiting enzyme of cholesterol synthesis. Given that the additional hydroxyl group renders oxysterols more hydrophilic, these molecules move more freely in the cytoplasmic environment than cholesterol and may function as membrane solubilizer (Ikonen, 2008). In mammalian cells, 25-OHC is an indicator of high cellular cholesterol levels, it can be esterified by sterols esterifying enzymes and also may act as cholesterol biosynthesis repressor (Brown and Jessup, 2009). So far, the precise role of 25-OHC in *E. bovis*-infected host cells is not known. However, since 25-OHC has also been shown to stimulate cholesterol esterification via SOAT (Brown, Dana and Goldstein, 1975), which may, in turn, be directly linked with enhanced LD formation, it is tempting to suggest a pivotal role for 25-OHC in cholesterol regulation of *E. bovis*-infected host cells.

It is worth noting that oxysterols are transported by cytosolic receptors, the oxysterol binding proteins (OSBPs) (Kandutsch and Shown, 1981). Interestingly, several OSBP-related proteins (ORPs) were identified in apicomplexan parasites, such as *C. parvum, Plasmodium* spp., *T. gondii* and *E. tenella* (Zeng, 2006). The fact that a *C. parvum*-derived ORP was reported to be localized in the PVM, suggests a role of these molecules in direct oxysterol uptake from the cytosol (Zeng and Zhu, 2006). However, future genome analyses have to clarify whether *E. bovis* also possesses ORPs and may therefore directly benefit from enhanced oxysterol synthesis.

Gene transcription and protein expression analyses also indicated an involvement of LDL-promoted up-take of cholesterol since both, LDLR and OLR1 gene transcripts and proteins were found up-regulated in *E. bovis*-infected host cells. Interestingly, the significant enhancement of LDLR and OLR1 gene transcripts

started 5 days earlier during macromeront development than that of *de novo* synthesis-associated molecules suggesting a defined chronology of cholesterol acquisition. Thus, the LDL-related pathway may represent the first action for cholesterol up-take in times of beginning parasite proliferation and afterwards, in times of maximum cholesterol need, i. e. when merozoites I are about to be formed, host cell *de novo* synthesis may additionally be triggered to satisfy the top demands. In accordance, enhanced levels of LDLR and OLR1 gene transcripts were also detected in *T. cruzi*-infected macrophages (Chiribao et al., 2014). Cholesterol acquisition via the LDL-incorporation is a common feature in apicomplexan parasites and will be discussed more in detail in chapter **5.2.3**.

5.2.2 ***Inhibition of host cellular cholesterol de novo synthesis and esterification blocks parasite growth***

Inhibitor experiments were performed to verify the actual role of different steps of host cellular *de novo* cholesterol biosynthesis as well of cholesterol esterification and fatty acid synthesis in *E. bovis* macromeront formation. Thus, different inhibitors were applied targeting HMG-CoA reductase (lovastatin), squalene synthase (zaragozic acid), acyl-CoA cholesterol acyltransferase (CI976) and fatty acid synthase (C75).

Intracellular *E. bovis* macromeront formation is a long lasting process that may take up to 30 days *in vitro*. This has important implications on inhibitor experiments since the compounds have to act for many days without exhibiting detrimental effects on the cultures themselves. Therefore extensive experiments were performed to estimate toxic effects of long-term treatments with lovastatin, zaragozic acid, CI976 and C75 in bovine endothelial cell cultures. Overall, BUVEC reacted rather sensitive and, in most cases, did not tolerate compound concentrations used in other reports dealing with other coccidian species in different host cell types (Ehrenman et al. 2013, Nishikawa et al. 2011, Sonda et al. 2001) when being continuously treated for at least 15-20 days. In consequence, a final concentration of 1 µM (lovastatin) and 5 µM (all other compounds) was used

in the current inhibition study. Compared to other reports this rather signifies low dose treatments.

Referring to dose effect curves and calculated IC_{50} values, lovastatin proved as the most effective anti-proliferative compound. Lovastatin belongs to the well-known group of statins, a class of drugs widely used to lower plasma cholesterol levels (Brown, 2001, Brautbar and Ballantyne, 2011). Statins are reversible inhibitors of the microsomal enzyme HMG-CoA reductase, which represents the early rate-limiting step in cholesterol biosynthesis (Istvan and Deisenhofer, 2001). It has to be mentioned that mevalonate is not exclusively used as substrate for sterol synthesis but is also needed for protein isoprenylation and the synthesis of non-sterol products that are critical for the growth and proliferation of eukaryotic cells (Liao, 2002). Consequently, effects may partially also be attributed to the blockage of other molecules than cholesterol. However, low dose (1 µM) treatments of *E.bovis*-infected endothelial host cells resulted in a significant arrest of meront formation and almost total blockage of merozoite production (>99 % reduction). Interestingly, *E. bovis*-infected host cells appear to be significantly more sensitive to this drug (IC_{50}: 0.1 µM) than other coccidian species, since the IC_{50} value of lovastatin was approximately 170-fold higher for *T. gondii*-infected macrophages (Nishikawa et al., 2011, IC_{50} = 17,1 µM) and the use of 10-fold doses of lovastatin resulted only in a 50 % reduced filipin staining and a 2.5-fold reduction of the PV size of *C. parvum* in epithelial cells (Ehrenman et al, 2013). In agreement, treatments of *T. gondii*-infected macrophages with different statins resulted in >50% inhibition in the case of simvastatin only at doses of 30-40 µg/ml (corresponds to 72-96 µM) whilst rosuvastatin and atorvastatin even failed to do so (Cortez et al., 2009). The higher sensitivity of *E.bovis* may be explained by the fact that the numbers of merozoites I to be produced per infected host cell is at least 1000-fold higher than in *T. gondii* or *C.parvum*, and most probably result in a much higher need for cholesterol for membrane biogenesis in the replicative phase of infection.

Zaragozic acid affects with squalene synthase the first enzymatic step of the mevalonate pathway, which directly targets sterol synthesis and therefore is considered as more specific for cholesterol blockage than statin treatments (Lindsey and Harwood, 1995). In infected BUVEC, 5 µM zaragozic acid treatments resulted in an arrest of meront formation and induced strong anti-proliferative effects (reduction of 70.2 % of merozoite I production) confirming that *E. bovis* development clearly depends on host cell *de novo* synthesis. However, the fact that meront growth is not completely blocked after zaragozic acid treatment and and still produces smaller (but mostly degraded) meronts I argues for an additional source of cholesterol than *de novo* synthesis. Thus, the simultaneous exploitation of the LDL-mediated pathway may help in forming smaller meronts, but, however, the parasite finally fails to produce adequate numbers of offspring.

In contrast to *E. bovis*, only moderate effects of 15 µM zaragozic acid treatments (as indicated by 25 % of growth delay) were estimated in *C. parvum*-infected epithelial cells (Ehrenman et al., 2013). Comparable rates of reduction were also reported in *T. gondii*-infected macrophages applying 1-10 µM zaragozic acid (Nishikawa et al., 2011). In addition, squalene synthase-defective CHO cells revealed no significant anti-proliferative effects on *T. gondii* development compared to non-defective controls (Coppens et al., 2000). However, Martins-Duarte et al. (2006) applied two quinuclidine-based inhibitors of squalene synthase in *T. gondii*-infected epithelial cells and reported on anti-proliferative effects of both compounds achieving up to 48-58 % reduction of tachyzoite replication at 3 µM dosage.

Overall, the data on lovastatin and zaragozic acid treatments clearly indicate that successful *E. bovis* macromeront development and merozoite I production significantly depends on the host cell cholesterol *de novo* synthesis.

CI976 is an inhibitor of SOAT that also affects multiple membrane trafficking steps, including those found in the endocytic and secretory pathways (Chambers

et al., 2005, Kam et al., 1990, Schmidt and Brown, 2009). Treatments of *E. bovis*-infected BUVEC resulted in immediate arrest of parasite development irrespective of the onset of treatment. Overall, 5 µM CI976 treatments induced strong anti-proliferative effects since it almost entirely blocked merozoite I production (> 99 % reduction) indicating that cholesterol esterification and storage is of high relevance for successful *E. bovis* development and that SOAT may represent a key molecule in this aspect. In agreement, LDs/neutral lipids were increasingly accumulated in *E. bovis* meronts with ongoing development and lipid droplet deposition in infected host cells was blocked by CI976. These data are in line with several reports on *T. gondii* documenting the essential role of cholesterol esterification and lipid droplet formation in optimal parasite proliferation (Coppens et al., 2000, Sonda et al., 2001, Coppens and Vielemeyer, 2005, Nishikawa et al., 2005). Accordingly, the absence of host cellular SOAT or SOAT inhibition induced a considerable decrease of *T. gondii* replication (Sonda et al., 2001). However, the merozoite I reduction rates of approximately 60 and 70 % induced by 4 µM and 10 µM CI976 treatments, respectively, appeared lower for *T. gondii* than those detected in *E. bovis*-infected host cells after 5 µM treatments indicating a higher sensitivity of *E. bovis*. Importantly, it was shown for *T. gondii* that the parasite itself is able to synthesize and store cholesteryl esters, if host cell cholesterol is available (Sonda et al., 2001, Nishikawa et al., 2005). Given that two SOAT-like molecules were identified in *T. gondii* stages and proved sensitive to SOAT inhibitor treatments (Nishikawa et al., 2005, Lige et al., 2013), respective molecules may also exist in *E.bovis* stages. Thus, it remains to be elucidated whether the detrimental effects driven by CI976 accounted only to the host cell compartment or were also brought about by direct anti-parasitic effects.

Given that cholesteryl esters play a pivotal role in *E. bovis* development and that precursors thereof are cholesterol and fatty acids, the effects of fatty acid synthase blockage was additionaly investigated. Fatty acid synthase is a lipogenic enzyme that catalyzes the condensation of acetyl-CoA and malonyl-CoA to generate long-chain fatty acids (Chirala and Wakil, 2004, Menendez and Lupu, 2007). The synthetic α-methylene-γ-butyrolactone compound C75 inhibits fatty acid synthase

activity and has been studied for its anti-inflammatory and anti-tumoral activities (Kuhajda et al., 2000, Flavin et al., 2010, Matsuo et al., 2014). C75 treatments induced dose-dependent anti-proliferative effects on *E.bovis* merozoite I production and impeded proper macromeront development. In contrast, C75 was ineffective in directly inhibiting *T. cruzi* growth in infected macrophages (D'Avila et al., 2011). It is noteworthy, that treatments of *in vitro* parasite cultures with C75 resulted in enormous morphological alterations as detected by massive vacuolization of the *E. bovis* macromeronts indicating a high relevance of fatty acids for optimal intracellular parasite replication.

In summary, the results indicate that successful development of *E. bovis* macromeronts in endothelial cells significantly depends on host cellular *de novo* synthesis of cholesterol via the mevalonate biosynthesis pathway in addition to functional cholesterol esterification, fatty acid synthesis and lipid droplet formation.

5.2.3 ***Key role of host cellular LDL up-take in E. bovis development***

Besides *de novo* biosynthesis, exogenous cholesterol is acquired mainly via cellular lipoprotein internalization. LDL is particularly enriched in free cholesterol and cholesteryl esters rendering these molecules as a beneficial source of cholesterol. Hence, human LDL contain approximately 350 and 1400 molecules of free and esterified cholesterol molecules per particle, respectively, whilst HDL particles contain only 30 and 70 respective molecules (Wilson et al., 1992). In the blood or lymph, different modifications of LDL occur, such as acetylated (ac) or oxidized (ox) LDL. Whilst most cells are able to internalize non-modified LDL (Myant, 1990), acLDL up-take is restricted to certain cell types, such as endothelial cells and macrophages (Voyta, 1984). In order to address the question, whether LDL and acLDL internalization differed in *E. bovis*-infected endothelial host cells and in non-infected controls, we used (bodipy)LDL- and (bodipy)acLDL-enriched cell culture media and assayed for lipoprotein binding to endothelial (host) cells. Respective analyses revealed that *E. bovis*-infected host

cells were not restricted to LDL or acLDL up-take but showed enhanced capacities to scavenge cholesterol from both sources. Thus, fluorescence-based LDL and acLDL binding assays showed that both molecules were increasingly bound to the surface of macromeront-carrying host cells. Furthermore FACS analyses revealed a 37.5-fold and 5.2-fold increase of LDL and acLDL binding, respectively.

The current gene transcription profiles also indicate a role of oxLDL during macromeront formation. Thus, in agreement to recent microarray analyses of *E. bovis*-infected host cells (Taubert et al., 2010), a significant up-regulation of OLR1 gene transcripts were detected. These data were confirmed by enhanced OLR1 protein expression in *E. bovis*-infected BUVEC at 17 days p. i. To our knowledge, this represents the first report on the involvement of OLR1 in coccidian host cell infections. OLR1 (syn. LOX-1) is considered as the major receptor for oxLDL in vascular endothelial cells (Sawamura et al., 1997, Moriwaki et al., 1998, Kume et al., 1998) and belongs to the scavenger receptor class E molecules. OLR1 has vastly been investigated on the level of human artherosclertic lesions (for review see Pirillo et al., 2013). Given that oxLDL may also provide a good exogenous cholesterol source, OLR1-promoted uptake may also be involved in *E. bovis* macromeront formation. However, additional experiments are needed to confirm this assumption.

Prolonged supplementation of bodipy-LDL additionally resulted in signals within the meronts which may indicate the utilization of LDL by the parasites themselves. LDL has also been reported to serve as exogenous cholesterol source for other apicomplexan parasites, such as *T. gondii*, *C. parvum* and *Plasmodium* spp. (Coppens et al., 2000, Labaied et al., 2011, Ehrenmann et al., 2013). Thus, fluorescence-derived signals of exogenously supplied LDL-incorporated NBD-cholesterol were detected in the PV or parasite membranes of these parasites (Coppens et al., 2000, Labaied et al., 2011, Ehrenmann et al., 2013).

Given that LDL is mainly internalized via the classical LDLR we further analyzed this receptor in *E. bovis*-infected host cells. In agreement to recent transcriptome data on *E. bovis*-infected bovine endothelial cells (Taubert et al., 2010), LDLR gene transcripts were found significantly up-regulated throughout macromeront development. The transcriptional data were confirmed on the protein level since a significant, almost two-fold enhancement of surface LDLR expression was detected on infected host cells at 17 days p. i. via FACS analysis. The general involvement of LDLR in parasite-mediated LDL-uptake is in line with data on *T. gondii*-infected CHO cells showing that antibody-mediated blockage of LDLR leads to a dramatic decrease of cholesteryl ester delivery to the parasite (Coppens et al., 2000). In contrast, a 70-80 % reduced LDLR expression did not affect the liver stage burden in the case of *Plasmodium* spp. although this parasite in principle salvages LDL-derived cholesterol (Labaied et al., 2011). In concert with the later findings, *T. gondii* growth did not change in LDLR-deficient (KO) macrophages when compared to wild type cells indicating that parasite-driven LDL may also be acquired via other host cell receptors, such as scavenger receptors. In this context it is worth noting that the class B type I scavenger receptor being able to bind LDL (Horiuchi et al., 2003), was required for *P. berghei* infections (Rodrigues et al., 2008).

In order to assess whether enhanced disposability of LDL would be of benefit for the parasite development, infected host cells were cultured in LDL-enriched medium. Indeed, a significantly increased offspring production was detected in LDL-enriched cultures confirming the pivotal role of LDL for optimal parasite proliferation. Similar results were reported for *T. gondii*-infected CHO cells on the level of tachyzoite numbers per PV (Coppens et al., 2000) whilst excess LDL had no stimulatory effect on *Plasmodium* spp. and *C. parvum* proliferation (Labaied et al., 2011, Ehrenmann et al., 2013). However, exogenous LDL treatment also had no beneficial effect on *T. gondii* proliferation in macrophages (Nishikawa et al., 2011) indicating cell type specific reactions.

Overall, the current data indicate that *E. bovis* has the capacity to scavenge cholesterol from several sources at a time, which contrasts to *T. gondii* (Coppens, 2000) but is in principle in line with findings for *Plasmodium* spp. (Labaied et al., 2011). Nevertheless, *E. bovis* bears significant differences to *Plasmodium* spp., since, based on the enormous demand for cholesterol, *E. bovis* development clearly depends on both, cellular *de novo* synthesis and the LDL-mediated extracellular cholesterol internalization at a time, whilst *Plasmodium* spp. being suggested to exhibit moderate needs of sterols for optimal proliferation (Labaied et al., 2011), merely alternatively exploits these scavenger pathways. Given that cellular cholesterol synthesis is tightly regulated by a complex network of cellular mechanisms, more research is needed to understand how the parasite outwits this regulatory network.

6 SUMMARY

During first merogony *E. bovis* forms large-sized macromeronts containing >120,000 merozoites. Given thatobligate intracellular replicating coccidians are generally considered as auxotrophic for cholesterol synthesis and that asingle sporozoite stage cannot provide all components necessary for this nutrient and energy demanding process, the parasite needs to scavenge molecules from the endothelial host cell. Especially for the massive offspring membrane production, large amounts of cholesterol are indispensable for a successful replication process. Here, the influence of *E. bovis* infections on host cell cholesterol metabolism was analyzed.

Free cholesterol and neutral lipids were shown to be differentially distributed in sporozoite stages. Thus, free cholesterol mainly occurred in the apical complex and in the pellicles of sporozoite and merozoite I stages whilst neutral lipids accumulated in refractile bodies of the sporozoites. Both stages showed cytoplasmic lipid droplet (LD)-like structures indicating their capability for lipid storage. Kinetic analyses revealed enhanced levels of free cholesterol during *E. bovis* macromeront development. A massive increase of LD formation in immature macromeronts suggested these organelles and esterified cholesterol (which is stored in LDs) as important lipid source for *E. bovis*. In agreement, an artificial increase of cellular LDs led to improved merozoite I production and pharmacological blockage of cholesterol esterification abrogated *E. bovis* development.

Transcriptional profiling of infected host cells in times of macromeront formation indicated that *E. bovis* modulates both pathways of cholesterol acquisition, i. e. LDL-promoted uptake of extracellular cholesterol sources and host cellular *de novo* synthesis. Thus, the gene transcription of several molecules being involved in cellular cholesterol *de novo* synthesis via the mevalonate biosynthesis pathway (e. g. HMG-CoA synthase, HMG-CoA-reductase and squalene epoxidase) and of transcripts of the LDL-receptor (LDLR) and the oxidised LDL receptor 1 (OLR1) were equally found up-regulated in infected host cells. Furthermore, cellular

cholesterol processing appeared enhanced since key molecules, such as cholesterol-25-hydroxylase and acyl-CoA acetyltransferase, were significantly up-regulated in infected cells, the latter of which promotes cellular cholesteryl ester synthesis and lipid droplet biogenesis.

The key role of cholesterol *de novo* synthesis and processing was furthermore confirmed via pharmacological blockage applying the following inhibitors: lovastatin, zaragozic acid, CI976 and C75 targeting HMG-CoA-reductase, squalene synthase, acyl-CoA cholesterol acyltransferase and fatty acid synthase, respectively. In summary, all inhibitors significantly interfered with *E. bovis* macromeront formation and merozoite I production in a dose-dependent manner. Dose effect responses identified lovastatin as the most effective compound, followed by CI976, C75 and squalestatin, respectively. Overall, merozoite I production was inhibited by 99.6, 99.7, 84.6 and 70.2 % via lovastatin, CI976, C75 and zaragozic acid treatments, respectively. Concerning macromeront development, both, the rate and size of meronts were affected by inhibitor treatments. Respective effects were characterized by developmental arrest and meront degradation.

The pivotal role of LDL-promoted host cellular incorporation of exogenous cholesterol for parasite replication was underlined by enhanced binding of non-modified and acetylated LDL on *E. bovis*-infected cells. In addition, significantly increased levels of surface LDLR expression were detected on meront-carrying host cells. Furthermore, cholesterol and LDL enrichments of the cell culture medium boosted parasite replication. Besides LDLR, we additionally identified the scavenger receptor OLR1 (oxidized LDL receptor 1) as a key molecule of parasite-triggered LDL uptake since both, gene transcription and protein expression was found enhanced in infected cells.

Overall, these results indicate that *E. bovis* massively modulates the host cell cholesterol metabolism to guarantee its intracellular growth and replication.

7 ZUSAMMENFASSUNG

E. bovis bildet als strikt intrazellulärer Erreger im Rahmen der ersten Merogonie sog. Makromeronten aus, in denen mehr als 120.000 Merozoiten produziert werden. Dieser nährstoff- und energiefordernde Prozess kann nicht von Sporozoiten allein getragen werden. Dementsprechend muss der Parasit den Wirtszellmetabolismus modulieren, um seine erfolgreiche Replikation abzusichern. Dies betrifft aufgrund der massiv geforderten Membranbiogenese für die Merozoitenproduktion insbesondere den Cholesterolmetabolismus der infizierten Wirtszelle, der Gegenstand dieser Untersuchungen war.

In freien Stadien von *E. bovis* (Sporozoiten, Merozoiten I) zeigte sich eine unterschiedliche Verteilung von freiem Cholesterol und neutralen Fetten bzw. Lipidtröpfchen (LT). Während freies Cholesterol bevorzugt im Apikalkomplex und in der Pellikula nachgewiesen wurde, waren Cholesterylester bzw. neutrale Fette ausschließlich in refraktilen Körperchen nachzuweisen. Zudem wurden LT-ähnliche Strukturen im Zytoplasma beider Stadien gefunden, was auf die Befähigung zur Lipidspeicherung seitens des Parasiten schließen lässt.

Analysen zur *E. bovis*-Makromerontenreifung zeigten eine vermehrte Präsenz von von freiem Cholesterol in infizierten Zellen. Ein massiver Anstieg der LT-Bildung in immaturen Makromeronten wies auf eine entscheidende Rolle dieser Organelle bzw. ihrer Inhalte wie z. B. Cholesterylester als Lipidquelle hin. Die Relevanz von LT bzw. Cholesterylestern konnte über artifizielle Steigerung der LT in Wirtszellen über gesteigerte Merozoiten I-Produktion als auch über pharmakologische Blockade der Cholesterolveresterung mit ausbleibender Parasitenproliferation bestätigt werden.

Analysen zur Gentranskription von Wirtszellen während der Makromerontenbildung wiesen auf eine gleichzeitige Modulation beider Wege der Cholesterolakquise, d. h. von wirtszellulärer *de novo*-Synthese als auch der LDL-vermittelte Aufnahme exogenen Cholesterols, hin. Entsprechend waren Gentranskripte diverser, in die zelluläre *de novo*-Synthese von Cholesterol eingebundener Moleküle (z. B. HMG-CoA-Synthase, HMG-CoA-Reduktase,

Squalenepoxidase) als auch von LDL-Rezeptoren (LDL-Rezeptor, oxidised LDL-Rezeptor 1) gegen Ende der Merontenreifung hochreguliert. Zusätzlich wurde die Prozessierung zellulären Cholesterols über *E. bovis*-Infektionen verstärkt, da sowohl die Cholesterol-25-Hydroxylase als auch die Acyl-CoA-Acyltransferase hochreguliert wurden, wobei letztere die Synthese von Cholesterylestern sowie die Biosynthese der Lipidkörperchen vermittelt.

Die entscheidende Rolle der wirtszellulären *de novo*-Synthese von Cholesterol wurde zusätzlich über Inhibitionsstudien belegt, bei der Inhibitoren zur Blockade der HMG-CoA-Reduktase (Lovastatin), Squalensynthase (Zaragozic Acid), Acyl-CoA:cholesterol acyltransferase (CI976) and Fettsäuresynthase (C75) verwendet wurden. Hier zeigte sich, dass alle verwendeten Inhibitoren einen blockierenden, dosis-abhängigen Einfluss auf die Makromerontenbildung und Merozoiten I-Produktion hatten. So wurde die Merozoiten I-Synthese zu 99,6, 99,7, 84,6 und 70,2 % überLovastatin, CI976, C75 and Zaragozic Acid gehemmt. Zusätzlich wurde die Größenentwicklung der Makromeronten als auch respektive Infektionsraten negativ beeinflusst und es zeigten sich Entwicklungsabbrüche als auch Degradierungseffekte bei Makromeronten.

Die entscheidende Rolle der LDL-vermittelten Cholesterolaufnahme für die Parasitenproliferation wurde über signifikant gesteigerte Bindungsreaktionen von nicht-modifizierten und acetyliertem LDL an Meronten-tragenden Wirtszellen als auch über eine signifikant erhöhte Oberflächenexpression von LDL-Rezeptoren bei infizierten Zellen untermauert. Zudem führte eine Anreicherung des Zellkulturmediums mit LDL oder Cholesterol zu einer gesteigerten Merozoiten I-Produktion. Neben dem klassischen LDL Rezeptor konnten wir mit OLR1 einen zusätzlichen, sog. „Scavenger“-Rezeptor identifizieren, der sowohl auf Transkript- als auch Proteinebene in infizierten Zellen hochreguliert war und aller Wahrscheinlichkeit nach an die *E. bovis*-vermittelte Steigerung der wirtszellulären LDL-Aufnahme beteiligt ist.

Zusammenfassend zeigen vorliegende Ergebnisse, dass *E. bovis* massivst in den Cholesterolhaushalt der Zelle eingreift, um sein intrazelluläres Wachstum und Entwicklung abzusichern.

8 REFERENCES

ADL, S. M., SIMPSON, A. G., FARMER, M. A., ANDERSEN, R. A., ANDERSON, O. R., BARTA, J. R., BOWSER, S. S., BRUGEROLLE, G., FENSOME, R. A., FREDERICQ, S., JAMES, T. Y., KARPOV, S., KUGRENS, P., KRUG, J., LANE, C. E., LEWIS, L. A., LODGE, J., LYNN, D. H., MANN, D. G., MCCOURT, R. M., MENDOZA, L., MOESTRUP, O., MOZLEY-STANDRIDGE, S. E., NERAD, T. A., SHEARER, C. A., SMIRNOV, A. V., SPIEGEL, F. W. & TAYLOR, M. F. 2005. The new higher level classification of eukaryotes with emphasis on the taxonomy of protists. *J Eukaryot Microbiol,* 52**,** 399-451.

ALBERTS, B., JOHNSON, A., LEWIS, J., RAFF, M., ROBERTS, K. & WALTER, P. 2008. *Molecular biology of the cell.* New York: Garland Science.

ALTSCHUL, S. F., GISH, W., MILLER, W., MYERS, E. W. & LIPMAN, D. J. 1990. Basic local alignment search tool. *J Mol Biol,* 215**,** 403-10.

ANONYMOUS a._. Lipid droplets fluorescence assay kit. *Manual booklet. Cayman Chemical*, 11.

ANONYMOUS b._. Mini trans-blot electrophoretic transfer cell. *Instruction manual. Bio-Rad*, 7.

BALINT, S., VERDENY VILANOVA, I., SANDOVAL ALVAREZ, A. & LAKADAMYALI, M. 2013. Correlative live-cell and superresolution microscopy reveals cargo transport dynamics at microtubule intersections. *Proc Natl Acad Sci U S A,* 110**,** 3375-80.

BANO, N., ROMANO, J. D., JAYABALASINGHAM, B. & COPPENS, I. 2007. Cellular interactions of *Plasmodium* liver stage with its host mammalian cell. *Int J Parasitol,* 37**,** 1329-41.

BANSAL, D., BHATTI, H. S. & SEHGAL, R. 2005. Role of cholesterol in parasitic infections. *Lipids Health Dis,* 4**,** 10.

BEHRENDT, J. H., CLAUSS, W., ZAHNER, H. & HERMOSILLA, C. 2004. Alternative mechanism of *Eimeria bovis* sporozoites to invade cells *in vitro* by breaching the plasma membrane. *J Parasitol,* 90**,** 1163-5.

BELLER, M., THIEL, K., THUL, P. J. & JACKLE, H. 2010. Lipid droplets: a dynamic organelle moves into focus. *FEBS Lett,* 584**,** 2176-82.

BERGSTROM, J. D., DUFRESNE, C., BILLS, G. F., NALLIN-OMSTEAD, M. & BYRNE, K. 1995. Discovery, biosynthesis, and mechanism of action of the zaragozic acids: potent inhibitors of squalene synthase. *Annu Rev Microbiol,* 49**,** 607-39.

BESTEIRO, S., BERTRAND-MICHEL, J., LEBRUN, M., VIAL, H. & DUBREMETZ, J. F. 2008. Lipidomic analysis of *Toxoplasma gondii* tachyzoites rhoptries: further insights into the role of cholesterol. *Biochem J,* 415**,** 87-96.

BEYER, T. V., SVEZHOVA, N. V., RADCHENKO, A. I. & SIDORENKO, N. V. 2002. Parasitophorous vacuole: morphofunctional diversity in different coccidian genera (a short insight into the problem). *Cell Biol Int,* 26**,** 861-71.

BICKEL, P. E., TANSEY, J. T. & WELTE, M. A. 2009. PAT proteins, an ancient family of lipid droplet proteins that regulate cellular lipid stores. *Biochim Biophys Acta,* 1791**,** 419-40.

BLACKMAN, M. J. & BANNISTER, L. H. 2001. Apical organelles of Apicomplexa: biology and isolation by subcellular fractionation. *Mol Biochem Parasitol,* 117**,** 11-25.

BLADER, I. J., MANGER, I. D. & BOOTHROYD, J. C. 2001. Microarray analysis reveals previously unknown changes in *Toxoplasma gondii*-infected human cells. *J Biol Chem,* 276**,** 24223-31.

BOTTOVA, I., HEHL, A. B., STEFANIC, S., FABRIAS, G., CASAS, J., SCHRANER, E., PIETERS, J. & SONDA, S. 2009. Host cell P-glycoprotein is essential for cholesterol uptake and replication of *Toxoplasma gondii*. *J Biol Chem,* 284**,** 17438-48.

BOZZA, P. T., MELO, R. C. & BANDEIRA-MELO, C. 2007. Leukocyte lipid bodies regulation and function: contribution to allergy and host defense. *Pharmacol Ther,* 113**,** 30-49.

BRADFORD, M. M. 1976. A rapid and sensitive method for the quantitation of microgram quantities of protein utilizing the principle of protein-dye binding. *Anal Biochem,* 72**,** 248-54.

BRASAEMLE, D. L., DOLIOS, G., SHAPIRO, L. & WANG, R. 2004. Proteomic analysis of proteins associated with lipid droplets of basal and lipolytically stimulated 3T3-L1 adipocytes. *J Biol Chem,* 279**,** 46835-42.

BRAUTBAR, A. & BALLANTYNE, C. M. 2011. Pharmacological strategies for lowering LDL cholesterol: statins and beyond. *Nat Rev Cardiol,* 8**,** 253-65.

BROWN, A. J. & JESSUP, W. 2009. Oxysterols: Sources, cellular storage and metabolism, and new insights into their roles in cholesterol homeostasis. *Mol Aspects Med,* 30**,** 111-22.

BROWN, M. S. & GOLDSTEIN, J. L. 1975a. Lipoprotein receptors and genetic control of cholesterol metabolism in cultured human cells. *Naturwissenschaften,* 62**,** 385-9.

BROWN, M. S. & GOLDSTEIN, J. L. 1975b. Regulation of the activity of the low density lipoprotein receptor in human fibroblasts. *Cell,* 6**,** 307-16.

BROWN, M. S. & GOLDSTEIN, J. L. 1986. A receptor-mediated pathway for cholesterol homeostasis. *Science,* 232**,** 34-47.

BROWN, M. S., DANA, S. E. & GOLDSTEIN, J. L. 1975a. Cholesterol ester formation in cultured human fibroblasts. Stimulation by oxygenated sterols. *J Biol Chem,* 250**,** 4025-7.

BROWN, M. S., FAUST, J. R. & GOLDSTEIN, J. L. 1975b. Role of the low density lipoprotein receptor in regulating the content of free and esterified cholesterol in human fibroblasts. *J Clin Invest,* 55**,** 783-93.

BROWN, W. J., WARFEL, J. & GREENSPAN, P. 1988. Use of Nile red stain in the detection of cholesteryl ester accumulation in acid lipase-deficient fibroblasts. *Arch* P*athol Lab Med,* 112**,** 295-7.

BROWN, W. V. 2001. Novel approaches to lipid lowering: what is on the horizon? *Am J Cardiol,* 87**,** 23b-27b.

BUHAESCU, I. & IZZEDINE, H. 2007. Mevalonate pathway: a review of clinical and therapeutical implications. *Clin Biochem,* 40**,** 575-84.

BUHMAN, K. F., ACCAD, M. & FARESE, R. V. 2000. Mammalian acyl-CoA:cholesterol acyltransferases. *Biochim Biophys Acta,* 1529**,** 142-54.

BURGER, H.J. 1983. *Eimeria*-Infektionen beim Rind. Berl. Munch. Tierarztl. Wochenschr. 96, 350-357.

BURGESS, A., VIGNERON, S., BRIOUDES, E., LABBE, J. C., LORCA, T. & CASTRO, A. 2010. Loss of human Greatwall results in G2 arrest and multiple mitotic defects due to deregulation of the cyclin B-Cdc2/PP2A balance. *Proc Natl Acad Sci U S A,* 107**,** 12564-9.

BUSTIN, S. A., BENES, V., GARSON, J. A., HELLEMANS, J., HUGGETT, J., KUBISTA, M., MUELLER, R., NOLAN, T., PFAFFL, M. W., SHIPLEY, G. L., VANDESOMPELE, J. & WITTWER, C. T. 2009. The MIQE guidelines: minimum information for publication of quantitative real-time PCR experiments. *Clin Chem,* 55**,** 611-22.

CAAMANO, J., TATO, C., CAI, G., VILLEGAS, E. N., SPEIRS, K., CRAIG, L., ALEXANDER, J. & HUNTER, C. A. 2000. Identification of a role for NF-kappa B2 in the regulation of apoptosis and in maintenance of T cell-mediated immunity to *Toxoplasma gondii*. *J Immunol,* 165**,** 5720-8.

CARMEN, J. C., HARDI, L. & SINAI, A. P. 2006. *Toxoplasma gondii* inhibits ultraviolet light-induced apoptosis through multiple interactions with the mitochondrion-dependent programmed cell death pathway. *Cell Microbiol,* 8**,** 301-15.

CARRUTHERS, V. B. & SIBLEY, L. D. 1997. Sequential protein secretion from three distinct organelles of *Toxoplasma gondii* accompanies invasion of human fibroblasts. *Eur J Cell Biol,* 73**,** 114-23.

CHAMBERS, K., JUDSON, B. & BROWN, W. J. 2005. A unique lysophospholipid acyltransferase (LPAT) antagonist, CI-976, affects secretory and endocytic membrane trafficking pathways. *J Cell Sci,* 118**,** 3061-71.

CHANG, T. Y., CHANG, C. C., OHGAMI, N. & YAMAUCHI, Y. 2006. Cholesterol sensing, trafficking, and esterification. *Annu Rev Cell Dev Biol,* 22**,** 129-57.

CHANG, T. Y., LI, B. L., CHANG, C. C. & URANO, Y. 2009. Acyl-coenzyme A:cholesterol acyltransferases. *Am J Physiol Endocrinol Metab,* 297**,** E1-9.

CHARRON, A. J. & SIBLEY, L. D. 2002. Host cells: mobilizable lipid resources for the intracellular parasite *Toxoplasma gondii*. *J Cell Sci,* 115**,** 3049-59.

CHEN, X. M., GORES, G. J., PAYA, C. V. & LARUSSO, N. F. 1999. *Cryptosporidium parvum* induces apoptosis in biliary epithelia by a Fas/Fas ligand-dependent mechanism. *Am J Physiol,* 277**,** G599-608.

CHEN, X. M., LEVINE, S. A., SPLINTER, P. L., TIETZ, P. S., GANONG, A. L., JOBIN, C., GORES, G. J., PAYA, C. V. & LARUSSO, N. F. 2001. *Cryptosporidium parvum* activates nuclear factor kappaB in biliary epithelia preventing epithelial cell apoptosis. *Gastroenterology,* 120**,** 1774-83.

CHIRALA, S. S. & WAKIL, S. J. 2004. Structure and function of animal fatty acid synthase. *Lipids,* 39**,** 1045-53.

CHIRIBAO, M. L., LIBISCH, G., PARODI-TALICE, A. & ROBELLO, C. 2014. Early *Trypanosoma cruzi* infection reprograms human epithelial cells. *Biomed Res Int,* 2014**,** 439501.

CHOBOTAR, B & SCHOLTYSECK, E. 1982. Ultrastructure .in Long. P.L.: *The biology of the coccidia.* Baltimore: University Park Press.

CHRISTIAN, A. E., HAYNES, M. P., PHILLIPS, M. C. & ROTHBLAT, G. H. 1997. Use of cyclodextrins for manipulating cellular cholesterol content. *J Lipid Res,* 38**,** 2264-72.

COPPENS, I. & JOINER, K. A. 2003. Host but not parasite cholesterol controls *Toxoplasma* cell entry by modulating organelle discharge. *Mol Biol Cell,* 14**,** 3804-20.

COPPENS, I. & VIELEMEYER, O. 2005. Insights into unique physiological features of neutral lipids in Apicomplexa: from storage to potential mediation in parasite metabolic activities. *Int J Parasitol,* 35**,** 597-615.

COPPENS, I. 2006. Contribution of host lipids to *Toxoplasma* pathogenesis. *Cell Microbiol,* 8**,** 1-9.

COPPENS, I. 2013. Targeting lipid biosynthesis and salvage in apicomplexan parasites for improved chemotherapies. *Nat Rev Microbiol,* 11**,** 823-35.

COPPENS, I., DUNN, J. D., ROMANO, J. D., PYPAERT, M., ZHANG, H., BOOTHROYD, J. C. & JOINER, K. A. 2006. *Toxoplasma gondii* sequesters lysosomes from mammalian hosts in the vacuolar space. *Cell,* 125**,** 261-74.

COPPENS, I., SINAI, A. P. & JOINER, K. A. 2000. *Toxoplasma gondii* exploits host low-density lipoprotein receptor-mediated endocytosis for cholesterol acquisition. *J Cell Biol,* 149**,** 167-80.

CORNELISSEN, A. W., VERSTEGEN, R., VAN DEN BRAND, H., PERIE, N. M., EYSKER, M., LAM, T. J. & PIJPERS, A. 1995. An observational study of *Eimeria* species in housed cattle on Dutch dairy farms. *Vet Parasitol,* 56**,** 7-16.

CORTEZ, E., STUMBO, A. C., OLIVEIRA, M., BARBOSA, H. S. & CARVALHO, L. 2009. Statins inhibit *Toxoplasma gondi*i multiplication in macrophages *in vitro*. *Int J Antimicrob Agents,* 33**,** 185-6.

CRUZ, K. D., CRUZ, T. A., VERAS DE MORAES, G., PAREDES-SANTOS, T. C., ATTIAS, M. & DE SOUZA, W. 2013. disruption of lipid rafts interferes with the interaction of *Toxoplasma gondii* with macrophages and epithelial Cells. *Biomed Res Int,* 2013**,** 687835.

DAUGSCHIES, A. & NAJDROWSKI, M. 2005. Eimeriosis in cattle: current understanding. *J Vet Med B Infect Dis Vet Public Health,* 52**,** 417-27.

DAUGSCHIES, A., AKIMARU, M. & BURGER, H. J. 1986. [Experimental *Eimeria bovis* infections in the calf: 1. Parasitologic and clinical findings]. *Dtsch Tierarztl Wochenschr,* 93**,** 393-7.

D'AVILA, H., FREIRE-DE-LIMA, C. G., ROQUE, N. R., TEIXEIRA, L., BARJA-FIDALGO, C., SILVA, A. R., MELO, R. C., DOSREIS, G. A., CASTRO-FARIA-NETO, H. C. & BOZZA, P. T. 2011. Host cell lipid bodies triggered by *Trypanosoma cruzi* infection and enhanced by the uptake of apoptotic cells are associated with prostaglandin E(2) generation and increased parasite growth. *J Infect Dis,* 204**,** 951-61.

D'AVILA, H., MAYA-MONTEIRO, C. M. & BOZZA, P. T. 2008. Lipid bodies in innate immune response to bacterial and parasite infections. *Int Immunopharmacol,* 8**,** 1308-15.

DE SOUZA, W & ATTIAS, M. 2010. Subpellicular microtubules in Apicomplexa and Trypanosomatids. In de Souza, W.: *Structures and Organelles in Pathogenic Protist*. Berlin: Springer Verlag.

DE VENEVELLES, P., FRANCOIS CHICH, J., FAIGLE, W., LOMBARD, B., LOEW, D., PERY, P. & LABBE, M. 2006. Study of proteins associated with the *Eimeria tenella* refractile body by a proteomic approach. *Int J Parasitol,* 36**,** 1399-407.

DEL CACHO, E., GALLEGO, M., LOPEZ-BERNAD, F., QUILEZ, J. & SANCHEZ-ACEDO, C. 2004. Expression of anti-apoptotic factors in cells parasitized by second-generation schizonts of *Eimeria tenella* and *Eimeria necatrix*. *Vet Parasitol,* 125**,** 287-300.

DIDONATO, D. & BRASAEMLE, D. L. 2003. Fixation methods for the study of lipid droplets by immunofluorescence microscopy. *J Histochem Cytochem,* 51**,** 773-80.

DOOLAN, D. L. & HOFFMAN, S. L. 2000. The complexity of protective immunity against liver-stage malaria. *J Immunol,* 165**,** 1453-62.

DUBREMETZ, J. F. & ELSNER, Y. Y. 1979. Ultrastructural study of schizogony of *Eimeria bovis* in cell cultures. *J Protozool,* 26**,** 367-76.

DUBREMETZ, J. F., GARCIA-REGUET, N., CONSEIL, V. & FOURMAUX, M. N. 1998. Apical organelles and host-cell invasion by Apicomplexa. *Int J Parasitol,* 28**,** 1007-13.

EBERLE, D., HEGARTY, B., BOSSARD, P., FERRE, P. & FOUFELLE, F. 2004. SREBP transcription factors: master regulators of lipid homeostasis. *Biochimie,* 86**,** 839-48.

EBNET, K. & VESTWEBER, D. 1999. Molecular mechanisms that control leukocyte extravasation: the selectins and the chemokines. *Histochem Cell Biol,* 112**,** 1-23.

EDWARDS, P. A., TABOR, D., KAST, H. R. & VENKATESWARAN, A. 2000. Regulation of gene expression by SREBP and SCAP. *Biochim Biophys Acta,* 1529**,** 103-13.

EHRENMAN, K., WANYIRI, J. W., BHAT, N., WARD, H. D. & COPPENS, I. 2013. *Cryptosporidium parvum* scavenges LDL-derived cholesterol and micellar cholesterol internalized into enterocytes. *Cell Microbiol,* 15**,** 1182-97.

ENTZEROTH, R., MATTIG, F. R. & WERNER-MEIER, R. 1998. Structure and function of the parasitophorous vacuole in *Eimeria* species. *Int J Parasitol,* 28**,** 1015-8.

FABER, J. E., KOLLMANN, D., HEISE, A., BAUER, C., FAILING, K., BURGER, H. J. & ZAHNER, H. 2002. *Eimeria* infections in cows in the periparturient phase and their calves: oocyst excretion and levels of specific serum and colostrum antibodies. *Vet Parasitol,* 104**,** 1-17.

FARESE, R. V., JR. & WALTHER, T. C. 2009. Lipid droplets finally get a little R-E-S-P-E-C-T. *Cell,* 139**,** 855-60.

FAYER, R. & HAMMOND, D. M. 1967. Development of first-generation schizonts of *Eimeria bovis* in cultured bovine cells. *J Protozool,* 14**,** 764-72.

FERNANDES, M. C., CORTEZ, M., GERALDO YONEYAMA, K. A., STRAUS, A. H., YOSHIDA, N. & MORTARA, R. A. 2007. Novel strategy in *Trypanosoma cruzi* cell invasion: implication of cholesterol and host cell microdomains. *Int J Parasitol,* 37**,** 1431-41.

FISCH, S., GRAY, S., HEYMANS, S., HALDAR, S. M., WANG, B., PFISTER, O., CUI, L., KUMAR, A., LIN, Z., SEN-BANERJEE, S., DAS, H., PETERSEN, C. A., MENDE, U., BURLEIGH, B. A., ZHU, Y., PINTO, Y. M., LIAO, R. & JAIN, M. K. 2007. Kruppel-like factor 15 is a regulator of cardiomyocyte hypertrophy. *Proc Natl Acad Sci U S A,* 104**,** 7074-9.

FITZGERALD, P. R. 1980. The economic impact of coccidiosis in domestic animals. *Adv. Vet. Sci. Comp. Med*. 24, 121–143.

FLAVIN, R., PELUSO, S., NGUYEN, P. L. & LODA, M. 2010. Fatty acid synthase as a potential therapeutic target in cancer. *Future Oncol,* 6**,** 551-62.

FLEIGE, S., WALF, V., HUCH, S., PRGOMET, C., SEHM, J. & PFAFFL, M. W. 2006. Comparison of relative mRNA quantification models and the impact of RNA integrity in quantitative real-time RT-PCR. *Biotechnol Lett,* 28**,** 1601-13.

FOUSSARD, F., GALLOIS, Y., GIRAULT, A. & MENEZ, J. F. 1991a. Lipids and fatty acids of tachyzoites and purified pellicles of *Toxoplasma gondii*. *Parasitol Res,* 77**,** 475-7.

FOUSSARD, F., LERICHE, M. A. & DUBREMETZ, J. F. 1991b. Characterization of the lipid content of *Toxoplasma gondii* rhoptries. *Parasitology,* 102 Pt 3**,** 367-70.

FOX, J.E. 1985. Coccidiosis in cattle. *Mod. Vet. Pract.* 66, 113-116.

FRIAS, M. A., REBSAMEN, M. C., GERBER-WICHT, C. & LANG, U. 2007. Prostaglandin E2 activates Stat3 in neonatal rat ventricular cardiomyocytes: A role in cardiac hypertrophy. *Cardiovasc Res,* 73**,** 57-65.

FROLOV, A., WOODFORD, J. K., MURPHY, E. J., BILLHEIMER, J. T. & SCHROEDER, F. 1996. Spontaneous and protein-mediated sterol transfer between intracellular membranes. *J Biol Chem,* 271**,** 16075-83.

FUJIMOTO, T. & PARTON, R. G. 2011. Not just fat: the structure and function of the lipid droplet. *Cold Spring Harb Perspect Biol,* 3.

FUJIMOTO, T. 2004. [Lipid droplet as an independent organelle]. *Seikagaku,* 76**,** 578-84.

FUJIMOTO, T., OHSAKI, Y., CHENG, J., SUZUKI, M. & SHINOHARA, Y. 2008. Lipid droplets: a classic organelle with new outfits. *Histochem Cell Biol,* 130**,** 263-79.

FURLONG, S. T. 1989. Sterols of parasitic protozoa and helminths. *Exp Parasitol,* 68**,** 482-5.

GAVET, O. & PINES, J. 2010. Activation of cyclin B1-Cdk1 synchronizes events in the nucleus and the cytoplasm at mitosis. *J Cell Biol,* 189**,** 247-59.

GIMM, T., WIESE, M., TESCHEMACHER, B., DEGGERICH, A., SCHODEL, J., KNAUP, K. X., HACKENBECK, T., HELLERBRAND, C., AMANN, K., WIESENER, M. S., HONING, S., ECKARDT, K. U. & WARNECKE, C.

2010. Hypoxia-inducible protein 2 is a novel lipid droplet protein and a specific target gene of hypoxia-inducible factor-1. *Faseb j,* 24**,** 4443-58.

GIMPL, G. & GEHRIG-BURGER, K. 2007. Cholesterol reporter molecules. *Biosci Rep,* 27**,** 335-58.

GIMPL, G. & GEHRIG-BURGER, K. 2011. Probes for studying cholesterol binding and cell biology. *Steroids,* 76**,** 216-31.

GOCZE, P. M. & FREEMAN, D. A. 1994. Factors underlying the variability of lipid droplet fluorescence in MA-10 Leydig tumor cells. *Cytometry,* 17**,** 151-8.

GOEBEL, S., LUDER, C. G. & GROSS, U. 1999. Invasion by *Toxoplasma gondii* protects human-derived HL-60 cells from actinomycin D-induced apoptosis. *Med Microbiol Immunol,* 187**,** 221-6.

GOEBEL, S., LUDER, C. G., LUGERT, R., BOHNE, W. & GROSS, U. 1998. *Toxoplasma gondii* inhibits the in vitro induced apoptosis of HL-60 cells. *Tokai J Exp Clin Med,* 23**,** 351-6.

GOLDMAN, S. D. & KRISE, J. P. 2010. Niemann-Pick C1 functions independently of Niemann-Pick C2 in the initial stage of retrograde transport of membrane-impermeable lysosomal cargo. *J Biol Chem,* 285**,** 4983-94.

GOLDSTEIN, J. L. & BROWN, M. S. 1990. Regulation of the mevalonate pathway. *Nature,* 343**,** 425-30.

GOLDSTEIN, J. L. & BROWN, M. S. 2009. The LDL receptor. *Arterioscler Thromb Vasc Biol,* 29**,** 431-8.

GOLDSTEIN, J. L., DEBOSE-BOYD, R. A. & BROWN, M. S. 2006. Protein sensors for membrane sterols. *Cell,* 124**,** 35-46.

GOLDSTEIN, J. L., HO, Y. K., BASU, S. K. & BROWN, M. S. 1979. Binding site on macrophages that mediates uptake and degradation of acetylated low density lipoprotein, producing massive cholesterol deposition. P*roc Natl Acad Sci U S A,* 76**,** 333-7.

GOMES, A. F., MAGALHAES, K. G., RODRIGUES, R. M., DE CARVALHO, L., MOLINARO, R., BOZZA, P. T. & BARBOSA, H. S. 2014. *Toxoplasma gondii*-skeletal muscle cells interaction increases lipid droplet biogenesis and positively modulates the production of IL-12, IFN-g and PGE2. *Parasit Vectors,* 7**,** 47.

GRAFNER, G. & GRAUBMANN, H. D. 1979. [Remarks on the pathogenicity of *Eimeria* species exemplified by cattle coccidiosis]. *Angew Parasitol,* 20**,** 202-9.

GREEN, D. R. & REED, J. C. 1998. Mitochondria and apoptosis. *Science,* 281**,** 1309-12.

GREEN, D. R. 1998. Apoptotic pathways: the roads to ruin. *Cell,* 94**,** 695-8.

GREEN, D. R. 2000. Apoptotic pathways: paper wraps stone blunts scissors. *Cell,* 102**,** 1-4.

GREENSPAN, P., MAYER, E. P. & FOWLER, S. D. 1985. Nile red: a selective fluorescent stain for intracellular lipid droplets. *J Cell Biol,* 100**,** 965-73.

GRELLIER, P., RIGOMIER, D. & SCHREVEL, J. 1990. [*In vitro* induction of *Plasmodium falciparum* schizogony by human high density lipoproteins (HDL)]. *C R Acad Sci III,* 311**,** 361-7.

GRUNDY, S. M. 1983. Absorption and metabolism of dietary cholesterol. *Annu Rev Nutr,* 3**,** 71-96.

GUL, A., CICEK, M. & KILINC, O. 2008. Prevalence of *Eimeria* spp., *Cryptosporidium* spp. and *Giardia* spp. in calves in the Van province. *Turkiye Parazitol Derg,* 32**,** 202-4.

HAMMOND, D. M., ANDERSEN F. L.&MINER M. L. 1963. The occurrence of a second asexual generation in the life cycle of *Eimeria bov*is in calves. *J.Parasitol*, 49, 3: 428-434.

HAMMOND, D. M., BOWMAN G. W., DAVIS L. R., & SIMMS B. T. 1946. The endogenous phase of the life cycle of *Eimeria bovis. J.Parasitol*, 32, 409-427.

HAMMOND, D. M., CHOBOTAR B.& ERNST J. V. 1968. Cytological observations on sporozoites of *Eimeria bovis* and *E. auburnensis* and an *Eimeria* species from the ord kangaroo rat. *J.Parasitol*, 54, 3: 550-558.

HAMMOND, D. M., SPEER, C. A. & ROBERTS, W. 1970. Occurrence of refractile bodies in merozoites of *Eimeria* species. *J Parasitol,* 56**,** 189-91.

HAMMOND, D.M., ERNST, J.V. & MINER, M.L. 1966. The development of first generation schizonts of *Eimeria bovis*. J. Protozool, 13, 559564.

HARA, A. & RADIN, N. S. 1978. Lipid extraction of tissues with a low-toxicity solvent. *Anal Biochem,* 90**,** 420-6.

HEISE, A., PETERS, W. & ZAHNER, H. 1999a. Microneme antigens of *Eimeria bovis* recognized by two monoclonal antibodies. *Parasitol Res,* 85**,** 457-67.

HEISE, A., PETERS, W. & ZAHNER, H. 1999b. A monoclonal antibody reacts species-specifically with amylopectin granules of *Eimeria bovis* merozoites. *Parasitol Res,* 85**,** 500-3.

HERMOSILLA, C., BARBISCH, B., HEISE, A., KOWALIK, S. & ZAHNER, H. 2002. Development of *Eimeria bovis in vitro*: suitability of several bovine, human and porcine endothelial cell lines, bovine fetal gastrointestinal, Madin-Darby bovine kidney (MDBK) and African green monkey kidney (VERO) cells. *Parasitol Res,* 88**,** 301-7.

HERMOSILLA, C., BURGER, H. J. & ZAHNER, H. 1999. T cell responses in calves to a primary *Eimeria bovis* infection: phenotypical and functional changes. *Vet Parasitol,* 84**,** 49-64.

HERMOSILLA, C., RUIZ, A. & TAUBERT, A. 2012. *Eimeria bovis*: an update on parasite-host cell interactions. *Int J Med Microbiol,* 302**,** 210-5.

HERMOSILLA, C., SCHROPFER, E., STOWASSER, M., ECKSTEIN-LUDWIG, U., BEHRENDT, J. H. & ZAHNER, H. 2008. Cytoskeletal changes in *Eimeria bovis*-infected host endothelial cells during first merogony. *Vet Res Commun,* 32**,** 521-31.

HERMOSILLA, C., ZAHNER, H. & TAUBERT, A. 2006. *Eimeria bovis* modulates adhesion molecule gene transcription in and PMN adhesion to infected bovine endothelial cells. *Int J Parasitol,* 36**,** 423-31.

HEUSSLER, V. T., KUENZI, P. & ROTTENBERG, S. 2001. Inhibition of apoptosis by intracellular protozoan parasites. *Int J Parasitol,* 31**,** 1166-76.

HEUSSLER, V. T., MACHADO, J., JR., FERNANDEZ, P. C., BOTTERON, C., CHEN, C. G., PEARSE, M. J. & DOBBELAERE, D. A. 1999. The intracellular parasite *Theileria parva* protects infected T cells from apoptosis. *Proc Natl Acad Sci U S A,* 96**,** 7312-7.

HOOSHMAND-RAD, P., SVENSSON, C. & UGGLA, A. 1994. Experimental *Eimeria alabamensis* infection in calves. *Vet Parasitol,* 53**,** 23-32.

HORIUCHI, S., SAKAMOTO, Y. & SAKAI, M. 2003. Scavenger receptors for oxidized and glycated proteins. *Amino Acids,* 25**,** 283-92

HORTON, J. D., GOLDSTEIN, J. L. & BROWN, M. S. 2002. SREBPs: activators of the complete program of cholesterol and fatty acid synthesis in the liver. *J Clin Invest,* 109**,** 1125-31.

HUA-HONG, Y., XIANG-MEI, L, ZE-YUAN, D. 2010. Effect of oleic acid on proliferation of human umbilical vein endothelial cells [J]. *Food Science*, 31, 372-374.

IKONEN, E. 2008. Cellular cholesterol trafficking and compartmentalization. *Nat Rev Mol Cell Biol,* 9**,** 125-38.

ISTVAN, E. S. & DEISENHOFER, J. 2001. Structural mechanism for statin inhibition of HMG-CoA reductase. *Science,* 292**,** 1160-4.

JACKSON, A. R. 1964. THE ISOLATION OF VIABLE COCCIDIAL SPOROZOITES. *Parasitology,* 54**,** 87-93.

JACKSON, K. E., KLONIS, N., FERGUSON, D. J., ADISA, A., DOGOVSKI, C. & TILLEY, L. 2004. Food vacuole-associated lipid bodies and heterogeneous lipid environments in the malaria parasite, *Plasmodium falciparum*. *Mol Microbiol,* 54**,** 109-22.

JAFFE, E. A., NACHMAN, R. L., BECKER, C. G. & MINICK, C. R. 1973. Culture of human endothelial cells derived from umbilical veins. Identification by morphologic and immunologic criteria. *J Clin Invest,* 52**,** 2745-56.

JOHNDROW, C., NELSON, R., TANOWITZ, H., WEISS, L. M. & NAGAJYOTHI, F. 2014. *Trypanosoma cruzi* infection results in an increase in intracellular cholesterol. *Microbes Infect,* 16**,** 337-44.

JONAS, A. 2004. Lipoprotein structure. In VANCE D. E. & VANCE J. E., *Biochemistry of lipids, lipoproteins, and membranes, 4th edition*. Amsterdam: Elsevier B.V.

JUNGST, C., KLEIN, M. & ZUMBUSCH, A. 2013. Long-term live cell microscopy studies of lipid droplet fusion dynamics in adipocytes. *J Lipid Res,* 54**,** 3419-29.

KAM, N. T., ALBRIGHT, E., MATHUR, S. & FIELD, F. J. 1990. Effect of lovastatin on acyl-CoA: cholesterol O-acyltransferase (ACAT) activity and the basolateral-membrane secretion of newly synthesized lipids by CaCo-2 cells. *Biochem J,* 272**,** 427-33.

KANDUTSCH, A. A. & SHOWN, E. P. 1981. Assay of oxysterol-binding protein in a mouse fibroblast, cell-free system. Dissociation constant and other properties of the system. *J Biol Chem,* 256**,** 13068-73.

KELLER, P., SCHAUMBURG, F., FISCHER, S. F., HACKER, G., GROSS, U. & LUDER, C. G. 2006. Direct inhibition of cytochrome c-induced caspase activation in vitro by *Toxoplasma gondii* reveals novel mechanisms of interference with host cell apoptosis. *FEMS Microbiol Lett,* 258**,** 312-9.

KUENZI, P., SCHNEIDER, P. & DOBBELAERE, D. A. 2003. *Theileria parva*-transformed T cells show enhanced resistance to Fas/Fas ligand-induced apoptosis. *J Immunol,* 171**,** 1224-31.

KUERSCHNER, L., MOESSINGER, C. & THIELE, C. 2008. Imaging of lipid biosynthesis: how a neutral lipid enters lipid droplets. *Traffic,* 9**,** 338-52.

KUHAJDA, F. P., PIZER, E. S., LI, J. N., MANI, N. S., FREHYWOT, G. L. & TOWNSEND, C. A. 2000. Synthesis and antitumor activity of an inhibitor of fatty acid synthase. *Proc Natl Acad Sci U S A,* 97**,** 3450-4.

KUME, N., MURASE, T., MORIWAKI, H., AOYAMA, T., SAWAMURA, T., MASAKI, T. & KITA, T. 1998. Inducible expression of lectin-like oxidized LDL receptor-1 in vascular endothelial cells. *Circ Res,* 83**,** 322-7.

LABAIED, M., JAYABALASINGHAM, B., BANO, N., CHA, S. J., SANDOVAL, J., GUAN, G. & COPPENS, I. 2011. *Plasmodium* salvages cholesterol internalized by LDL and synthesized *de novo* in the liver. *Cell Microbiol,* 13**,** 569-86.

LALIBERTE, J. & CARRUTHERS, V. B. 2008. Host cell manipulation by the human pathogen *Toxoplasma gondii*. *Cell Mol Life Sci,* 65**,** 1900-15.

LANG, M., KANN, M., ZAHNER, H., TAUBERT, A. & HERMOSILLA, C. 2009. Inhibition of host cell apoptosis by *Eimeria bovis* sporozoites. *Vet Parasitol,* 160**,** 25-33.

LANGE, Y. 1991. Disposition of intracellular cholesterol in human fibroblasts. *J Lipid Res,* 32**,** 329-39.

LAUER, S., VANWYE, J., HARRISON, T., MCMANUS, H., SAMUEL, B. U., HILLER, N. L., MOHANDAS, N. & HALDAR, K. 2000. Vacuolar uptake of host components, and a role for cholesterol and sphingomyelin in malarial infection. *EMBO J,* 19**,** 3556-64.

LECOEUR, H., GIRAUD, E., PREVOST, M. C., MILON, G. & LANG, T. 2013. Reprogramming neutral lipid metabolism in mouse dendritic leucocytes hosting live *Leishmania amazonensis* amastigotes. *PLoS Negl Trop Dis,* 7**,** e2276.

LEMGRUBER, L. & LUPETTI, P. 2012. Crystalloid body, refractile body and virus-like particles in Apicomplexa: what is in there? *Parasitology,* 139**,** 285-93.

LEUTENEGGER, C. M., ALLUWAIMI, A. M., SMITH, W. L., PERANI, L. & CULLOR, J. S. 2000. Quantitation of bovine cytokine mRNA in milk cells of healthy cattle by real-time TaqMan polymerase chain reaction. *Vet Immunol Immunopathol,* 77**,** 275-87.

LEVINE, N. D., CORLISS, J. O., COX, F. E., DEROUX, G., GRAIN, J., HONIGBERG, B. M., LEEDALE, G. F., LOEBLICH, A. R., 3RD, LOM, J., LYNN, D., MERINFELD, E. G., PAGE, F. C., POLJANSKY, G., SPRAGUE, V., VAVRA, J. & WALLACE, F. G. 1980. A newly revised classification of the protozoa. *J Protozool,* 27**,** 37-58.

LIAO, J. K. 2002. Isoprenoids as mediators of the biological effects of statins. *J Clin Invest,* 110**,** 285-8.

LIGE, B., SAMPELS, V. & COPPENS, I. 2013. Characterization of a second sterol-esterifying enzyme in *Toxoplasma* highlights the importance of cholesterol storage pathways for the parasite. *Mol Microbiol,* 87**,** 951-67.

LINDSEY, S. & HARWOOD, H. J., JR. 1995. Inhibition of mammalian squalene synthetase activity by zaragozic acid A is a result of competitive inhibition

followed by mechanism-based irreversible inactivation. *J Biol Chem,* 270**,** 9083-96.

LISCUM, L. & UNDERWOOD, K. W. 1995. Intracellular cholesterol transport and compartmentation. *J Biol Chem,* 270**,** 15443-6.

LISCUM, L. 2004. Cholesterol biosynthesis. In VANCE D. E. & VANCE J. E., *Biochemistry of lipids, lipoproteins, and membranes, 4th edition*. Amsterdam: Elsevier B. V.

LIVAK, K. J. & SCHMITTGEN, T. D. 2001. Analysis of relative gene expression data using real-time quantitative PCR and the 2(-Delta Delta C(T)) Method. *Methods,* 25**,** 402-8.

LUDER, C. G. & GROSS, U. 2005. Apoptosis and its modulation during infection with *Toxoplasma gondii*: molecular mechanisms and role in pathogenesis. *Curr Top Microbiol Immunol,* 289**,** 219-37.

LUTZ, K. 2008. Charakterisierung des *Eimeria bovis* Mikronemenproteins 4 (EbMIC4) und erste Studien zur Modulation des Wirtszell-Proteoms durch *Eimeria bovis*. *PhD Dissertation*. Justus Liebig Universitaet. Giessen.

LUTZ, K., SCHMITT, S., LINDER, M., HERMOSILLA, C., ZAHNER, H. & TAUBERT, A. 2011. *Eimeria bovis*-induced modulation of the host cell proteome at the meront I stage. *Mol Biochem Parasitol,* 175**,** 1-9.

MAHLBERG, F. H., GLICK, J. M., JEROME, W. G. & ROTHBLAT, G. H. 1990. Metabolism of cholesteryl ester lipid droplets in a J774 macrophage foam cell model. *Biochim Biophys Acta,* 1045**,** 291-8.

MARTIN, S. & PARTON, R. G. 2006. Lipid droplets: a unified view of a dynamic organelle. *Nat Rev Mol Cell Biol,* 7**,** 373-8.

MARTIN, S., & PARTON, R. G. 2011. Characterization of Rab18, A lipid droplet-associated small GTPAse. In P. M. CONN, *Methods of enzymology*, 111-113. California: Academic Press Elsevier.

MARTINS-DUARTE, E. S., URBINA, J. A., DE SOUZA, W. & VOMMARO, R. C. 2006. Antiproliferative activities of two novel quinuclidine inhibitors against *Toxoplasma gondii* tachyzoites *in vitro*. *J Antimicrob Chemother,* 58**,** 59-65.

MATJILA, P. T. & PENZHORN, B. L. 2002. Occurrence and diversity of bovine coccidia at three localities in South Africa. *Vet Parasitol,* 104**,** 93-102.

MAXFIELD, F. R. & WUSTNER, D. 2012. Analysis of cholesterol trafficking with fluorescent probes. *Methods Cell Biol,* 108**,** 367-93.

MCDONOUGH, P. M., AGUSTIN, R. M., INGERMANSON, R. S., LOY, P. A., BUEHRER, B. M., NICOLL, J. B., PRIGOZHINA, N. L., MIKIC, I. & PRICE, J. H. 2009. Quantification of lipid droplets and associated proteins in cellular models of obesity via high-content/high-throughput microscopy and automated image analysis. *Assay Drug Dev Technol,* 7**,** 440-60.

MCMAHON, H. T. & BOUCROT, E. 2011. Molecular mechanism and physiological functions of clathrin-mediated endocytosis. *Nat Rev Mol Cell Biol,* 12**,** 517-33.

MELO, R. C., D'AVILA, H., FABRINO, D. L., ALMEIDA, P. E. & BOZZA, P. T. 2003. Macrophage lipid body induction by Chagas disease in vivo: putative

intracellular domains for eicosanoid formation during infection. *Tissue Cell,* 35**,** 59-67.

MELO, R. C., D'AVILA, H., WAN, H. C., BOZZA, P. T., DVORAK, A. M. & WELLER, P. F. 2011. Lipid bodies in inflammatory cells: structure, function, and current imaging techniques. *J Histochem Cytochem,* 59**,** 540-56.

MELO, R. C., FABRINO, D. L., DIAS, F. F. & PARREIRA, G. G. 2006. Lipid bodies: Structural markers of inflammatory macrophages in innate immunity. *Inflamm Res,* 55**,** 342-8.

MENENDEZ, J. A. & LUPU, R. 2007. Fatty acid synthase and the lipogenic phenotype in cancer pathogenesis. *Nat Rev Cancer,* 7**,** 763-77.

MERCIER, C., ADJOGBLE, K. D., DAUBENER, W. & DELAUW, M. F. 2005. Dense granules: are they key organelles to help understand the parasitophorous vacuole of all apicomplexa parasites? *Int J Parasitol,* 35**,** 829-49.

MORIWAKI, H., KUME, N., SAWAMURA, T., AOYAMA, T., HOSHIKAWA, H., OCHI, H., NISHI, E., MASAKI, T. & KITA, T. 1998. Ligand specificity of LOX-1, a novel endothelial receptor for oxidized low density lipoprotein. *Arterioscler Thromb Vasc Biol,* 18**,** 1541-7.

MORRISSETTE, N. S. & SIBLEY, L. D. 2002. Cytoskeleton of apicomplexan parasites. *Microbiol Mol Biol Rev,* 66**,** 21-38; table of contents.

MOTULSKY, H. J., & CHRISTOPOULOS, A. 2003. Fitting models to biological data using linear and nonlinear regression: a practical guide to curve fitting. Sand Diego. CA: GraphPad Software Inc.

MURPHY, S., MARTIN, S. & PARTON, R. G. 2009. Lipid droplet-organelle interactions; sharing the fats. *Biochim Biophys Acta,* 1791**,** 441-7.

MYANT, N. 1990. The LDL receptor: Biology and biochemistry. In *Cholesterol Metabolism, LDL, and the LDL Receptor, 1st edition.* London: Academic Press

NAGAJYOTHI, F., WEISS, L. M., SILVER, D. L., DESRUISSEAUX, M. S., SCHERER, P. E., HERZ, J. & TANOWITZ, H. B. 2011. *Trypanosoma cruzi* utilizes the host low density lipoprotein receptor in invasion. *PLoS Negl Trop Dis,* 5**,** e953.

NAWABI, P., LYKIDIS, A., JI, D. & HALDAR, K. 2003. Neutral-lipid analysis reveals elevation of acylglycerols and lack of cholesterol esters in *Plasmodium falciparum*-infected erythrocytes. *Eukaryot Cell,* 2**,** 1128-31.

NICHOLS, B. A., CHIAPPINO, M. L. & O'CONNOR, G. R. 1983. Secretion from the rhoptries of *Toxoplasma gondii* during host-cell invasion. *J Ultrastruct Res,* 83**,** 85-98.

NISHIKAWA, Y., IBRAHIM, H. M., KAMEYAMA, K., SHIGA, I., HIASA, J. & XUAN, X. 2011. Host cholesterol synthesis contributes to growth of intracellular *Toxoplasma gondii* in macrophages. *J Vet Med Sci,* 73**,** 633-9

NISHIKAWA, Y., QUITTNAT, F., STEDMAN, T. T., VOELKER, D. R., CHOI, J. Y., ZAHN, M., YANG, M., PYPAERT, M., JOINER, K. A. & COPPENS, I. 2005. Host cell lipids control cholesteryl ester synthesis and storage in intracellular *Toxoplasma*. *Cell Microbiol,* 7**,** 849-67.

OHASHI, R., MU, H., WANG, X., YAO, Q. & CHEN, C. 2005. Reverse cholesterol transport and cholesterol efflux in atherosclerosis. *QJM,* 98**,** 845-56.

OHVO-REKILA, H., RAMSTEDT, B., LEPPIMAKI, P. & SLOTTE, J. P. 2002. Cholesterol interactions with phospholipids in membranes. *Prog Lipid Res,* 41**,** 66-97.

OKUBO, K., YOKOYAMA, N., TAKABATAKE, N., OKAMURA, M. & IGARASHI, I. 2007. Amount of cholesterol in host membrane affects erythrocyte invasion and replication by *Babesia bovis*. *Parasitology,* 134**,** 625-30.

OLOFSSON, S. O., BOSTROM, P., ANDERSSON, L., RUTBERG, M., PERMAN, J. & BOREN, J. 2009. Lipid droplets as dynamic organelles connecting storage and efflux of lipids. *Biochim Biophys Acta,* 1791**,** 448-58.

PACHECO-SOARES, C. & DE SOUZA, W. 2000. Labeled probes inserted in the macrophage membrane are transferred to the parasite surface and internalized during cell invasion by *Toxoplasma gondii*. P*arasitol Res,* 86**,** 11-7.

PALACPAC, N. M., HIRAMINE, Y., MI-ICHI, F., TORII, M., KITA, K., HIRAMATSU, R., HORII, T. & MITAMURA, T. 2004. Developmental-stage-specific triacylglycerol biosynthesis, degradation and trafficking as lipid bodies in *Plasmodium falciparum*-infected erythrocytes. *J Cell Sci,* 117**,** 1469-80.

PARTON, R. G. & DEL POZO, M. A. 2013. Caveolae as plasma membrane sensors, protectors and organizers. *Nat Rev Mol Cell Biol,* 14**,** 98-112.

PFAFFL, M. W. 2001. A new mathematical model for relative quantification in real-time RT-PCR. *Nucleic Acids Res,* 29**,** e45.

PIRILLO, A., NORATA, G. D. & CATAPANO, A. L. 2013. LOX-1, OxLDL, and atherosclerosis. *Mediators Inflamm,* 2013**,** 152786

POL, A., GROSS, S. P. & PARTON, R. G. 2014. Review: biogenesis of the multifunctional lipid droplet: lipids, proteins, and sites. *J Cell Biol,* 204**,** 635-46.

POLI, G., BIASI, F. & LEONARDUZZI, G. 2013. Oxysterols in the pathogenesis of major chronic diseases. *Redox Biol,* 1**,** 125-30.

PORCHET-HENNERE, E. & NICOLAS, G. 1983. Are rhoptries of Coccidia really extrusomes? *J Ultrastruct Res,* 84**,** 194-203.

PUCADYIL, T. J., TEWARY, P., MADHUBALA, R. & CHATTOPADHYAY, A. 2004. Cholesterol is required for *Leishmania donovani* infection: implications in leishmaniasis. *Mol Biochem Parasitol,* 133**,** 145-52.

RADHAKRISHNAN, A., IKEDA, Y., KWON, H. J., BROWN, M. S. & GOLDSTEIN, J. L. 2007. Sterol-regulated transport of SREBPs from endoplasmic reticulum to Golgi: oxysterols block transport by binding to Insig. *Proc Natl Acad Sci U S A,* 104**,** 6511-8.

RAVINDRAN, S. & BOOTHROYD, J. C. 2008. Secretion of proteins into host cells by Apicomplexan parasites. *Traffic,* 9**,** 647-56.

RICK, B., DUBREMETZ, J. F. & ENTZEROTH, R. 1998. A merozoite-specific 22-kDa rhoptry protein of the coccidium *Eimeria nieschulzi* (Sporozoa, Coccidia) is exocytosed in the parasitophorous vacuole upon host cell invasion. *Parasitol Res,* 84**,** 291-6.

ROBERTS, W. L. & HAMMOND, D. M. (1970): Ultrastructural and cytologic studies of the sporozoites of four *Eimeria* species. *J.Protozool*, 17, 76-86.

ROBINET, P., WANG, Z., HAZEN, S. L. & SMITH, J. D. 2010. A simple and sensitive enzymatic method for cholesterol quantification in macrophages and foam cells. *J Lipid Res,* 51**,** 3364-9.

RODRIGUES, C. D., HANNUS, M., PRUDENCIO, M., MARTIN, C., GONCALVES, L. A., PORTUGAL, S., EPIPHANIO, S., AKINC, A., HADWIGER, P., JAHN-HOFMANN, K., ROHL, I., VAN GEMERT, G. J., FRANETICH, J. F., LUTY, A. J., SAUERWEIN, R., MAZIER, D., KOTELIANSKY, V., VORNLOCHER, H. P., ECHEVERRI, C. J. & MOTA, M. M. 2008. Host scavenger receptor SR-BI plays a dual role in the establishment of malaria parasite liver infection. *Cell Host Microbe,* 4**,** 271-82

RODRIGUEZ-ACOSTA, A., FINOL, H. J., PULIDO-MENDEZ, M., MARQUEZ, A., ANDRADE, G., GONZALEZ, N., AGUILAR, I., GIRON, M. E. & PINTO, A. 1998. Liver ultrastructural pathology in mice infected with *Plasmodium berghei*. *J Submicrosc Cytol Pathol,* 30**,** 299-307

ROSS, J. L., ALI, M. Y. & WARSHAW, D. M. 2008. Cargo transport: molecular motors navigate a complex cytoskeleton. *Curr Opin Cell Biol,* 20**,** 41-7.

RUIZ, A., BEHRENDT, J. H., ZAHNER, H., HERMOSILLA, C., PEREZ, D., MATOS, L., MUNOZ MDEL, C., MOLINA, J. M. & TAUBERT, A. 2010. Development of *Eimeria ninakohlyakimovae in vitro* in primary and permanent cell lines. *Vet Parasitol,* 173**,** 2-10.

RUSSELL, D. W. 2000. Oxysterol biosynthetic enzymes. *Biochim Biophys Acta,* 1529**,** 126-35.

SAM-YELLOWE, T. Y. 1996. Rhoptry organelles of the apicomplexa: Their role in host cell invasion and intracellular survival. *Parasitol Today,* 12**,** 308-16.

SAWAMURA, T., KUME, N., AOYAMA, T., MORIWAKI, H., HOSHIKAWA, H., AIBA, Y., TANAKA, T., MIWA, S., KATSURA, Y., KITA, T. & MASAKI, T. 1997. An endothelial receptor for oxidized low-density lipoprotein. *Nature,* 386**,** 73-7.

SCHMIDT, J. A. & BROWN, W. J. 2009. Lysophosphatidic acid acyltransferase 3 regulates Golgi complex structure and function. *J Cell Biol,* 186**,** 211-8.

SCHMITTGEN, T. D. & LIVAK, K. J. 2008. Analyzing real-time PCR data by the comparative CT method. *Nature* P*rotocols,* 3**,** 1101-1108.

SCHOLTYSECK, E. 1979. *Fine structure of parasitic protozoa. An atlas of micrographs, drawings and diagrams.* Berlin: Springer-Verlag.

SCHROEDER, F., JEFFERSON, J. R., KIER, A. B., KNITTEL, J., SCALLEN, T. J., WOOD, W. G. & HAPALA, I. 1991. Membrane cholesterol dynamics: cholesterol domains and kinetic pools. *Proc Soc Exp Biol Med,* 196**,** 235-52.

SEHGAL, A., BETTIOL, S., PYPAERT, M., WENK, M. R., KAASCH, A., BLADER, I. J., JOINER, K. A. & COPPENS, I. 2005. Peculiarities of host cholesterol transport to the unique intracellular vacuole containing *Toxoplasma*. *Traffic,* 6**,** 1125-41.

SEO, T., OELKERS, P. M., GIATTINA, M. R., WORGALL, T. S., STURLEY, S. L. & DECKELBAUM, R. J. 2001. Differential modulation of ACAT1 and ACAT2 transcription and activity by long chain free fatty acids in cultured cells. *Biochemistry,* 40**,** 4756-62

SHEFFIELD, H.G & HAMMOND; D.M. Fine structure of first-generation merozoites of *Eimeria bovis*. J. *Parasit*, 52, 595-606.

SHIMANO, H. 2001. Sterol regulatory element-binding proteins (SREBPs): transcriptional regulators of lipid synthetic genes. *Prog Lipid Res,* 40**,** 439-52.

SHRIVASTAVA, S., HALDAR, S., GIMPL, G. & CHATTOPADHYAY, A. 2009. Orientation and dynamics of a novel fluorescent cholesterol analogue in membranes of varying phase. *J* P*hys Chem B,* 113**,** 4475-81.

SIMONS, K. & IKONEN, E. 2000. How cells handle cholesterol. *Science,* 290**,** 1721-6.

SIMONS, K. & TOOMRE, D. 2000. Lipid rafts and signal transduction. *Nat Rev Mol Cell Biol,* 1**,** 31-9.

SINAI, A. P. & JOINER, K. A. 2001. The *Toxoplasma gondii* protein ROP2 mediates host organelle association with the parasitophorous vacuole membrane. *J Cell Biol,* 154**,** 95-108.

SINAI, A. P. 2008. Biogenesis of and activities at the *Toxoplasma gondii* parasitophorous vacuole membrane. *Subcell Biochem,* 47**,** 155-64.

SONDA, S., TING, L. M., NOVAK, S., KIM, K., MAHER, J. J., FARESE, R. V., JR. & ERNST, J. D. 2001. Cholesterol esterification by host and parasite is essential for optimal proliferation of *Toxoplasma gondii*. *J Biol Chem,* 276**,** 34434-40.

SOUZA, W. 2006. Secretory organelles of pathogenic protozoa. *An Acad Bras Cienc,* 78**,** 271-91.

SPANN, N. J. & GLASS, C. K. 2013. Sterols and oxysterols in immune cell function. *Nat Immunol,* 14**,** 893-900.

SPEER, C.A. 1988. Ultrasturcture of two types of first-generation merozoites of *Eimeria bovis*. *J. Protozool*, 35, 379-381.

SUHWOLD, A., HERMOSILLA, C., SEEGER, T., ZAHNER, H. & TAUBERT, A. 2010. T cell reactions of *Eimeria bovis* primary and challenge-infected calves. *Parasitol Res,* 106**,** 595-605.

SUSS-TOBY, E., ZIMMERBERG, J. & WARD, G. E. 1996. *Toxoplasma* invasion: the parasitophorous vacuole is formed from host cell plasma membrane and pinches off via a fission pore. *Proc Natl Acad Sci U S A,* 93**,** 8413-8.

SYLVESTER, P. W. 2011. Optimization of the tetrazolium dye (MTT) colorimetric assay for cellular growth and viability. *Methods Mol Biol,* 716**,** 157-68.

TABAS, I. 2002. Consequences of cellular cholesterol accumulation: basic concepts and physiological implications. *J Clin Invest,* 110**,** 905-11.

TALL, A. R. 1998. An overview of reverse cholesterol transport. *Eur Heart J,* 19 Suppl A**,** A31-5.

TAUBERT, A., BEHRENDT, J. H., SUHWOLD, A., ZAHNER, H. & HERMOSILLA, C. 2009. Monocyte- and macrophage-mediated immune reactions against *Eimeria bovis*. *Vet Parasitol,* 164**,** 141-53.

TAUBERT, A., HERMOSILLA, C., SUHWOLD, A. & ZAHNER, H. 2008. Antigen-induced cytokine production in lymphocytes of *Eimeria bovis* primary and challenge infected calves. *Vet Immunol Immunopathol,* 126**,** 309-20.

TAUBERT, A., KRULL, M., ZAHNER, H. & HERMOSILLA, C. 2006a. *Toxoplasma gondii* and *Neospora caninum* infections of bovine endothelial cells induce endothelial adhesion molecule gene transcription and subsequent PMN adhesion. *Vet Immunol Immunopathol,* 112**,** 272-83.

TAUBERT, A., WIMMERS, K., PONSUKSILI, S., JIMENEZ, C. A., ZAHNER, H. & HERMOSILLA, C. 2010. Microarray-based transcriptional profiling of *Eimeria bovis*-infected bovine endothelial host cells. *Vet Res,* 41**,** 70.

TAUBERT, A., ZAHNER, H. & HERMOSILLA, C. 2006b. Dynamics of transcription of immunomodulatory genes in endothelial cells infected with different coccidian parasites. *Vet Parasitol,* 142**,** 214-22.

TAUBERT, A., ZAHNER, H. & HERMOSILLA, C. 2007. *Eimeria bovis* infection enhances adhesion of peripheral blood mononuclear cells to and their transmigration through an infected bovine endothelial cell monolayer *in vitro*. *Parasitol Res,* 101**,** 591-8.

TEDDER, T. F., STEEBER, D. A., CHEN, A. & ENGEL, P. 1995. The selectins: vascular adhesion molecules. *FASEB J,* 9**,** 866-73.

TEWARY, P., VEENA, K., PUCADYIL, T. J., CHATTOPADHYAY, A. & MADHUBALA, R. 2006. The sterol-binding antibiotic nystatin inhibits entry of non-opsonized *Leishmania donovani* into macrophages. *Biochem Biophys Res Commun,* 339**,** 661-6.

TWIGG, M. W., FREESTONE, K., HOMER-VANNIASINKAM, S. & PONNAMBALAM, S. 2012. The LOX-1 scavenger receptor and its implications in the treatment of vascular disease. *Cardiol Res* P*ract,* 2012**,** 632408.

VAN DE SAND, C., HORSTMANN, S., SCHMIDT, A., STURM, A., BOLTE, S., KRUEGER, A., LUTGEHETMANN, M., POLLOK, J. M., LIBERT, C. & HEUSSLER, V. T. 2005. The liver stage of *Plasmodium berghei* inhibits host cell apoptosis. *Mol Microbiol,* 58**,** 731-42.

VAN DER MEER-JANSSEN, Y. P., VAN GALEN, J., BATENBURG, J. J. & HELMS, J. B. 2010. Lipids in host-pathogen interactions: pathogens exploit the complexity of the host cell lipidome. *Prog Lipid Res,* 49**,** 1-26.

VAN MEER, G. 2001. Caveolin, cholesterol, and lipid droplets? *J Cell Biol,* 152**,** F29-34.

VAN MEERLOO, J., KASPERS, G. J. & CLOOS, J. 2011. Cell sensitivity assays: the MTT assay. *Methods Mol Biol,* 731**,** 237-45.

VANCE D. E. & VANCE J. E., *Biochemistry of li*p*ids, li*po*proteins, and membranes, 4th edition*. Amsterdam: Elsevier B.V.

VIELEMEYER, O., MCINTOSH, M. T., JOINER, K. A. & COPPENS, I. 2004. Neutral lipid synthesis and storage in the intraerythrocytic stages of *Plasmodium falciparum*. *Mol Biochem Parasitol,* 135**,** 197-209

VOYTA, J. C., VIA, D. P., BUTTERFIELD, C. E. & ZETTER, B. R. 1984. Identification and isolation of endothelial cells based on their increased uptake of acetylated-low density lipoprotein. *J Cell Biol,* 99**,** 2034-40.

WAGNER, J. G. & ROTH, R. A. 2000. Neutrophil migration mechanisms, with an emphasis on the pulmonary vasculature. *Pharmacol Rev,* 52**,** 349-74.

WARD, G. E., MILLER, L. H. & DVORAK, J. A. 1993. The origin of parasitophorous vacuole membrane lipids in malaria-infected erythrocytes. *J Cell Sci,* 106 (Pt 1)**,** 237-48.

WASAN, K. M., RISOVIC, V., SIVAK, O., LEE, S. D., MASON, D. X., CHIKLIS, G. R., MCSHANE, J., LYNN, M., WONG, N. & ROSSIGNOL, D. P. 2008. Influence of plasma cholesterol and triglyceride concentrations and eritoran (E5564) micelle size on its plasma pharmacokinetics and *ex vivo* activity following single intravenous bolus dose into healthy female rabbits. *Pharm Res,* 25**,** 176-82.

WENK, M. R. 2006. Lipidomics of host-pathogen interactions. *FEBS Lett,* 580**,** 5541-51.

WIEGAND, V., CHANG, T. Y., STRAUSS, J. F., 3RD, FAHRENHOLZ, F. & GIMPL, G. 2003. Transport of plasma membrane-derived cholesterol and the function of Niemann-Pick C1 Protein. *Faseb j,* 17**,** 782-4.

WILSON, H. M., GRIFFIN, B. A., WATT, C. & SKINNER, E. R. 1992. The isolation and characterization of high-density-lipoprotein subfractions containing apolipoprotein E from human plasma. *Biochem J,* 284 (Pt 2)**,** 477-81

XU, F., RYCHNOVSKY, S. D., BELANI, J. D., HOBBS, H. H., COHEN, J. C. & RAWSON, R. B. 2005. Dual roles for cholesterol in mammalian cells. P*roc Natl Acad Sci U S A,* 102**,** 14551-6.

YOKOYAMA, S. 2005. Assembly of high density lipoprotein by the ABCA1/apolipoprotein pathway. *Curr Opin Lipidol,* 16**,** 269-79.

ZENG, B. & ZHU, G. 2006. Two distinct oxysterol binding protein-related proteins in the parasitic protist *Cryptosporidium parvum* (Apicomplexa). *Biochem Biophys Res Commun,* 346**,** 591-99.

ZENG, B. 2006. Functional characterization of acyl-coa binding protein (ACBP) and oxysterol binding protein-related proteins (ORPS) from *Cryptosporidium parvum. PhD Dissertation.* Texas A&M University. Texas.

ZIDOVETZKI, R. & LEVITAN, I. 2007. Use of cyclodextrins to manipulate plasma membrane cholesterol content: evidence, misconceptions and control strategies. *Biochim Biophys Acta,* 1768**,** 1311-24.

9 APPENDIX

Statistical analysis

DATA			STATISTIC TEST	P VALUE	NOTE
Fig. 4.11	4 days p.i		multiple *t*-tests with days analyzed individually	0.00565457	significant
	14 days p.i		multiple *t*-tests with days analyzed individually	0.00361334	significant
	17 days p.i		multiple *t*-tests with days analyzed individually	0.00168995	significant
Fig. 4.12	controls vs. infected monolayers on 8 days p.i		*t*-tests	0.1825	not significant
	controls vs. infected monolayers on 17 days p.i		*t*-tests	< 0.0001	significant
	controls vs. infected monolayers on 21 days p.i		*t*-tests	< 0.0001	significant
Fig. 4.13	controls vs. cholesterol treated monolayer		*t*-tests	0.0150	significant
	controls vs. desmosterol treated monolayer		*t*-tests	0.0492	significant
Fig. 4.14	controls vs. host depleted		*t*-tests	0.0085	significant
	controls vs. parasite depleted		*t*-tests	< 0.0001	significant
	parasite vs. host depleted		*t*-tests	0.0083	significant
	3 groups of treatments		one-way ANOVA	0.0045	significant
Fig. 4.20	controls vs. 17 days p.i-infected monolayer		*t*-tests	< 0.000	significant
Fig. 4.22	controls vs. 17 days p.i-infected monolayer		*t*-tests	< 0.0001	significant
Fig. 4.23	controls vs. 17 days p.i-infected monolayer		*t*-tests	< 0.0001	significant
Fig. 4.24	controls vs. LDL enriched monolayer		*t*-tests	0.0069	significant
Fig. 4.28	ACAT1	12 days p.i	multiple *t*-tests with days analyzed individually	0.104044	not significant
		14 days p.i	multiple *t*-tests with days analyzed individually	0.0490754	not significant
		17 days p.i	multiple *t*-tests with days analyzed individually	0.00096642	significant
		20 days p.i	multiple *t*-tests with days analyzed individually	0.250879	not significant
	ACAT2	12 days p.i	multiple *t*-tests with days analyzed individually	0.974228	not significant
		14 days p.i	multiple *t*-tests with days analyzed individually	0.140826	not significant
		17 days p.i	multiple *t*-tests with days analyzed individually	0.00301399	significant
		20 days p.i	multiple *t*-tests with days analyzed individually	0.0955433	significant
Fig. 4.29	HMGCS1	12 days p.i	multiple *t*-tests with days analyzed individually	0.316054	not significan
		14 days p.i	multiple *t*-tests with days analyzed individually	0.599271	not significant
		17 days p.i	multiple *t*-tests with days analyzed individually	0.0134597	significant
		20 days p.i	multiple *t*-tests with days analyzed individually	0.00483933	significant
	SQLE	12 days p.i	multiple *t*-tests with days analyzed individually	0.881355	not significant
		14 days p.i	multiple *t*-tests with days analyzed individually	0.350306	not significant
		17 days p.i	multiple *t*-tests with days analyzed individually	0.00417226	significant
		20 days p.i	multiple *t*-tests with days analyzed individually	0.0149898	significant
	HMGCR	12 days p.i	multiple *t*-tests with days analyzed individually	0.203995	not significant
		14 days p.i	multiple *t*-tests with days analyzed individually	0.00752577	significant
		17 days p.i	multiple *t*-tests with days analyzed individually	0.00106191	significant
		20 days p.i	multiple *t*-tests with days analyzed individually	0.00526938	significant
Fig. 4.30	SOAT1	12 days p.i	multiple *t*-tests with days analyzed individually	0.0395837	not significant
		14 days p.i	multiple *t*-tests with days analyzed individually	0.00141457	significant
		17 days p.i	multiple *t*-tests with days analyzed individually	0.00184057	significant
		20 days p.i	multiple *t*-tests with days analyzed individually	0.12705	not significant
	CH25H	12 days p.i	multiple *t*-tests with days analyzed individually	0.100908	not significant
		14 days p.i	multiple *t*-tests with days analyzed individually	3.532e-006	significant
		17 days p.i	multiple *t*-tests with days analyzed individually	8.786e-006	significant
		20 days p.i	multiple *t*-tests with days analyzed individually	0.00546593	significant
Fig. 4.31	LDLR	12 days p.i	multiple *t*-tests with days analyzed individually	0.0087123	significant
		14 days p.i	multiple *t*-tests with days analyzed individually	0.401059	not significant
		17 days p.i	multiple *t*-tests with days analyzed individually	0.00360332	significant
		20 days p.i	multiple *t*-tests with days analyzed individually	0.164666	not significant
	OLR1	12 days p.i	multiple *t*-tests with days analyzed individually	0.00082721	significant
		14 days p.i	multiple *t*-tests with days analyzed individually	0.0342785	significant

		17 days p.i	multiple *t*-tests with days analyzed individually	0.00230203	significant
		20 days p.i	multiple *t*-tests with days analyzed individually	0.00576825	significant
Fig. 4.36	cells carrying meronts	2 days p.i	multiple *t*-tests with days analyzed individually	0.915553	not significant
		6 days p.i	multiple *t*-tests with days analyzed individually	0.815788	not significant
		10 days p.i	multiple *t*-tests with days analyzed individually	0.00040596	significant
		14 days p.i	multiple *t*-tests with days analyzed individually	4.027e-006	significant
		18 days p.i	multiple *t*-tests with days analyzed individually	2.177e-006	significant
		22 days p.i	multiple *t*-tests with days analyzed individually	5.544e-008	significant
		26 days p.i	multiple *t*-tests with days analyzed individually	0.00013641	significant
		30 days p.i	multiple *t*-tests with days analyzed individually	0.00332221	significant
	meronts size	10 days p.i	multiple *t*-tests with days analyzed individually	0.575521	not significant
		14 days p.i	multiple *t*-tests with days analyzed individually	0.0241595	significant
		18 days p.i	multiple *t*-tests with days analyzed individually	9.881e-006	significant
		22 days p.i	multiple *t*-tests with days analyzed individually	0.00021066	significant
		26 days p.i	multiple *t*-tests with days analyzed individually	5.955e-008	significant
		30 days p.i	multiple *t*-tests with days analyzed individually	2.194e-015	significant
Fig. 4.37	controls vs. medium 0.04% aceton		*t*-tests	0.4426	not significant
	controls vs. 0.05 µM		*t*-tests	0.4276	not significant
	controls vs 0.01 µM		*t*-tests	0.2055	not significant
	controls vs 0.05 µM		*t*-tests	0.0106	significant
	controls vs 0.1 µM		*t*-tests	0.0016	significant
	controls vs. 0.5 µM		*t*-tests	< 0.0001	significant
	controls vs. 1 µM		*t*-tests	< 0.0001	significant
Fig. 4.38	cells carrying meronts	2 days p.i	multiple *t*-tests with days analyzed individually	0.945364	not significant
		6 days p.i	multiple *t*-tests with days analyzed individually	0.439344	not significant
		10 days p.i	multiple *t*-tests with days analyzed individually	0.0788531	not significant
		14 days p.i	multiple *t*-tests with days analyzed individually	0.00025488	significant
		18 days p.i	multiple *t*-tests with days analyzed individually	0.0010787	significant
		22 days p.i	multiple *t*-tests with days analyzed individually	7.041e-006	significant
		26 days p.i	multiple *t*-tests with days analyzed individually	0.00013871	significant
		30 days p.i	multiple *t*-tests with days analyzed individually	0.0432414	not significant
	meronts size	10 days p.i	multiple *t*-tests with days analyzed individually	0.869716	not significant
		14 days p.i	multiple *t*-tests with days analyzed individually	0.293938	not significant
		18 days p.i	multiple *t*-tests with days analyzed individually	0.908454	not significant
		22 days p.i	multiple *t*-tests with days analyzed individually	0.393091	not significant
		26 days p.i	multiple *t*-tests with days analyzed individually	0.00191343	significant
		30 days p.i	multiple *t*-tests with days analyzed individually	6.058e-008	significant
Fig. 4.39	controls vs. medium 0.07% ethanol		*t*-tests	0.9769	not significant
	controls vs. 0.025 µM		*t*-tests	0.9902	not significant
	controls vs. 0.05 µM		*t*-tests	0.9702	not significant
	controls vs. 0.25 µM		*t*-tests	0.9509	not significant
	controls vs. 0.5 µM		*t*-tests	0.8436	not significant
	controls vs 2.5 µM		*t*-tests	0.0017	significant
	controls vs 5 µM		*t*-tests	< 0.0001	significant
Fig. 4.40	cells carrying meronts (treatments since 1 day p.i)	2 days p.i	multiple *t*-tests with days analyzed individually	0.915553	not significant
		6 days p.i	multiple *t*-tests with days analyzed individually	0.815788	not significant
		10 days p.i	multiple *t*-tests with days analyzed individually	4.072e-006	significant
		14 days p.i	multiple *t*-tests with days analyzed individually	3.686e-006	significant
		18 days p.i	multiple *t*-tests with days analyzed individually	1.241e-008	significant
		22 days p.i	multiple *t*-tests with days analyzed individually	4.887e-007	significant
		26 days p.i	multiple *t*-tests with days analyzed individually	4.993e-006	significant
		30 days p.i	multiple *t*-tests with days analyzed individually	0.00129247	significant
	meronts size (treatments since 1 day p.i)	10 days p.i	multiple *t*-tests with days analyzed individually	0.00749911	significant
		14 days p.i	multiple *t*-tests with days analyzed individually	0.00319473	significant
		18 days p.i	multiple *t*-tests with days analyzed individually	5.489e-008	significant
		22 days p.i	multiple *t*-tests with days analyzed individually	3.058e-005	significant
		26 days p.i	multiple *t*-tests with days analyzed individually	8.532e-009	significant
		30 days p.i	multiple *t*-tests with days analyzed individually	1.336e-016	significant
	cells carrying meronts (treatments since 10 days p.i)	2 days p.i	multiple *t*-tests with days analyzed individually	0.915553	not significant
		6 days p.i	multiple *t*-tests with days analyzed individually	0.815788	not significant
		10 days p.i	multiple *t*-tests with days analyzed individually	0.831236	not significant
		14 days p.i	multiple *t*-tests with days analyzed individually	0.0582052	not significant
		18 days p.i	multiple *t*-tests with days analyzed individually	0.0010787	significant
		22 days p.i	multiple *t*-tests with days analyzed individually	3.199e-006	significant
		26 days p.i	multiple *t*-tests with days analyzed individually	4.830e-005	significant
		30 days p.i	multiple *t*-tests with days analyzed individually	0.0044847	significant

	meronts size (treatments since 10 days p.i)	10 days p.i	multiple *t*-tests with days analyzed individually	0.815806	not significant
		14 days p.i	multiple *t*-tests with days analyzed individually	0.839711	not significant
		18 days p.i	multiple *t*-tests with days analyzed individually	0.00011022	significant
		22 days p.i	multiple *t*-tests with days analyzed individually	0.00172376	significant
		26 days p.i	multiple *t*-tests with days analyzed individually	6.985e-007	significant
		30 days p.i	multiple *t*-tests with days analyzed individually	7.240e-012	significant
Fig. 4.41	Lipid droplet deposition (treatments and times dependency)		Two-way RM ANOVA	< 0.0001	significant
Fig. 4.42	controls vs. medium 0.04% DMSO		*t*-tests	0.7893	not significant
	controls vs. 0.025 µM		*t*-tests	0.2480	not significant
	controls vs. 0.05 µM		*t*-tests	0.0170	significant
	controls vs. 0.25 µM		*t*-tests	0.000	significant
	controls vs. 0.5 µM		*t*-tests	< 0.000	significant
	controls vs 2.5 µM		*t*-tests	< 0.0001	significant
	controls vs 5 µM		*t*-tests	< 0.0001	significant
Fig. 4.43	cells carrying meronts	2 days p.i	multiple *t*-tests with days analyzed individually	0.915553	not significant
		6 days p.i	multiple *t*-tests with days analyzed individually	0.815788	not significant
		10 days p.i	multiple *t*-tests with days analyzed individually	0.831236	not significant
		14 days p.i	multiple *t*-tests with days analyzed individually	0.0582052	not significant
		18 days p.i	multiple *t*-tests with days analyzed individually	0.0010787	significant
		22 days p.i	multiple *t*-tests with days analyzed individually	0.00039885	significant
		26 days p.i	multiple *t*-tests with days analyzed individually	0.00073310	significant
		30 days p.i	multiple *t*-tests with days analyzed individually	0.0250967	not significant
	meronts size	10 days p.i	multiple *t*-tests with days analyzed individually	0.00749911	significant
		14 days p.i	multiple *t*-tests with days analyzed individually	0.00319473	significant
		18 days p.i	multiple *t*-tests with days analyzed individually	5.489e-008	significant
		22 days p.i	multiple *t*-tests with days analyzed individually	0.00062292	significant
		26 days p.i	multiple *t*-tests with days analyzed individually	8.741e-006	significant
		30 days p.i	multiple *t*-tests with days analyzed individually	1.142e-011	significant
Fig. 4.44	controls vs. medium 0.025% DMSO		*t*-tests	0.7734	not significant
	controls vs. 0.025 µM		*t*-tests	0.6902	not significant
	controls vs. 0.05 µM		*t*-tests	0.5102	not significant
	controls vs. 0.25 µM		*t*-tests	0.0469	significant
	controls vs. 0.5 µM		*t*-tests	0.0013	significant
	controls vs 2.5 µM		*t*-tests	< 0.0001	significant
	controls vs 5 µM		*t*-tests	< 0.0001	significant

ACKNOWLEDGMENT

I am privileged to have the opportunity to do the research for my "*Doktorarbeit*" at Institute of Parasitology, Justus-Liebig University, Giessen. I am most grateful to my supervisor, Prof. Dr. habil. Anja Taubert for the opportunity to join the research group, scholarship recommendation, great patience and all the support throughout research process and writing period.

My warm thanks are going to PD Dr. habil. Carlos Hermosilla and Dr. Jörg Hirzmann for sharing, help, encouragement and discussion of initial experiments and writing. I am also very thankful to Dr. Christian Bauer who introduced me to my supervisor and helped me to establish my life during first days in Giessen. I would like to thank to Dr. Katharina Kerner for helping me quite a lot in flow cytometry and save my cells to escape during institute movement. My acknowledgement to Dr. Anne Holz for her guidance toward confocal microscopy. I would like to thank Prof. Dr. Günter Lochnit for discussion and cholesterol extraction experiments. I am also very thankful to Prof. Dr. Gerald Gimpl for fluorescent-cholesterol derivatives gift. I would like to acknowledge to A. Wehrend and K. Herzog for the continuous supply of bovine umbilical cords.

I also thank Dr. Sonja Kleinertz, Liliana, Tamara and Maria for togetherness in the research group. I would like to thank to Brigitte Hofmann, Christine Henrich and Klaus Becker for all helps in the cell culture, "mol-biol" laboratory and during oocyst passaging period. For all the kind help I have received, I acknowledge all staffs and members of Institute of Parasitology, Justus-Liebig University, Giessen.

I should appreciate to DIKTI (Direktorat Jenderal Pendidikan Tinggi Indonesia) for the financial support in my promotion period (2011-2014) and enable me to stay in Germany with its scholarship.

DECLARATION

"I hereby declare that I have completed the submitted doctoral thesis independently and without any unauthorised outside help and with only those forms of support mentioned in the thesis. All texts that have been quoted verbatim or by analogy from published and non-published writings and all details based on verbal information have been identified as such. In the analyses that I have conducted and to which I refer in this thesis, I have followed the principles of good scientific practice, as stated in the Statute of Justus Liebig University Giessen for Ensuring Good Scientific Practice."

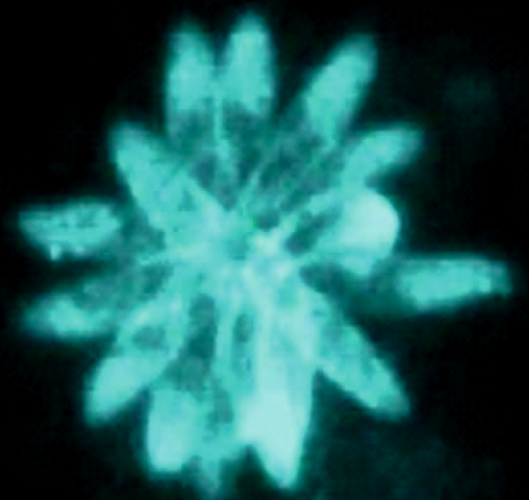

édition scientifique
VVB LAUFERSWEILER VERLAG

VVB LAUFERSWEILER VERLAG
STAUFENBERGRING 15
D-35396 GIESSEN

Tel: 0641-5599888 Fax: -5599890
redaktion@doktorverlag.de
www.doktorverlag.de

ISBN: 978-3-8359-6227-9